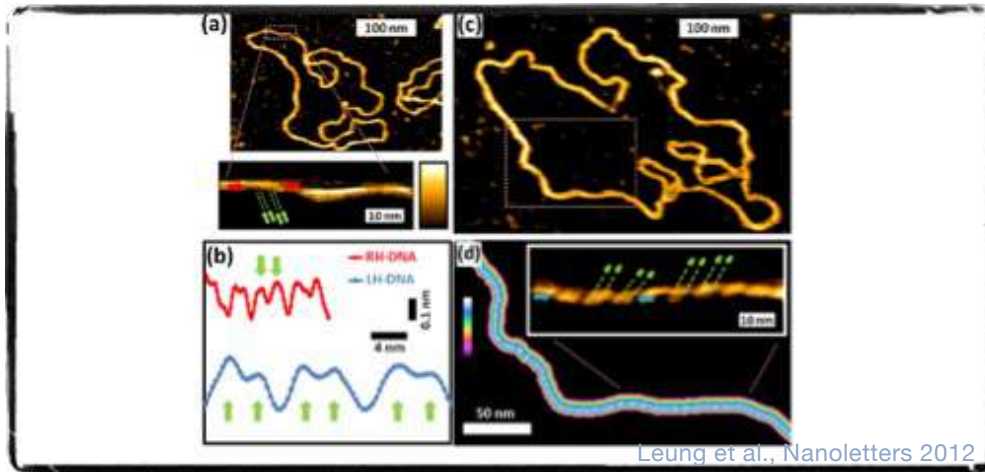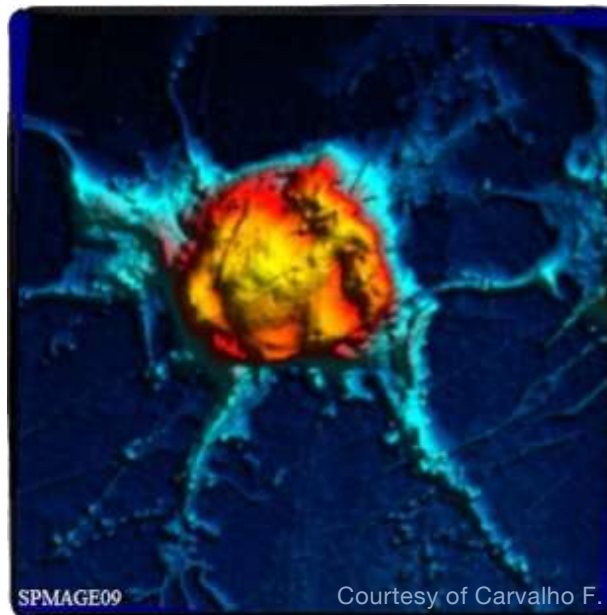# High Res/High Speed
AFM

AFM in Biology
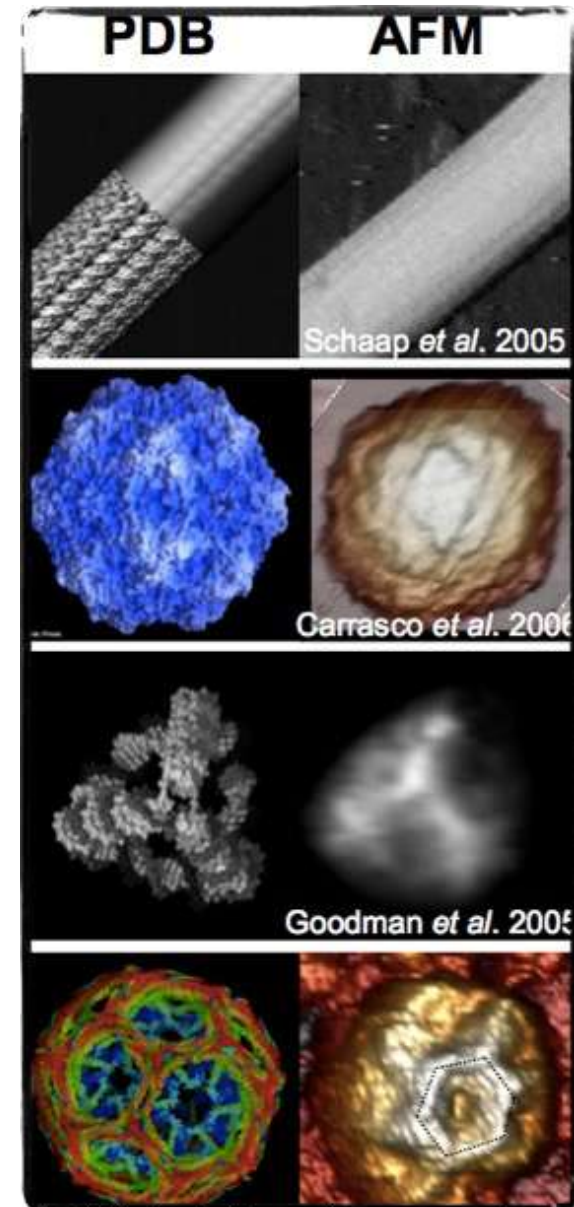
DNA

Leung et al., Nanoletters 2012

Cells

SPMAGE09 · Courtesy of Carvalho F.

Proteins

PDB · AFM

Schaap et al. 2005

Carrasco et al. 2006

Goodman et al. 2005

bio-molecules: working in liquid

Clare Waterman, NIH

laser

quadrant photo detector

AFM in liquid

Figure 1.8 Need of a liquid cell device for imaging in liquids. The incoming laser beam (red line) continuously changes direction due to surface waves at the gas–liquid interface. As a consequence, a nonsteady spot is o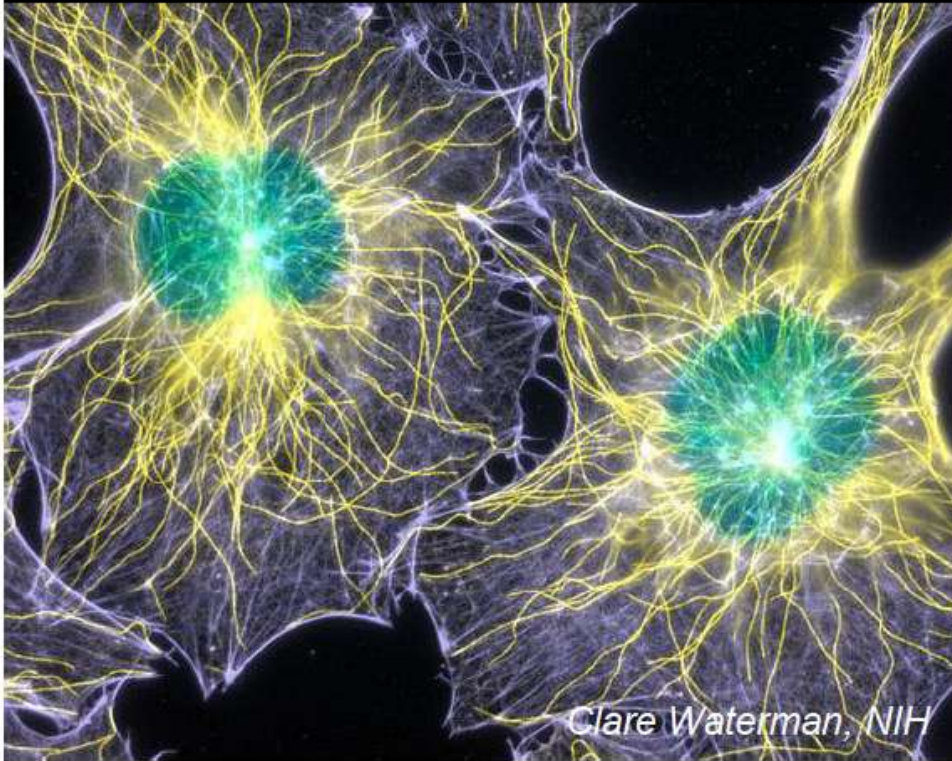btained (left). By using a transparent glass window, a well-defined interface is created and the laser light is transmitted without scattering in the liquid (middle). By means of two holes, liquid can be exchanged in the course of an experiment (right).

An important step of development, enabling biological AFM, was the development of a liquid cell in which cantilever, tip and sample are immersed in buffer solution.


Figure 1.12 Side view of a design of a liquid cell showing a possible mechanism to oscillate the cantilever. A piezoelectric ceramic is located below one of the supporting balls and far away from the liquid meniscus. This solution also moves the liquid, and that excites many other resonances of the liquid cell.
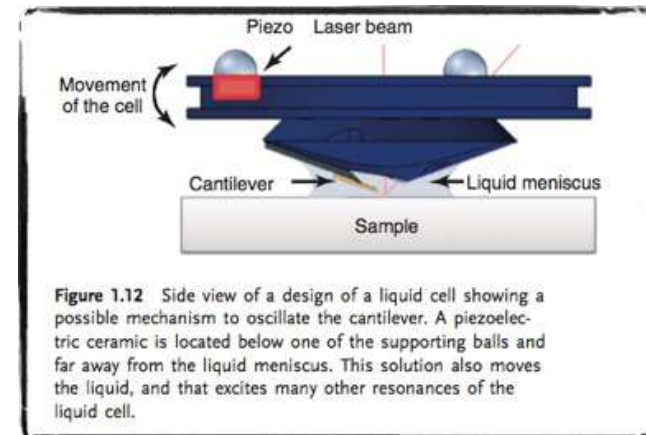
In the case of soft biological samples,non-destructive imaging at nanometer-resolution in physiological conditions (i.e. in aqueous buffer, at ambient temperature and pressure) requires the ability to control **forces < 100 pN.**
 With a high optical lever sensitivity, one is able to control normal forces applied by the cantilever down to about 50 pN in liquid, enabling **contact mode imaging of biological samples**. Although lateral scanning forces impose a restriction on the sample type to be imaged in contact mode, it has yielded fascinating insights into the organization of proteins in biological membranes

Balancing Electrostatic Forces

Main Forces in Liquid:

1) Van der Waals, globally attractive, short range.

2) Double layer forces: Repulsive, long range, dependent on pH and ionic strength. Due to ionic atmosphere over the surfaces of the tip and the surface. The 2 layers create the repulsive force.
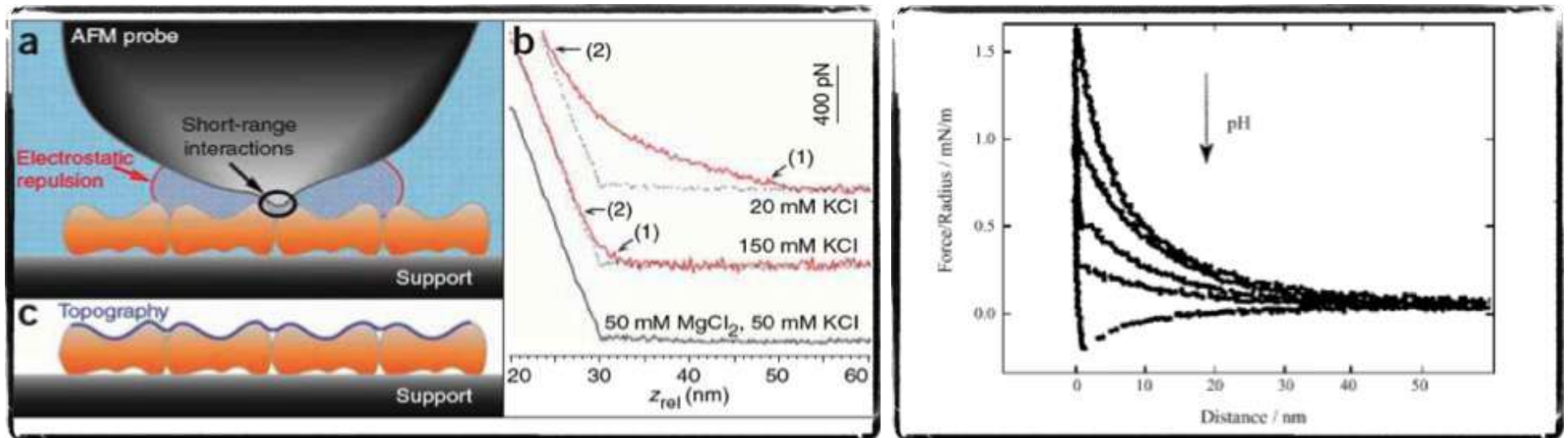
Fine tuning of electrolyte concentration is always required to minimize the distance of tip-sample electrostatic interactions and achieve high-resolution.
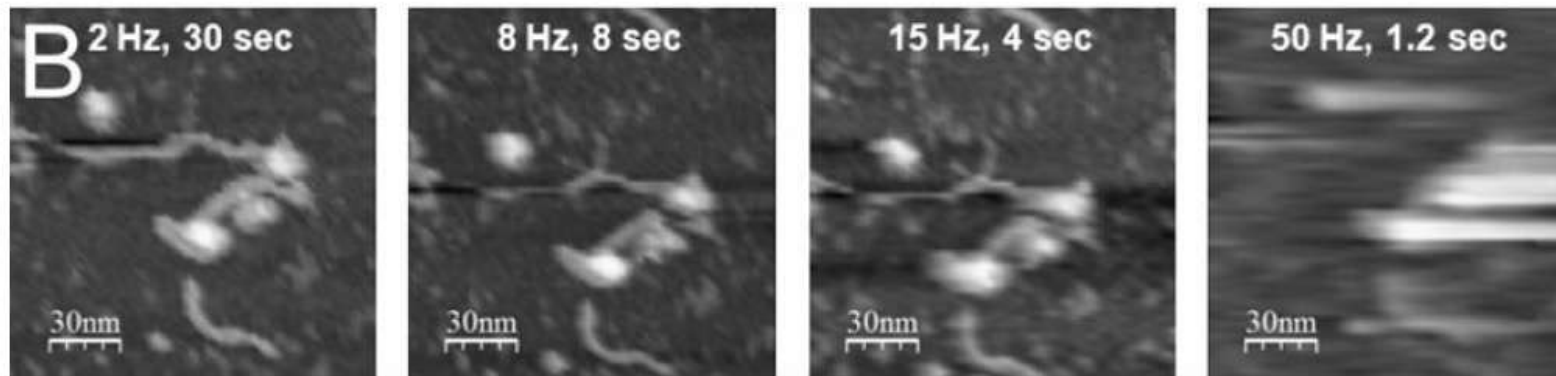
SPEED LIMITS OF AFM IMAGING
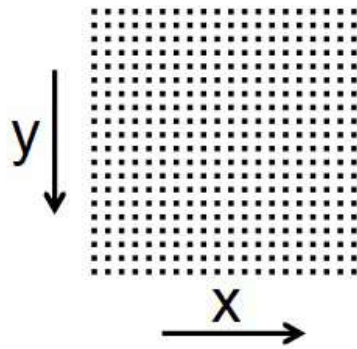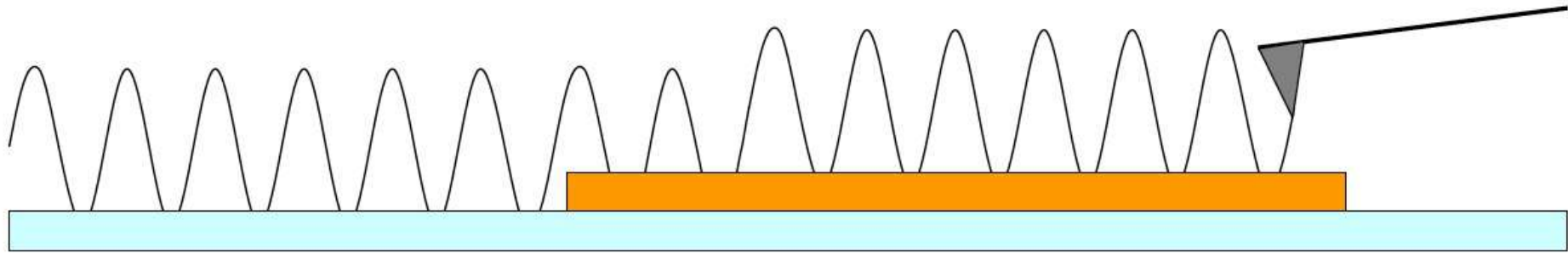
64 x 64 = 4096 px

need a few oscillations per pixel (~5)

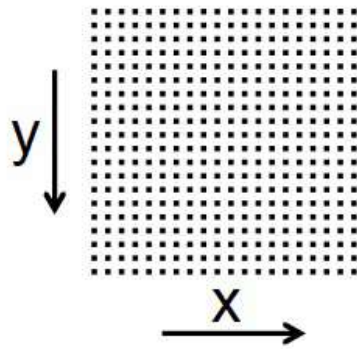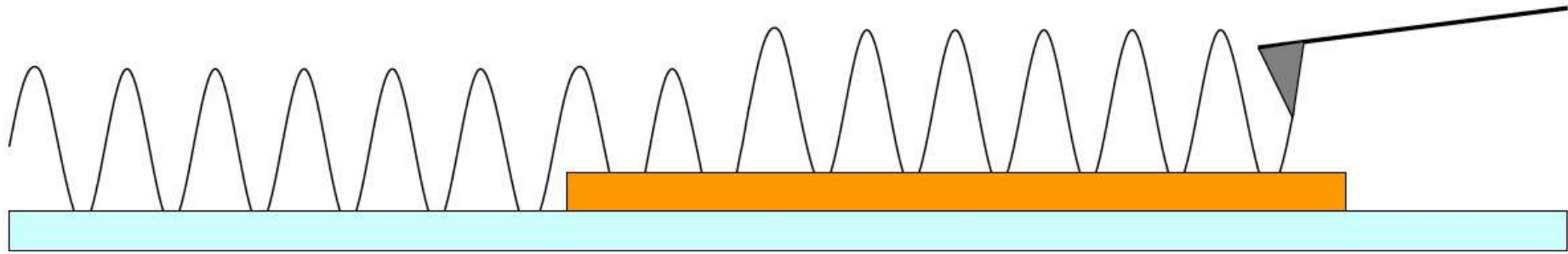fast bio-cantilever ~ 25 kHz

→ 0.04 ms * 5 * 4096 = 1 s

B. 2 Hz, 30 sec   8 Hz, 8 sec   15 Hz, 4 sec   50 Hz, 1.2 sec

30nm   30nm   30nm   30nm

(there are other limiting factors (z-piezo, feed-back loop)

Courtesy of I. Schaap

SPEED LIMITS OF AFM IMAGING

64 x 64 = 4096 px

need a few oscillations per pixel (~5)

fast bio-cantilever ~ 25 kHz

→ 0.04 ms * 5 * 4096 = 1 s

B 2 Hz, 30 sec   8 Hz, 8 sec   15 Hz, 4 sec   50 Hz, 1.2 sec

30nm   30nm   30nm   30nm
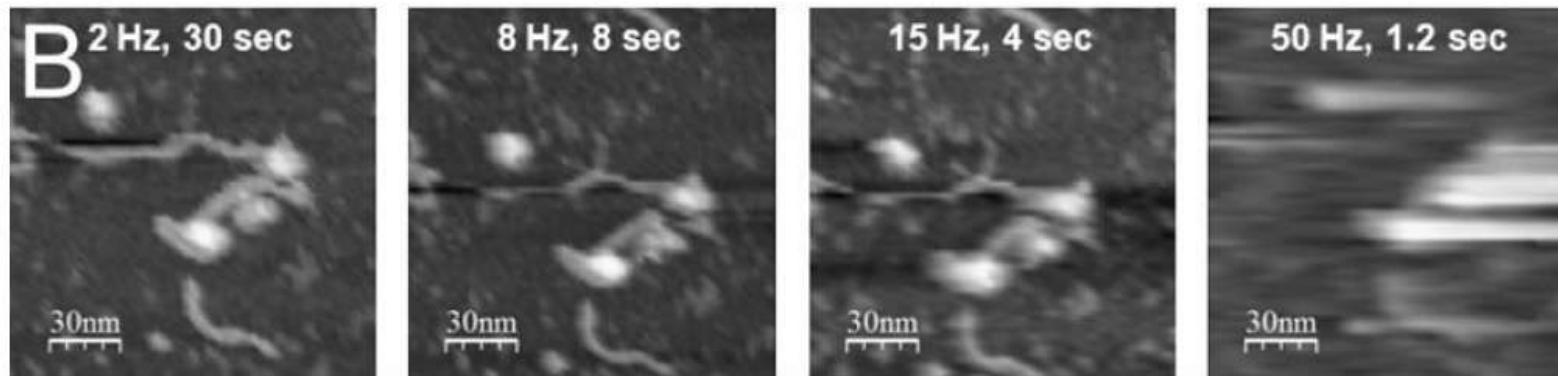
(there are other limiting factors (z-piezo, feed-back loop)

small cantilevers are faster

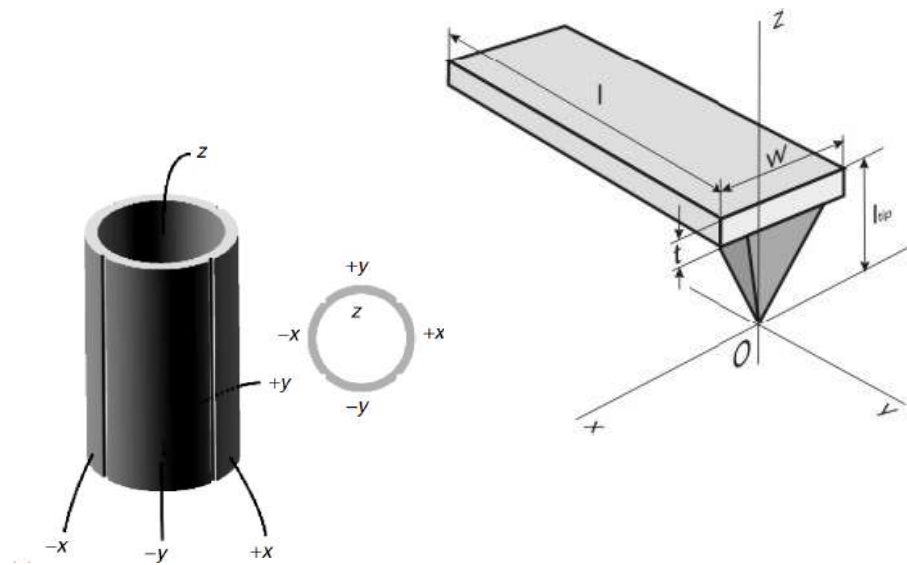|	l (μm)	w (μm)	t (μm)	ω_0 (kHz)	k (N/m)	
rc800	200	20	0.8	3	0.05	8 s
bl150	60	30	0.18	8	0.03	3 s
ac40	38	16	0.2	25	0.1	1 s
ac10	9	2	0.13	500	0.1	50 ms
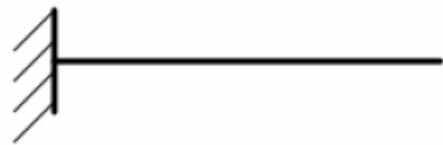
$$\omega_0 = \sqrt{k/m} = \sqrt{\frac{Et^2}{l^4 \rho}}$$

$$k = \frac{F}{d} = \frac{Ewt^3}{4l^3}$$

make cantilevers short to increase ω_0 and thinner to restore k

AFM in liquid

E= Young Modulus
ρ = density

$$k = \frac{Et^3 w}{4l^3}$$

$$f = \frac{1}{2\pi}\sqrt{\frac{k}{m}} = \frac{1}{4\pi}\frac{t}{l^2}\sqrt{\frac{E}{\rho}}$$

Main concern: electrical isolation of the piezo to avoid any shortcut due to wetting

For imaging in liquids: recommended to move the tip relative to the sample to minimize the added effective mass *m** (only the tip and parts of the tip holder are immersed in the buffer container)

AFM in liquid
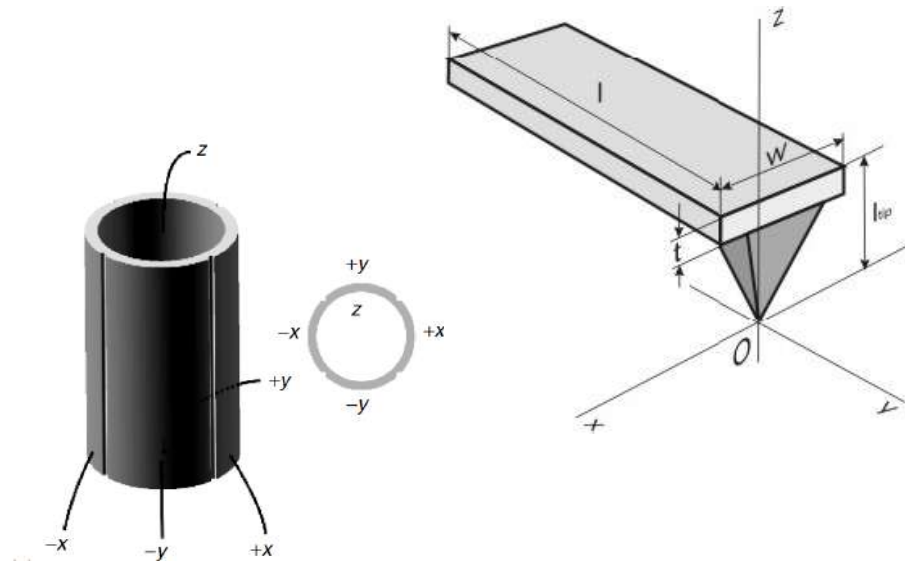
A cantilever in thermodynamic equilibrium with the thermal bath at temperature T has a thermal energy (Brownian motion) that increases the elastic energy stored in the cantilever, providing random vibrations.
To each degree of freedom, the equipartition theorem assign an average energy ½ $k_B T$

For a simple harmonic oscillator (like an AFM cantilever):

$$\frac{1}{2} k \langle x^2 \rangle = \frac{1}{2} k_B T$$

where:

- k = spring constant of the cantilever (N/m)
- $\langle x^2 \rangle$ = mean-square displacement due to thermal noise (m²)
- $k_B = 1.380649 \times 10^{-23} \, \text{J/K}$
- T = absolute temperature (K)

AFM in liquid

A cantilever in thermodynamic equilibrium with the thermal bath at temperature T has a thermal energy (Brownian motion) that increases the elastic energy stored in the cantilever, providing random vibrations.
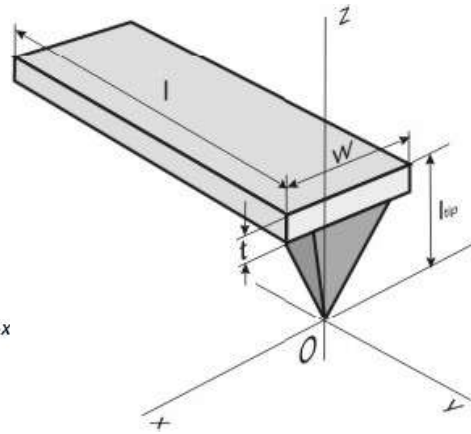To each degree of freedom, the equipartition theorem assign an average energy $\frac{1}{2} k_B T$
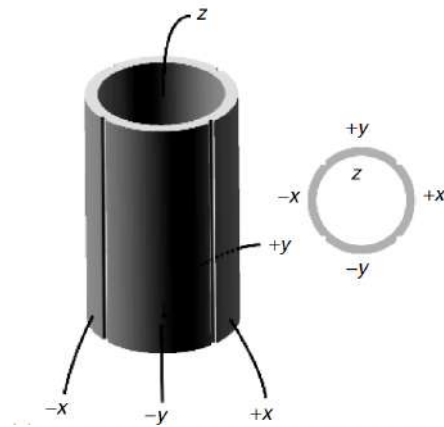
Rearranging:

$$x_{\mathrm{rms}} = \sqrt{\langle x^2 \rangle} = \sqrt{\frac{k_B T}{k}}$$

This gives the **root-mean-square amplitude** of thermal vibration.
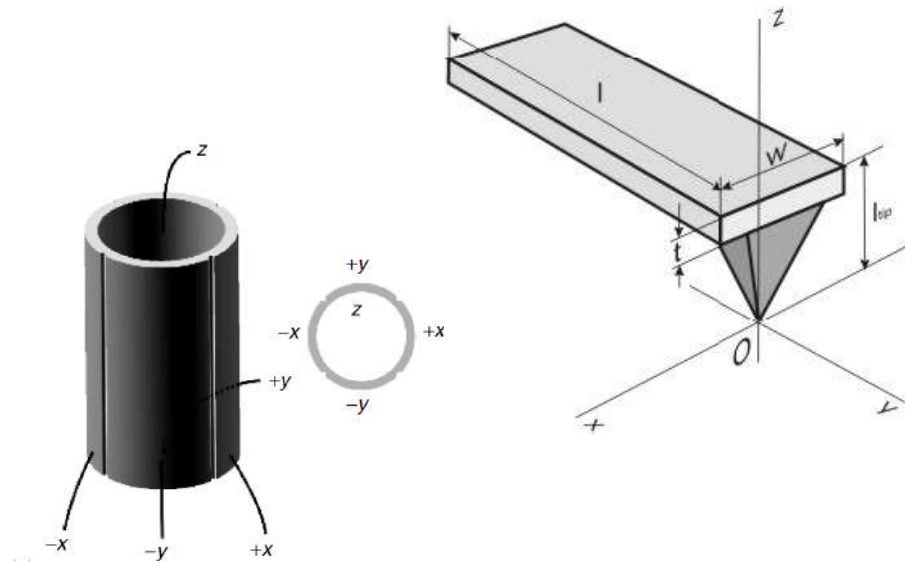
AFM in liquid

A cantilever in thermodynamic equilibrium with the thermal bath at temperature T has a thermal energy (Brownian motion) that increases the elastic energy stored in the cantilever, providing random vibrations.
To each degree of freedom, the equipartition theorem assign an average energy $\frac{1}{2} k_B T$

Suppose:

- $k = 1\,\text{N/m}$
- $T = 300\,\text{K}$

$$x_{\text{rms}} = \sqrt{\frac{1.38 \times 10^{-23} \times 300}{1}} = 2.0 \times 10^{-11}\,\text{m} = 20\,\text{pm}$$

So, a cantilever with $k = 1\,\text{N/m}$ at room temperature vibrates thermally with an RMS amplitude of about **20 picometers**.

- **Softer cantilevers** (smaller k) → larger thermal noise amplitude.

AFM in liquid

A cantilever in thermodynamic equilibrium with the thermal bath at temperature T has a thermal energy (Brownian motion) that increases the elastic energy stored in the cantilever, providing random vibrations.
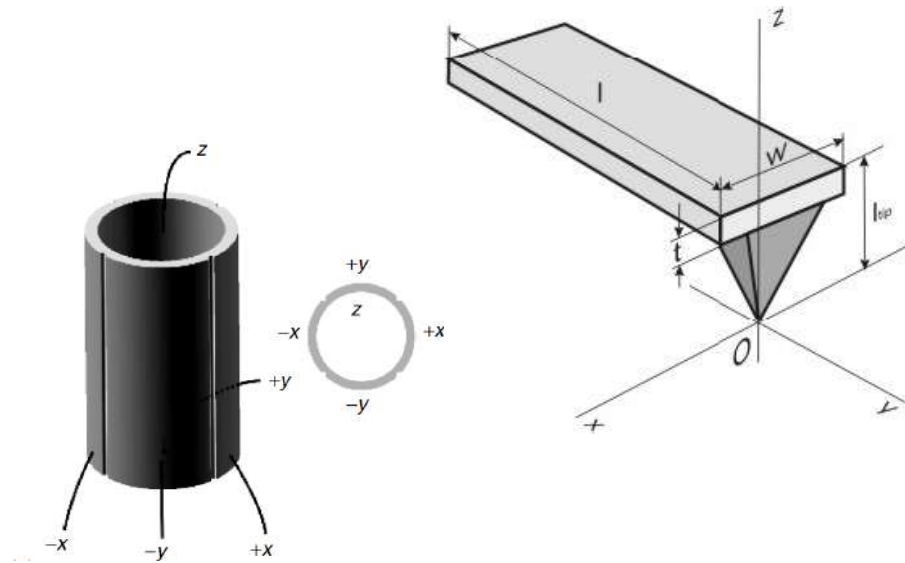To each degree of freedom, the equipartition theorem assign an average energy $\frac{1}{2} k_B T$

PSD describes how the **power (or variance)** of a signal is **distributed over frequency**.

- The **resonant frequency** and **quality factor** (Q) affect the **spectral density** of the noise, but **not** the total RMS amplitude given above.

- The **power spectral density (PSD)** of the thermal noise near resonance can be expressed as:

$$S_x(f) = \frac{4k_B T \, \gamma}{(k - m(2\pi f)^2)^2 + (2\pi f \gamma)^2}$$

where m is the effective mass and γ the damping coefficient.
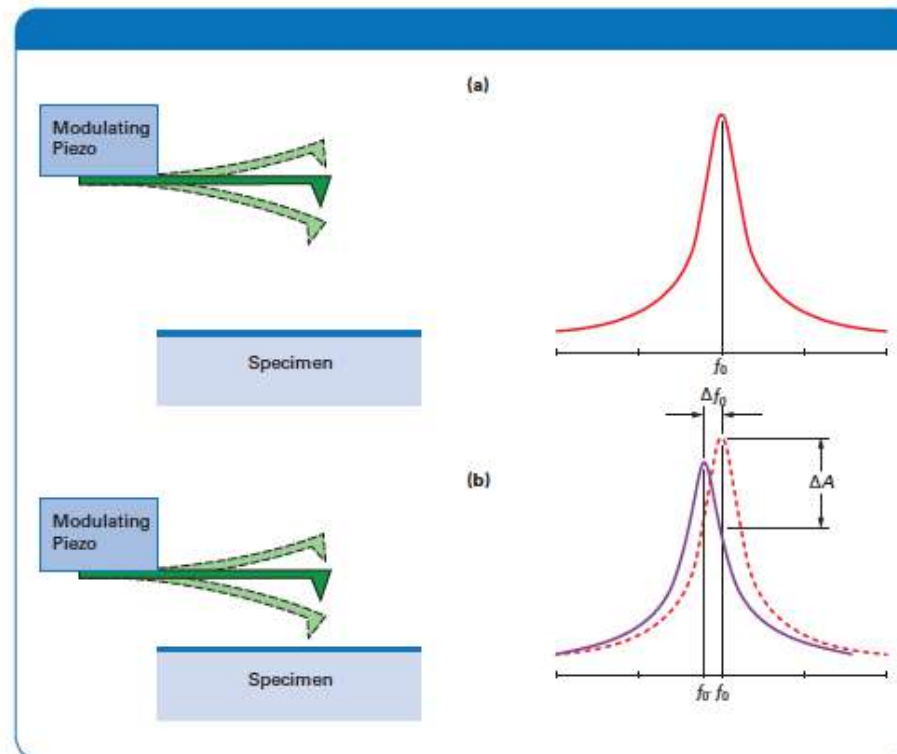
AFM tapping mode in liquid

Figure 6. Resonance curve of a TappingMode cantilever above and close to the surface. Note that the resonance shifts to lower frequencies and exhibits a drop in amplitude.

AFM tapping mode in liquid

For a harmonic oscillator (like a cantilever), the **quality factor** Q quantifies how underdamped the system is — i.e., how many oscillations occur before the energy decays significantly.

$$Q = 2\pi \frac{\text{Energy stored}}{\text{Energy dissipated per cycle}}$$

If we model the cantilever as a damped harmonic oscillator:

$$m\ddot{x} + \gamma\dot{x} + kx = 0$$

where

- m = effective mass
- k = spring constant
- γ = viscous damping coefficient (N·s/m)

The **resonant angular frequency** is:

$$\omega_0 = \sqrt{\frac{k}{m}}$$

Then, the **quality factor** is:

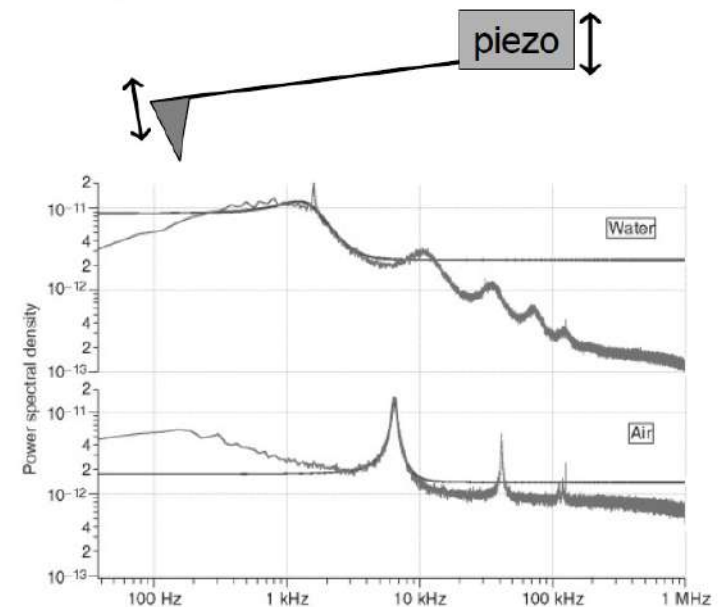$$Q = \frac{m\omega_0}{\gamma} = \frac{\sqrt{mk}}{\gamma}$$

AFM tapping mode in liquid

- **High viscous damping (large γ) → low Q**

    - Energy is lost quickly, oscillations die out rapidly.

- **Low damping (small γ) → high Q**

    - The cantilever oscillates for many cycles before energy loss.

For AFM cantilevers:

- In **vacuum**, damping is low → $Q \sim 10^3 - 10^5$

- In **air**, $Q \sim 100 - 1000$

- In **liquid**, viscous damping dominates → $Q \sim 1 - 10$

This is why AFM measurements in liquid have broader resonance peaks and lower force sensitivity.

AFM tapping mode in liquid

The **thermal noise power spectral density (PSD)** near resonance is:

$$S_x(f) = \frac{4k_B T \gamma}{(k - m(2\pi f)^2)^2 + (2\pi f \gamma)^2}$$

At resonance ($f = f_0$):

$$S_x(f_0) \propto \frac{Q}{k}$$

So, **higher Q** → **sharper and taller** resonance peak (narrowband noise),
lower Q → **broader and lower** noise peak (broadband noise).

AFM tapping mode in liquid

| Parameter	Symbol	Relation
Resonant frequency	$\omega_0 = \sqrt{k/m}$	—
Damping coefficient	γ	viscous loss
Quality factor	$Q = \dfrac{m\omega_0}{\gamma}$	inversely proportional to damping
Thermal noise amplitude	$x_{\mathrm{rms}} = \sqrt{k_B T/k}$	independent of Q
Noise PSD width	$\Delta f = \dfrac{f_0}{Q}$	narrower for higher Q

Operation modes in liquid

Contact Mode

Feedback set point chosen depending on exp. Conditions. Drawbacks: drift of free cantilever deflection photodiode signal; friction

Jumping Mode

Developed to minimize shear forces. At each pixel, a force-extension curve is perfomed. Accurate control of force; lateral motion performed out of contact. Not applicable in air due to capillary forces. Drawback: bit slow
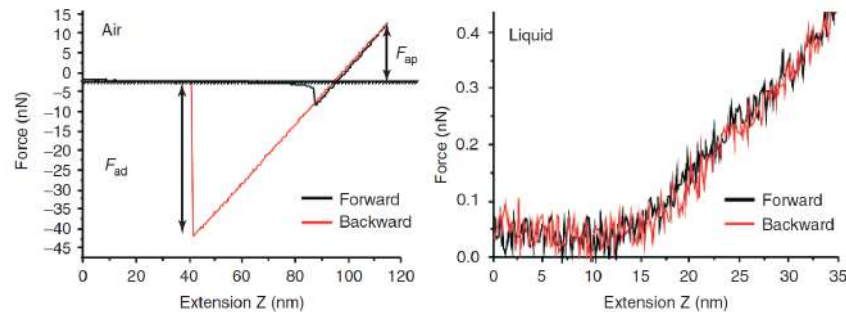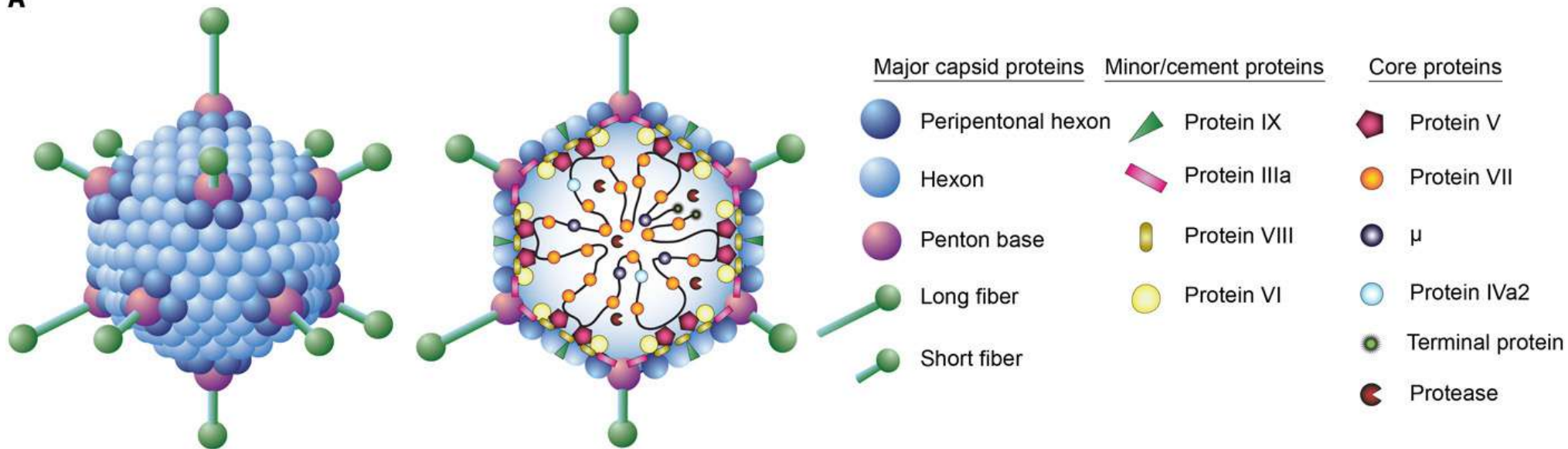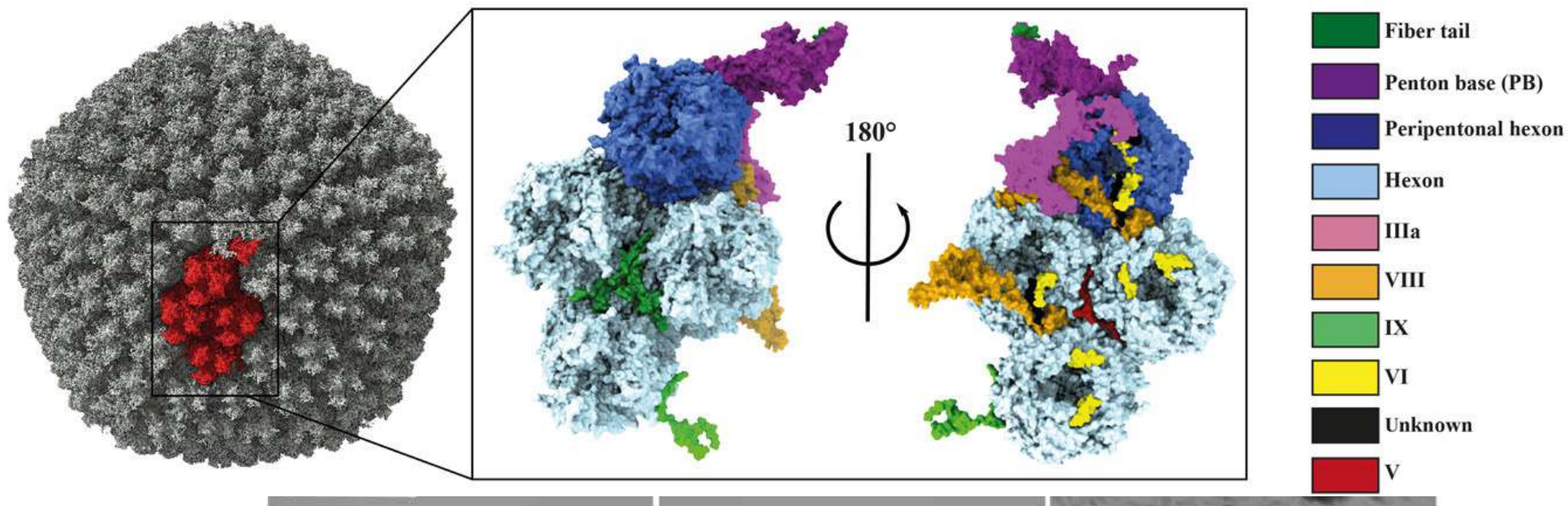

Dynamic Mode

Tapping mode: AM-AFM mode. Linear decrease of amplitude with tip-sample distance due to interaction with the surface. Reduction of amplitude in the tapping region gives the force. Comparable results, in liquid, to jumping mode, but much faster.

Atomic force microscopy of single virus shells

A

Major capsid proteins
- Peripentonal hexon
- Hexon
- Penton base
- Long fiber
- Short fiber

Minor/cement proteins
- Protein IX
- Protein IIIa
- Protein VIII
- Protein VI

Core proteins
- Protein V
- Protein VII
- μ
- Protein IVa2
- Terminal protein
- Protease

B

180°

- Fiber tail
- Penton base (PB)
- Peripentonal hexon
- Hexon
- IIIa
- VIII
- IX
- VI
- Unknown
- V

Imaging of single soft objects in liquid: jumping mode AFM

High resolution in dynamic mode requires a good control of the cantilever free oscillation, which is difficult on liquid, where the cantilever oscillation is the convolution of cantilever resonance and the mechanical resonance of the fluid cell ("forest of peaks"). As the liquid in the fluid cell changes shape, volume and composition throughout an experiment, these resonances shift, changing the tip-sample applied force.

New imaging modes needed!
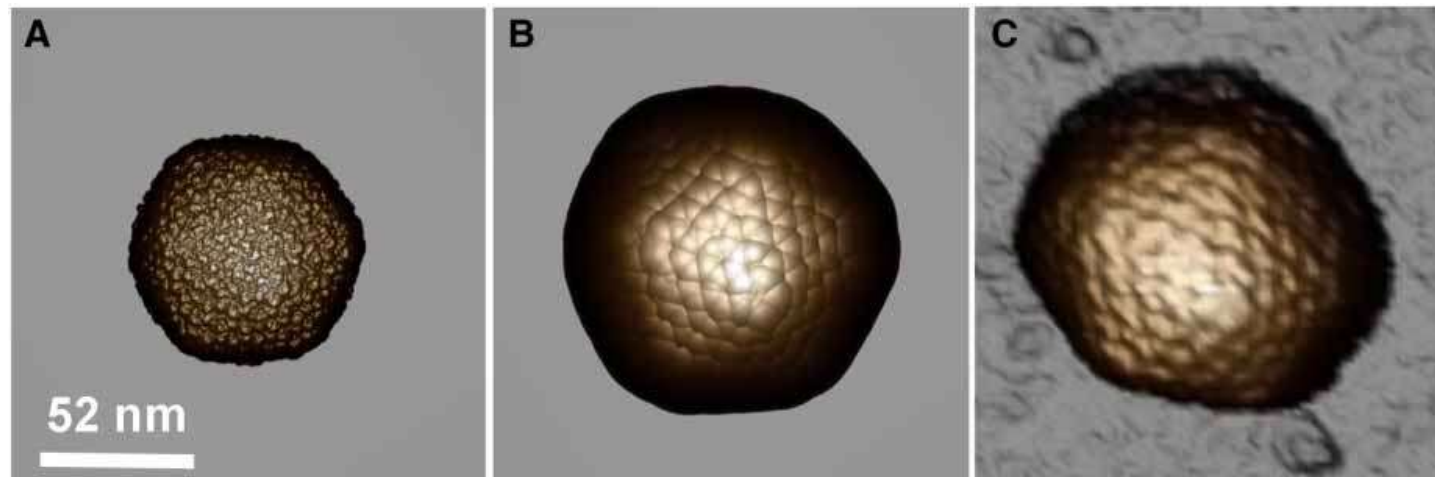
Jumping mode or "peak force" AFM

Jumping-mode AFM: quick F-Z scan at each point of the scanned area, moving laterally the tip at the farthest tip-sample distance to minimize lateral forces.

In order to reduce piezoelectric resonances, the F-Z is performed using a sinusoidal voltage wave al low frequency (few kHz, i.e. thousands F-Z curves per second) that is applied to the scanning piezoelectric.
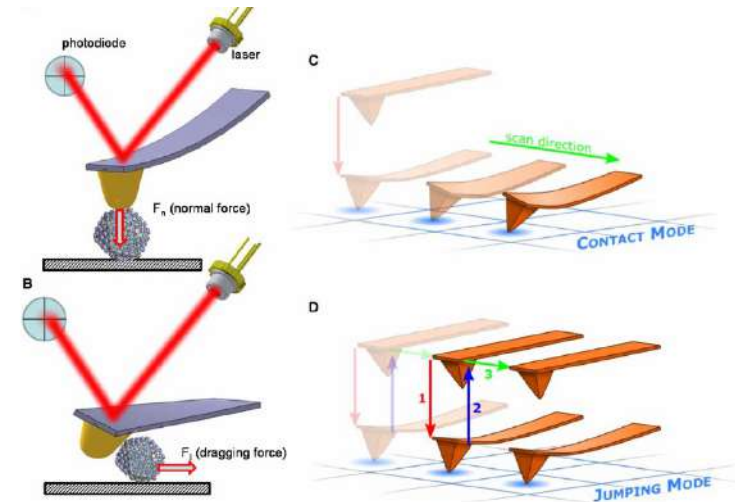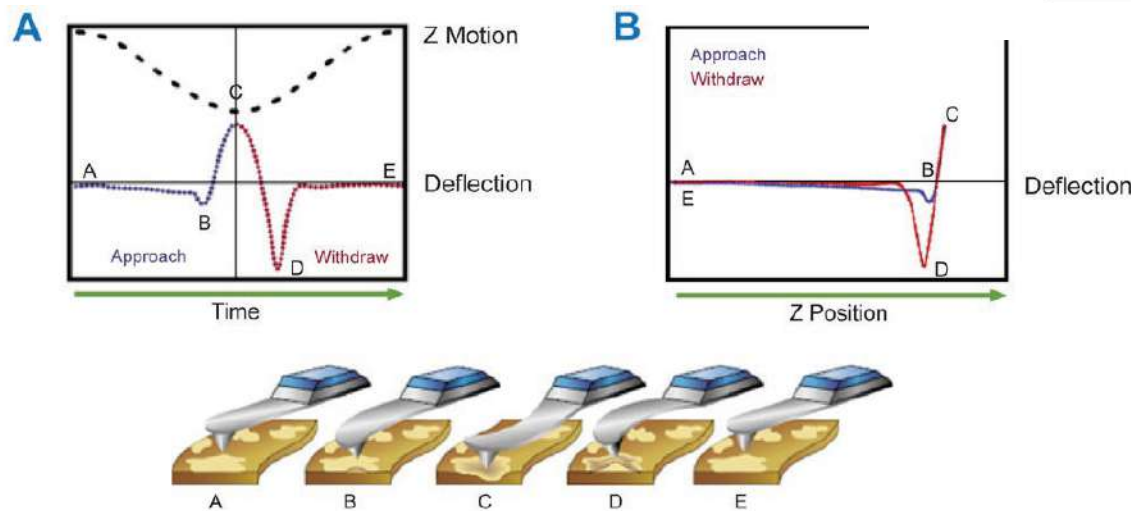

Figure 3. AFM working modes.
(A and B) The normal and lateral force concepts, respectively. (C and D) Contact and jumping modes, respectively.

When the AFM probe is brought into contact with the sample surface, the tip-sample interaction is controlled by maintaining the maximum force, or "peak force," between the tip and the sample constant

Jumping mode or "peak force" AFM

JM is particularly suitable for scanning in liquids, where the low adhesion forces allow using small Z displacement at each point. Because of the oscillation damping in liquid in amplitude modulation modes (NC, Tapping), JM although slow can give better performance. **N.B.: Dynamic modes use as feedback the oscillation amplitude. JM the cantilever deflection! Like in contact mode...easier. Is like a CM with the fine tuning of the zero interaction force**
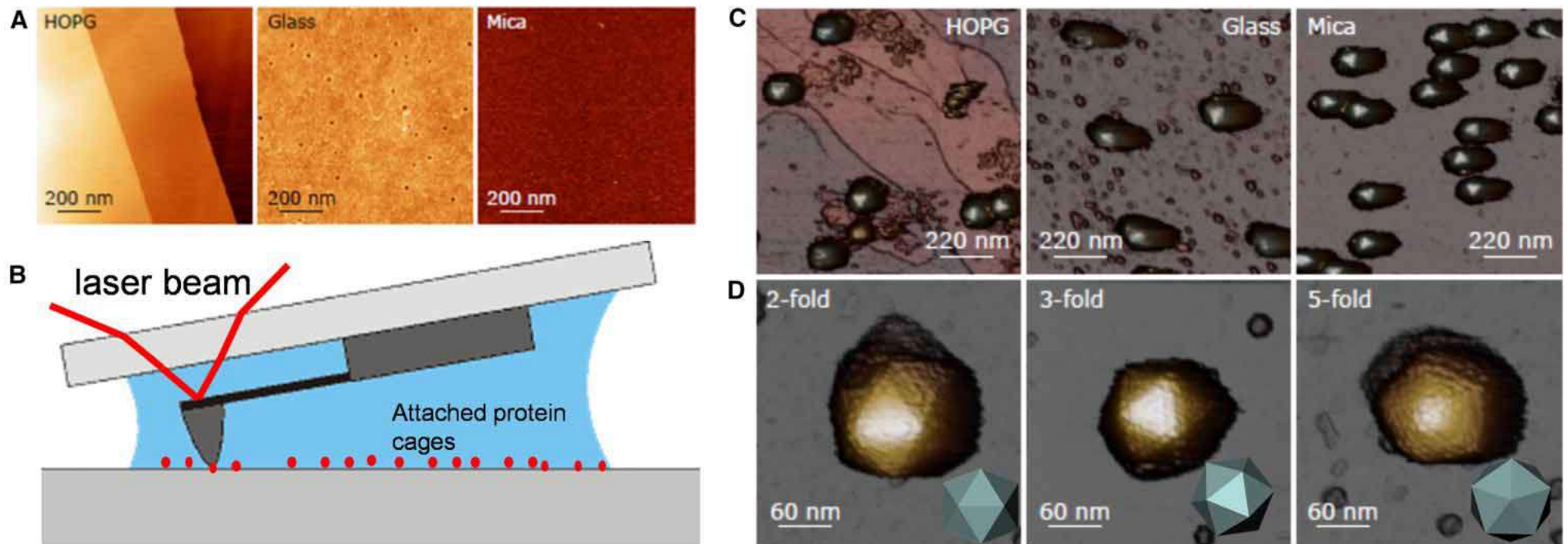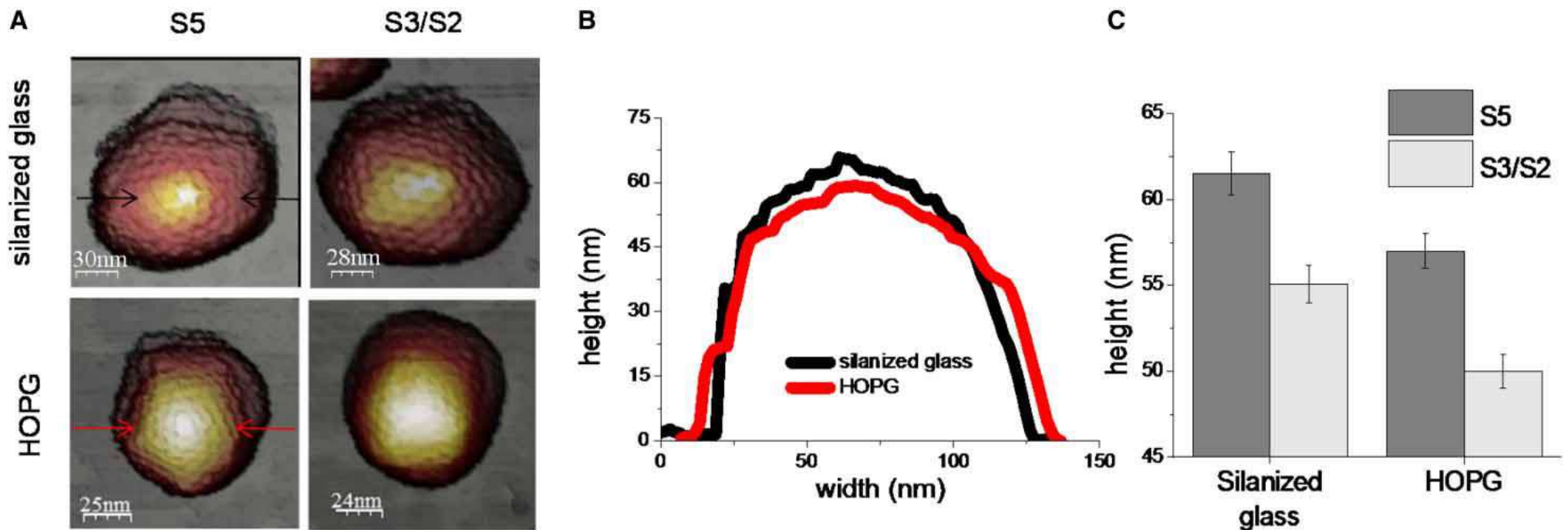

Figure 1. Attaching protein shells on surfaces.
(A) HOPG, glass, and mica bare substrates before attaching the samples. (B) Cartoon of the experimental system. Protein cages and cantilever are not in scale. (C) HAdv on HOPG, glass, and mica. (D) Individual HAdv particles showing 2-fold, 3-fold, and 5-fold symmetry axis orientations after adsorption on the surface. HAdV has a 95 nm diameter icosahedral, non enveloped capsid enclosing a ds DNA genome

Jumping mode or "peak force" AFM

JM is particularly suitable for scanning in liquids, where the low adhesion forces allow using small Z displacement at each point. Because of the oscillation damping in liquid in amplitude modulation modes (NC, Tapping), JM although slow can give better performance. **N.B.: Dynamic modes use as feedback the oscillation amplitude. JM the cantilever deflection! Like in contact mode...easier. Is like a CM with the fine tuning of the zero interaction force**

Figure 2. Protein shells collapse on the surface.

(A) P22 bacteriophage particles on glass and HOPG oriented to 5-fold and 3-/2- fold symmetry axes. (B) Comparison of topographical profiles obtained on two particles adsorbed on glass (black) and HOPG (red) obtained from A. (C) Comparison of average height of particles adsorbed at different orientations and substrates.

Jumping mode AFM
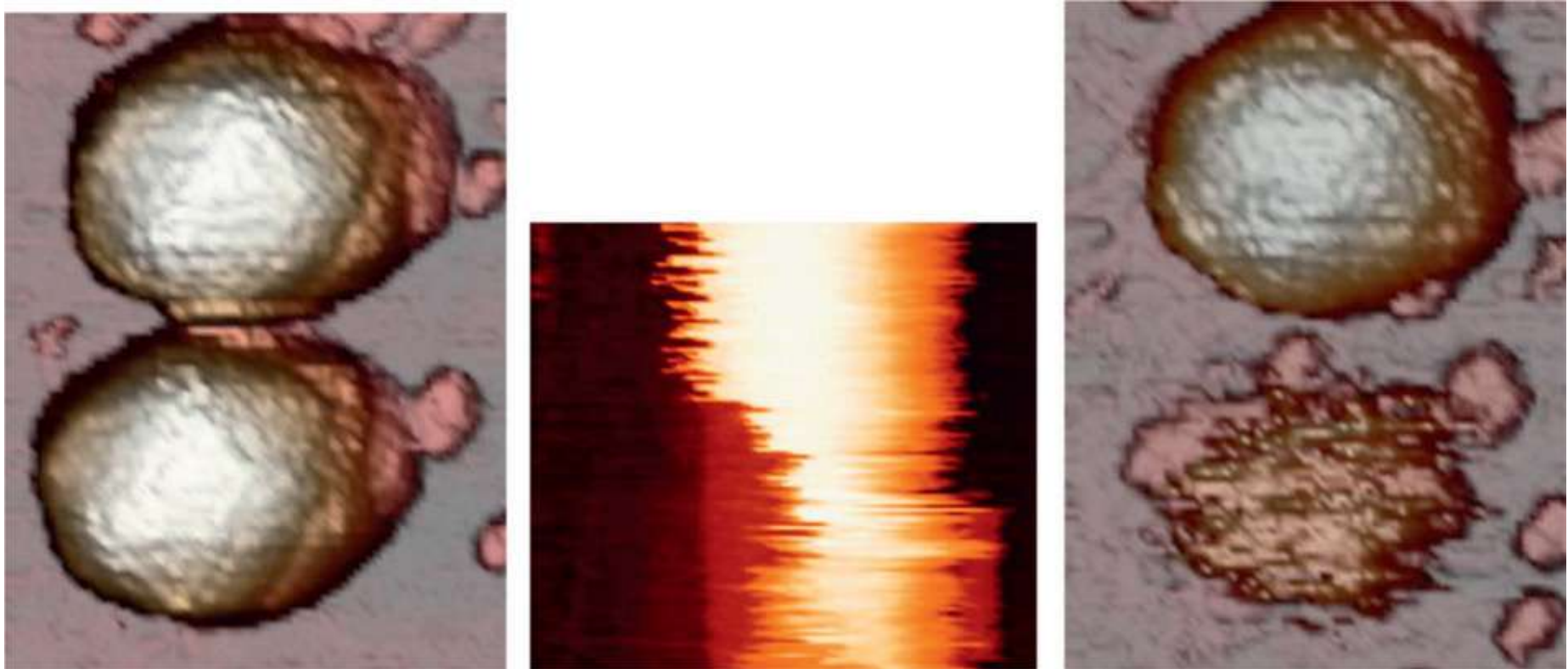
Fig. 4. (a) 250 nm × 330 nm AFM topography image of two HAdV particles acquired with JM+. (b) Time evolution (downwards) of the topography at the dashed line of figure (a). At the horizontal solid line the new algorithm is switched off, reverting to conventional JM. Notice the sudden change in the scanning profile. (c) Subsequent imaging of the same area with JM+ procedure demonstrates total destruction of the scanned virus while the other particle remains unmodified. Set point 150 pN.

under the new JM procedure, HAdV particles can be scanned for a long time without significant damage.

Jumping mode AFM
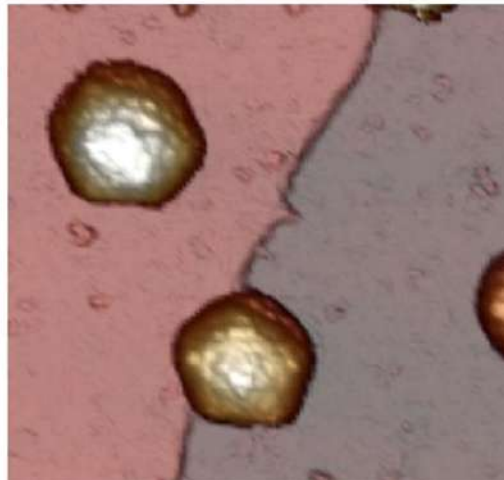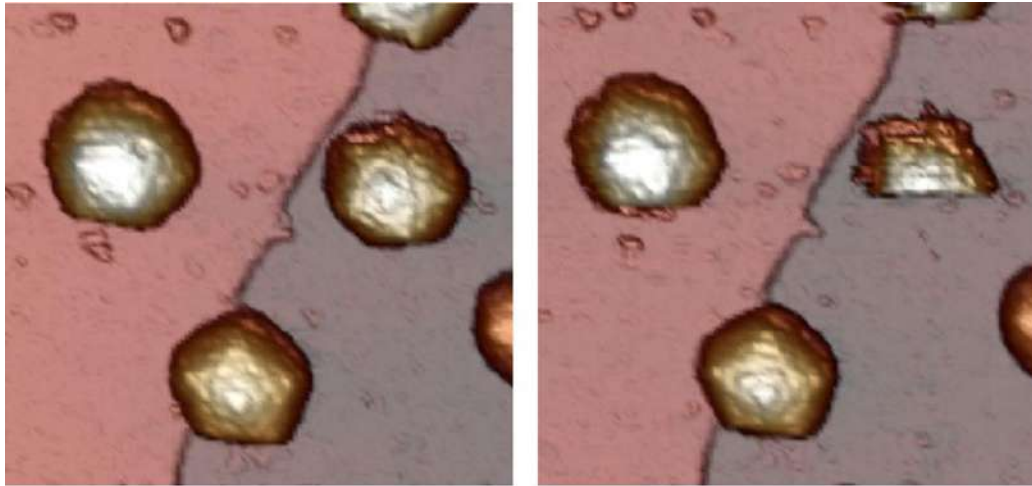
Bacteriophage T7 has an icosahedral capsid around 51nm diameter, with a triangulation number T=7, and a non-contractile tail. The shell is made of 415 copies of the gp10protein that encloses a dsDNA 40 kb in size.
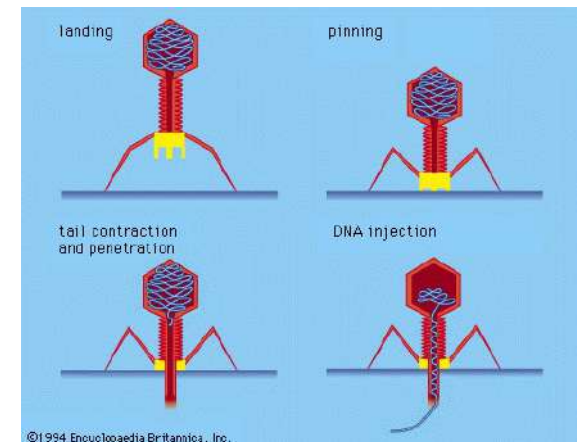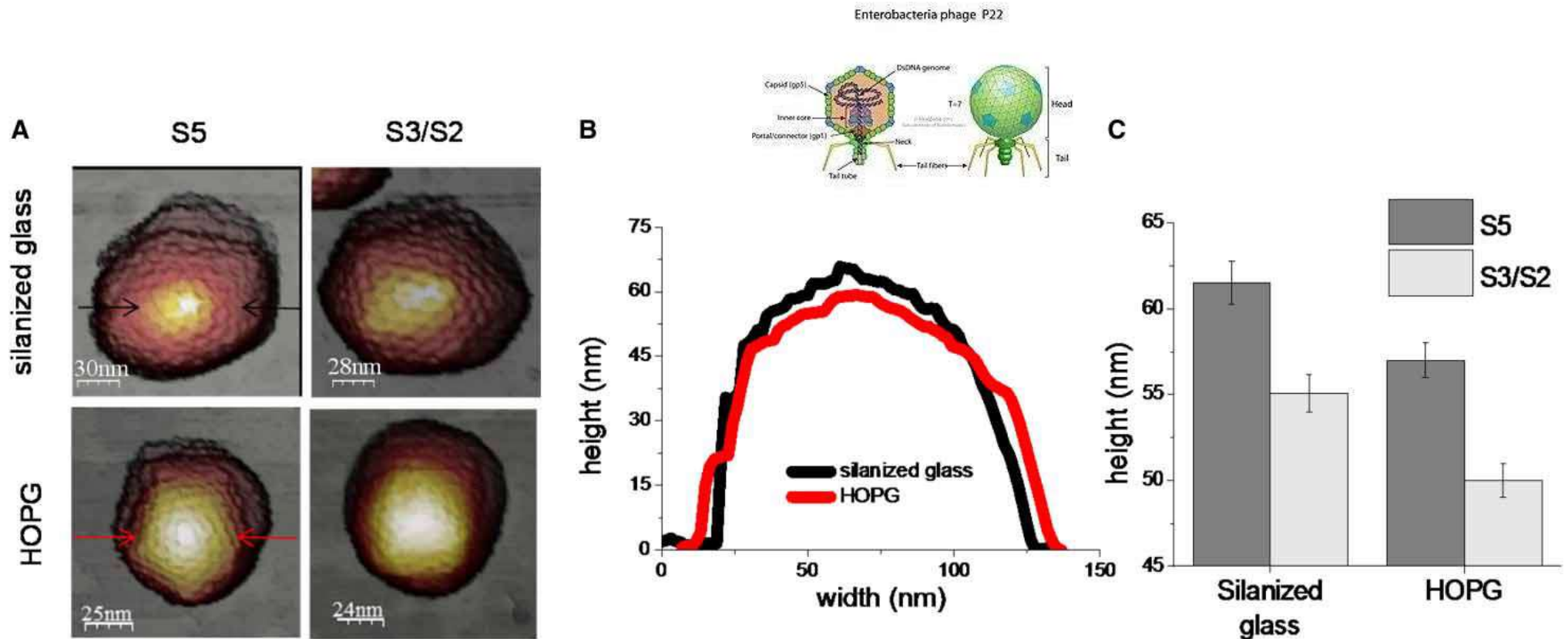

Fig. 5. (a) 500 nm × 500 nm AFM topography image acquired applying the new algorithms of bacteriophage T7. (b) When JM+ is switched off a particle is detached (circled particle in Fig. 5a). (c) Switching back to JM+ confirms that the particle has been completely removed. Set point 115 pN.

Imaging of single virus particles on different surfaces

**Figure 2. Protein shells collapse on the surface.**

(A) P22 bacteriophage particles on glass and HOPG oriented to 5-fold and 3-/2- fold symmetry axes. **(B)** Comparison of topographical profiles obtained on two particles adsorbed on glass (black) and HOPG (red) obtained from **A**. **(C)** Comparison of average height of particles adsorbed at different orientations and substrates.

Figure 5. Dilation effects in the protein shell of bacteriophage P22.
(A) The EM-1826 model of P22 bacteriophage oriented to the 2-fold symmetry axis. (B) Dilated data of (A) obtained with a tip of 10 nm in diameter by using the dilation algorithm of the WSxM software. (C) AFM image of a single P22 bacteriophage oriented to the 2-fold symmetry axis. The cartoon of (D) indicates the dilation as a function of the tip size: black, red, and blue curves are the topographical profiles obtained with tips of 0.5, 10, and 15 nm in diameter, respectively.
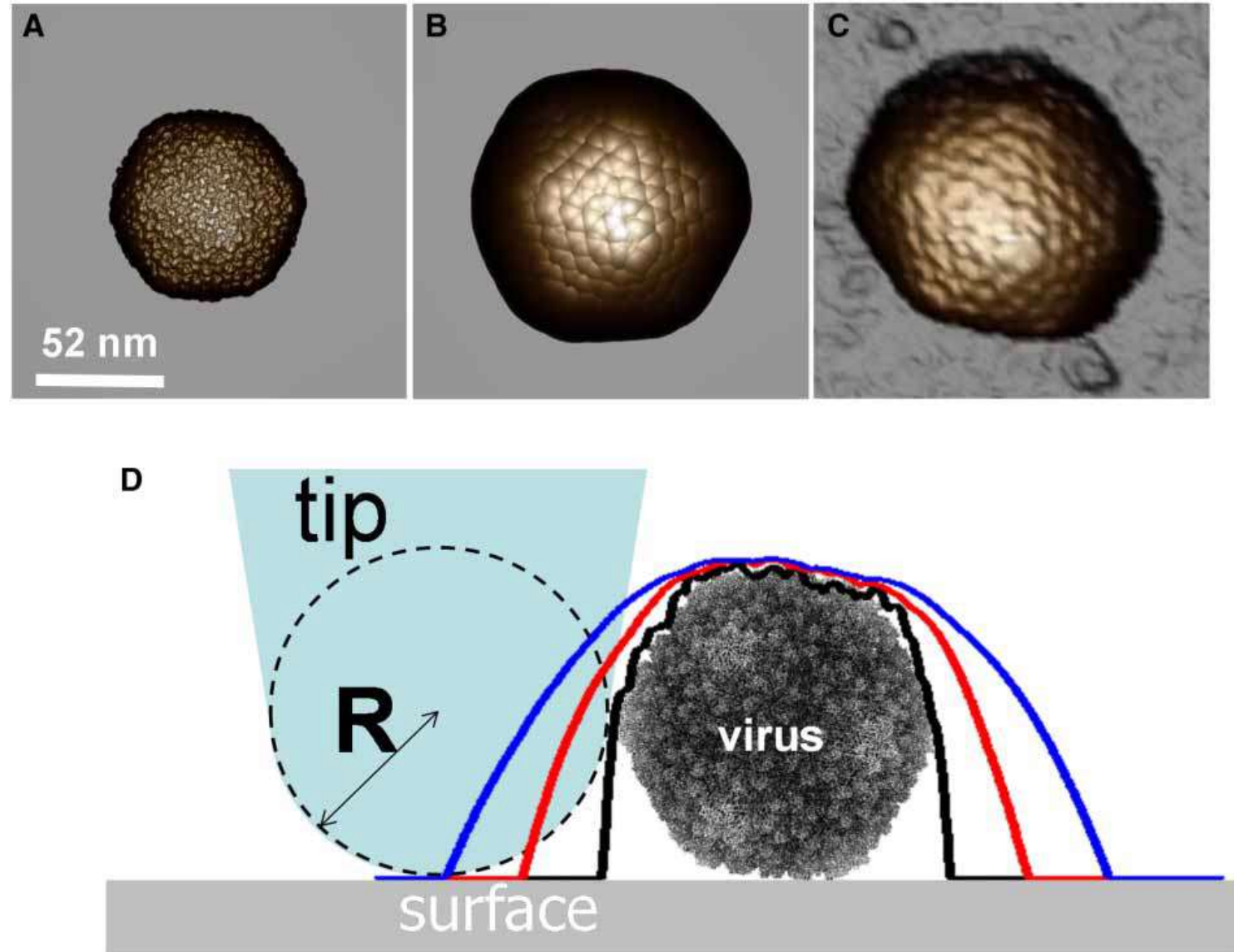
Nanoindentation
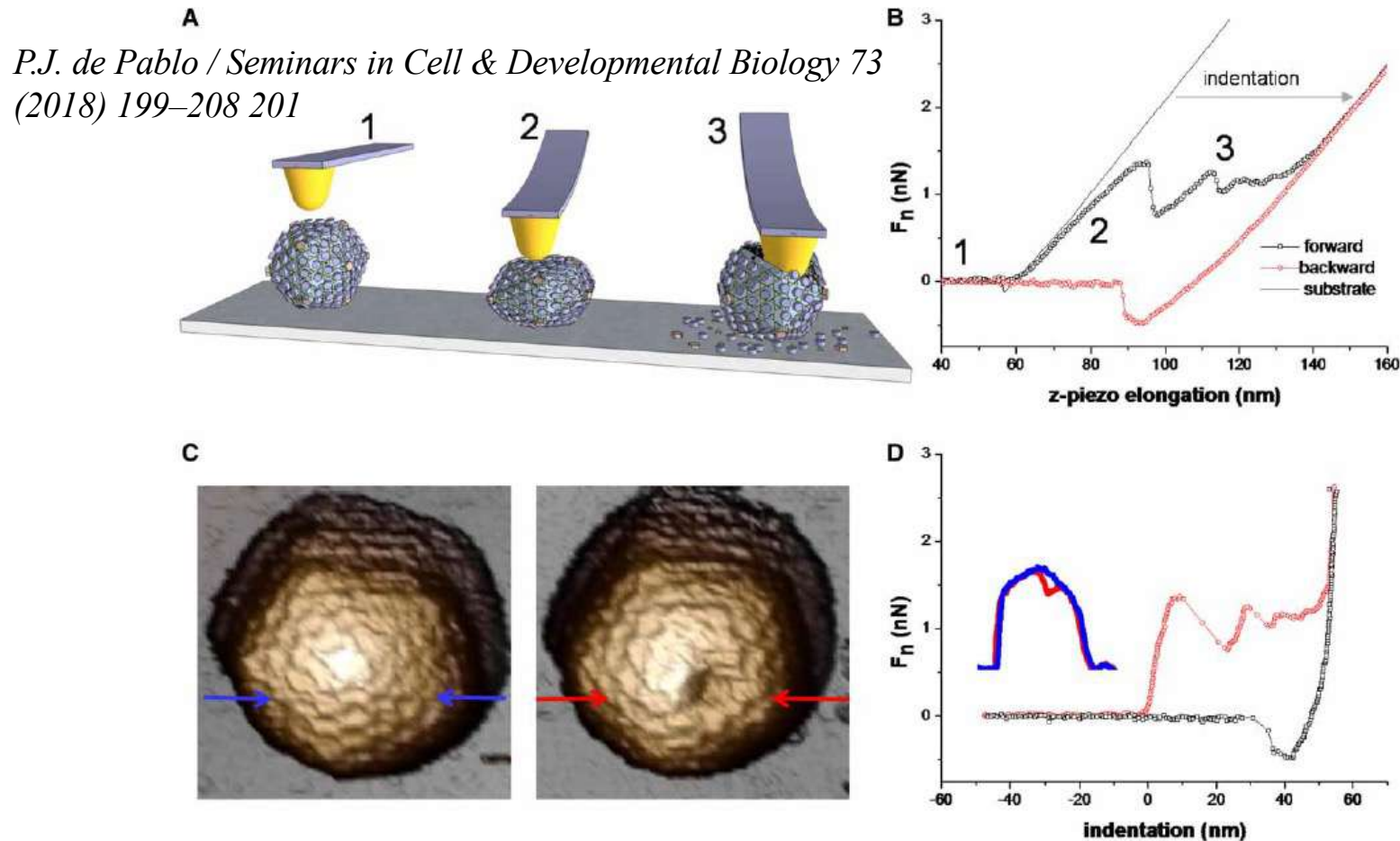
The subtraction of sample from substrate curves allows isolating the deformation of the cage (Figure 6D)

Figure 6. Single indentation assay.

Stiffness or spring constant: obtained by fitting the elastic part from 0 to 8 nm (k = 0.18 N/m);
breaking or yield force: force value when the elastic regime f nishes at 8 nm (Fb = 1.4 nN),
critical indentation δc :deformation of the virus when it breaks (8 nm).
Thin shell theory relates the protein shell stiffness with the Young' s modulus as k Et2=R , where t is the thickness of the shell and R is its radius
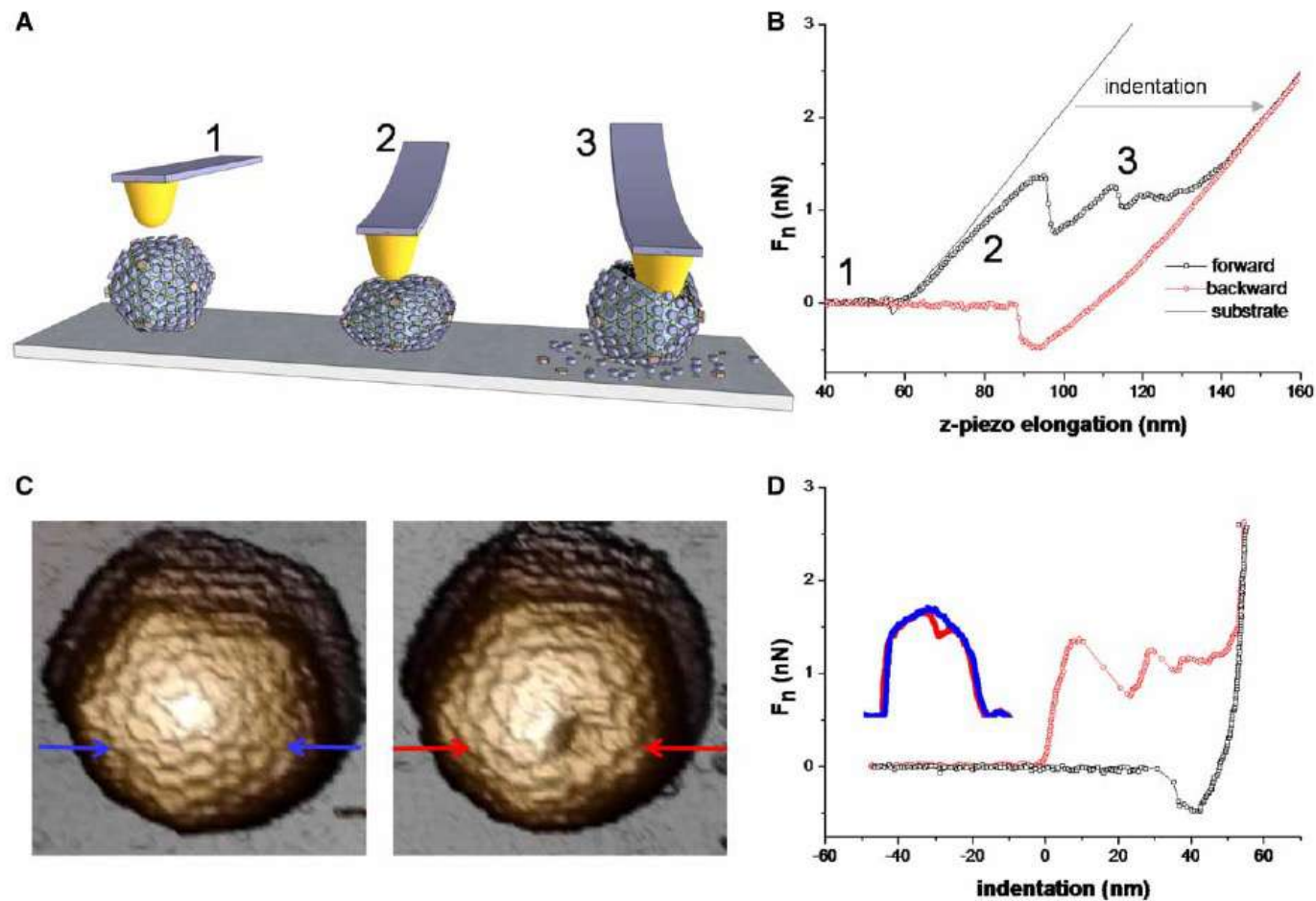
Figure 6. Single indentation assay.

The area enclosed between forward and backward curves from indentation 0 up to 8 nm is the energy used to break the cage. In this case, it is about 8.8 nm x nN, i.e. 8.8×10^{-18} J or $2141 k_B T$, which approaches the order of magnitude of the total energy for assembling all the proteins

The precise control of nanoindentation permits access to the inner cargo of protein cages. For instance, the consecutive application of nanoindentaion cycles in human adenovirus cracks open the shell in a controlled fashion to probe the mechanical properties of the core. These mechanical properties are related with the condensation state of dsDNA.
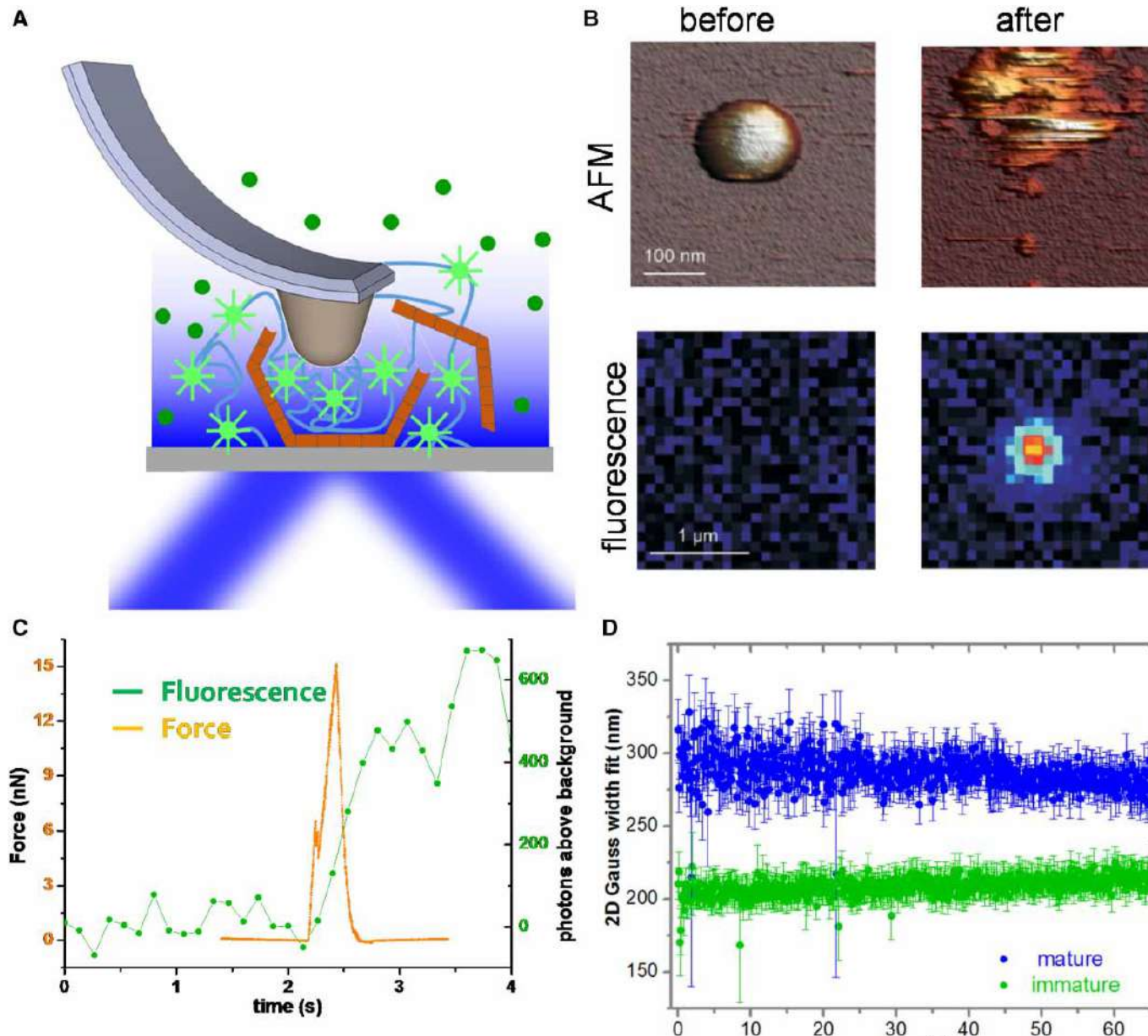
Figure 8. AFM/fluorescence combination for monitoring mechanical unpacking.
(A) Sketch of AFM/fluorescence combination for monitoring the access of YOYO-1 to released DNA. (B) AFM and fluorescence data of an HAdv particle before and after releasing DNA. (C) Simultaneous force (orange) and fluorescence (green) data during a nanoindentation experiment that disrupted the particle and released DNA. (D) Evolution of the fluorescence signal along time after particle disruption for mature (blue) and immature (green) particles (adapted from ref. [60]).

ATOMIC FORCE MICROSCOPY
Imaging in Biology_2
Examples

Single molecule imaging 1

Myosine V walking on actin filaments
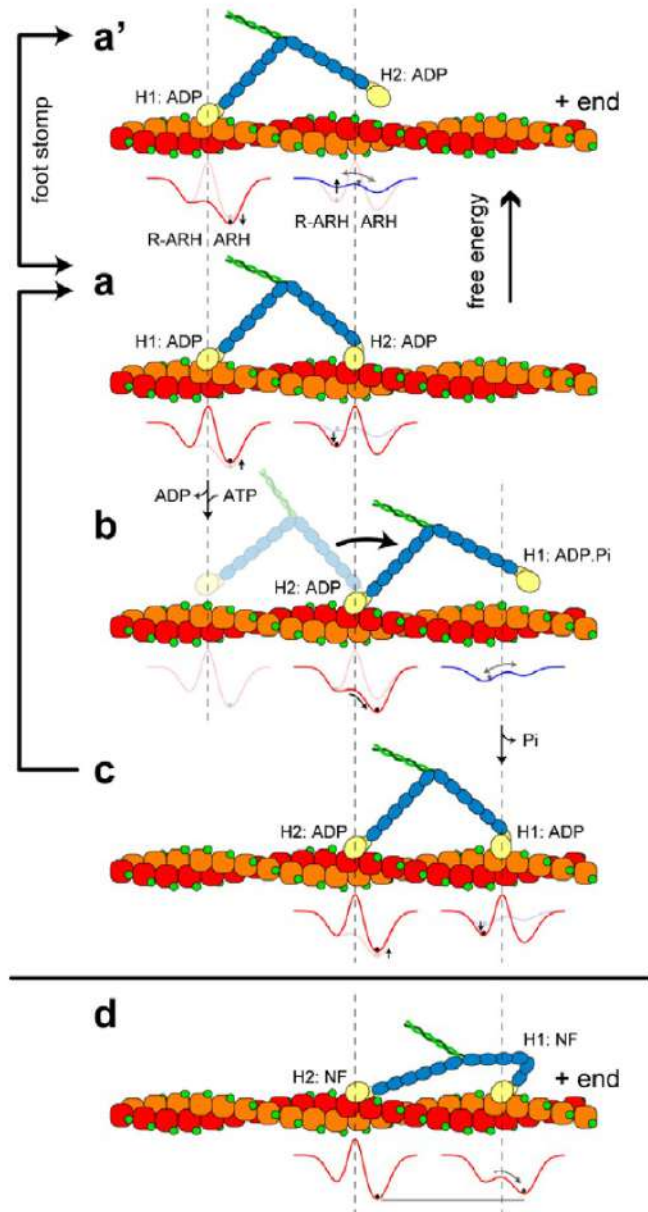
The molecular motor Myosin V walks along actin filaments in a "hand-over-hand" fashion, powered by ATP hydrolysis.
Prior work (optical tracking, fluorescence microscopy, etc.) had inferred stepping behavior, but imaging the actual molecular structure in motion had been elusive.

In dynamic HS-AFM the molecule itself is visualized while working and moving on its biological track, providing concomitant structural and dynamic data: not only did the observation confirm the hand-over-hand walking mechanism of myosin-V, it did reveal that the power stroke of this motor is driven by intramolecular mechanical tension

Myosine V walking on actin filaments

Each head of the double-headed myosin hydrolyzes ATP into ADP and inorganic phosphate (Pi). The ATPase rate is very low when myosin is alone but is markedly accelerated by its interaction with actin, where the chemical energy liberated by ATP hydrolysis is converted into mechanical work.
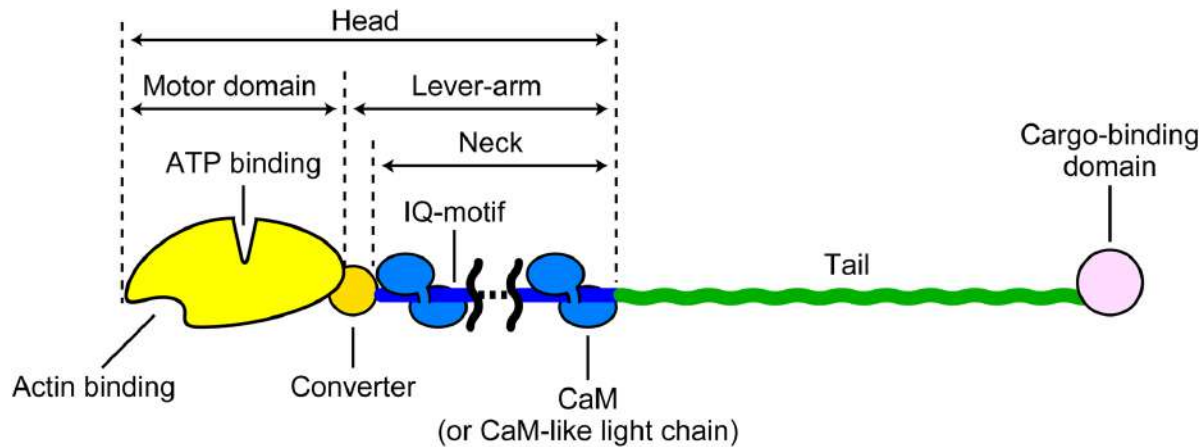
Myosine V walking on actin filaments

Using single-molecule fluorescence microscopy and optical-trap nanometry it has been shown that M5 moves along actin filaments toward the plus end in a "hand-over-hand" manner, advancing 36 nm per ATP hydrolysis cycle.

The 36 nm stride corresponds to a half pitch of the right-handed, double-helical structure of an actin filament, and, therefore, M5 moves approximately on a plane.
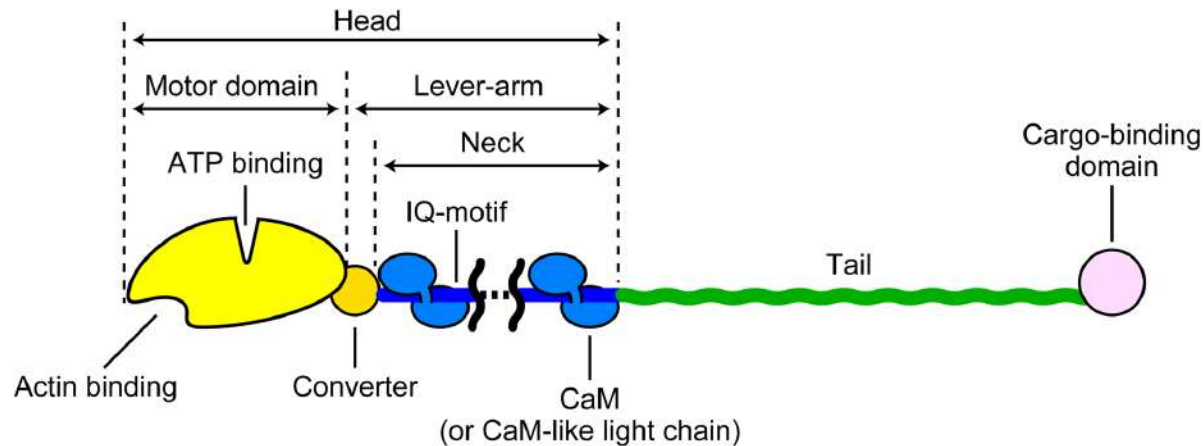

The mechanism underlying the alternate steps was suggested to arise from asymmetric kinetics of ADP dissociation from the two heads; ADP dissociation at the trailing head is more accelerated than at the leading head and/or ADP dissociation at the leading head is decelerated.

Myosine V walking on actin filaments

Using single-molecule fluorescence microscopy and optical-trap nanometry it has been shown that M5 moves along actin filaments toward the plus end in a "hand-over-hand" manner, advancing 36 nm per ATP hydrolysis cycle.

The 36 nm stride corresponds to a half pitch of the right-handed, double-helical structure of an actin filament, and, therefore, M5 moves approximately on a plane.
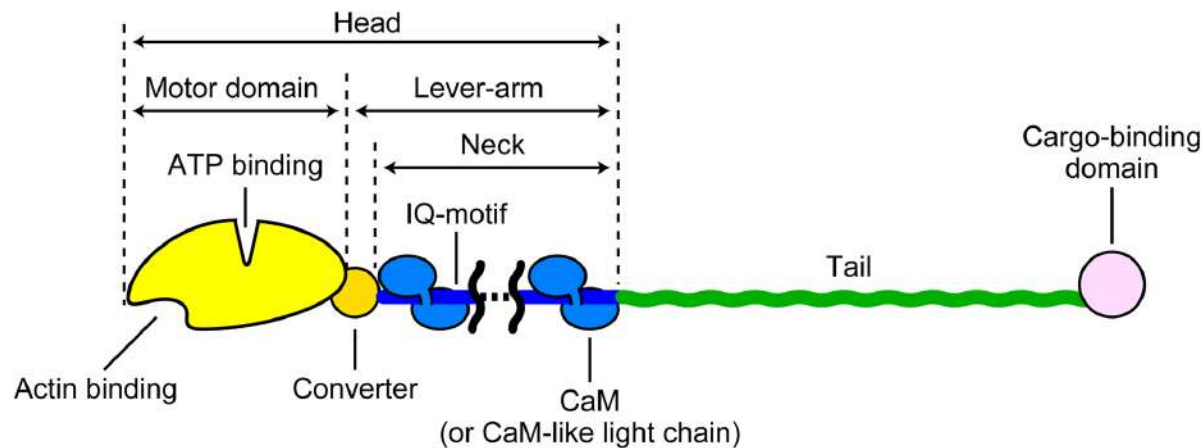
Actin binding and ATP binding sites are interacting

However, despite numerous and extensive studies, the heart of the motor mechanism, that is, how the tension for the forward step is generated in the molecule, coupled with the ATPase reaction, and how the energy liberated by ATP hydrolysis is used, has remained elusive.

Myosine V walking on actin filaments
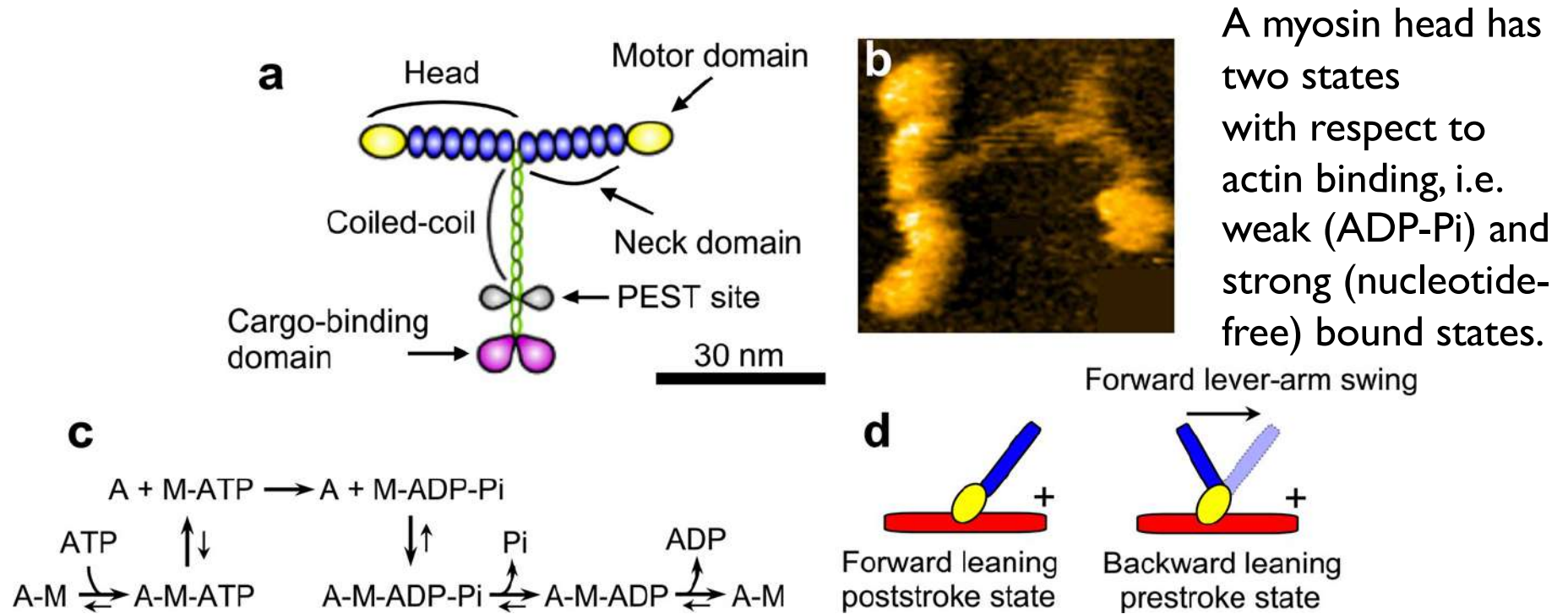
A myosin head has two states with respect to actin binding, i.e. weak (ADP-Pi) and strong (nucleotide-free) bound states.

The nucleotide-free head tightly bound to actin detaches from the actin immediately after binding to ATP, quickly followed by hydrolysis of the bound ATP to ADP−Pi.
When the ADP−Pi bound head is attached to actin, the bound Pi dissociates from the head, which is followed by the formation of a strongly bound tertiary complex A−M−ADP (A and M denote actin and myosin, respectively) and then by ADP dissociation, completing one ATPase cycle.
The main role of actin in the ATPase reaction is to accelerate the otherwise very slow Pi and ADP dissociation from a myosin head.

Energy in the cell: ATP

In the cell reactions that require energy are associated with ATP hydrolysis (hydrolysis= breaking down). ATP hydrolysis is an exothermic reaction, and the energy generated can be used to drive a non-spontaneous reaction.

Adenosine Tri/Di/Mono phosphate

ATP $\mapsto$ ADP + P
(ΔH = -30 kJ/mol)

ATP $\mapsto$ AMP + PP$_i$
(ΔH =-30 kJ/mol)

phosphodiester bonds have a large energy of hydrolysis (about 30 kJ/mol)

ATP

ADP

AMP
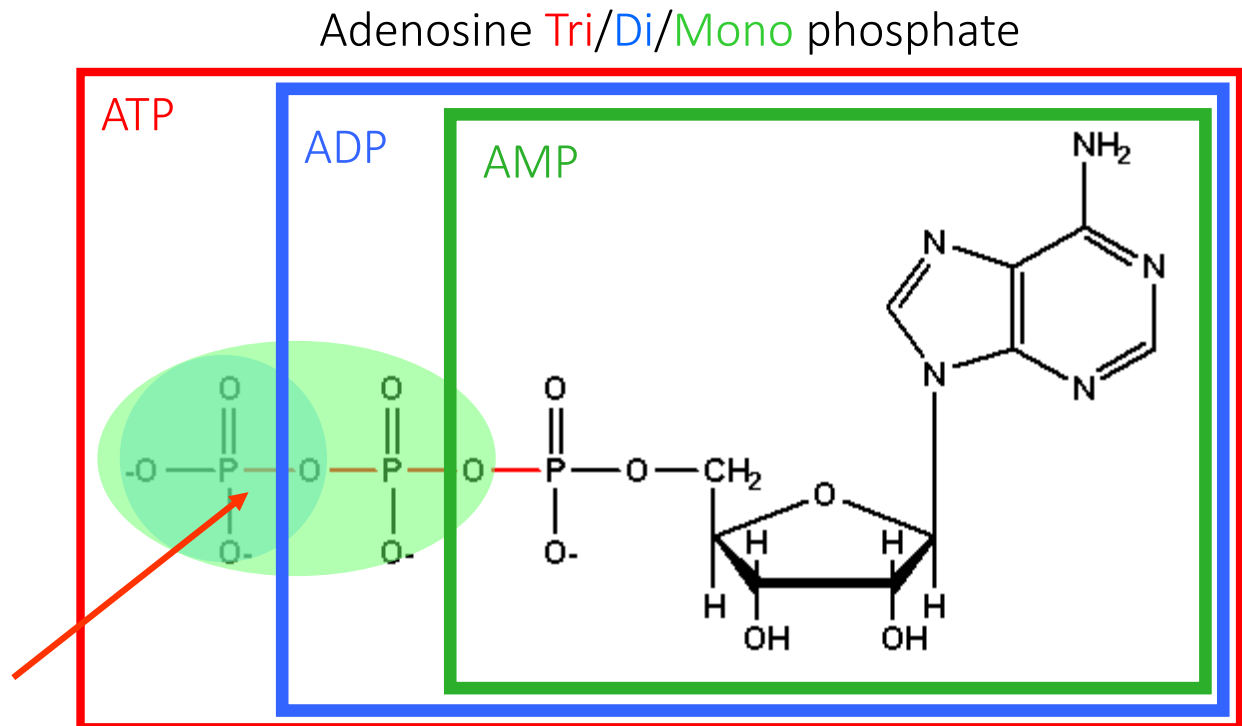
Energy production: accumulation of ATP

Energy consumption: breaking down (hydrolysis) of ATP $\mapsto$ ADP or AMP

Myosine V walking on actin filaments
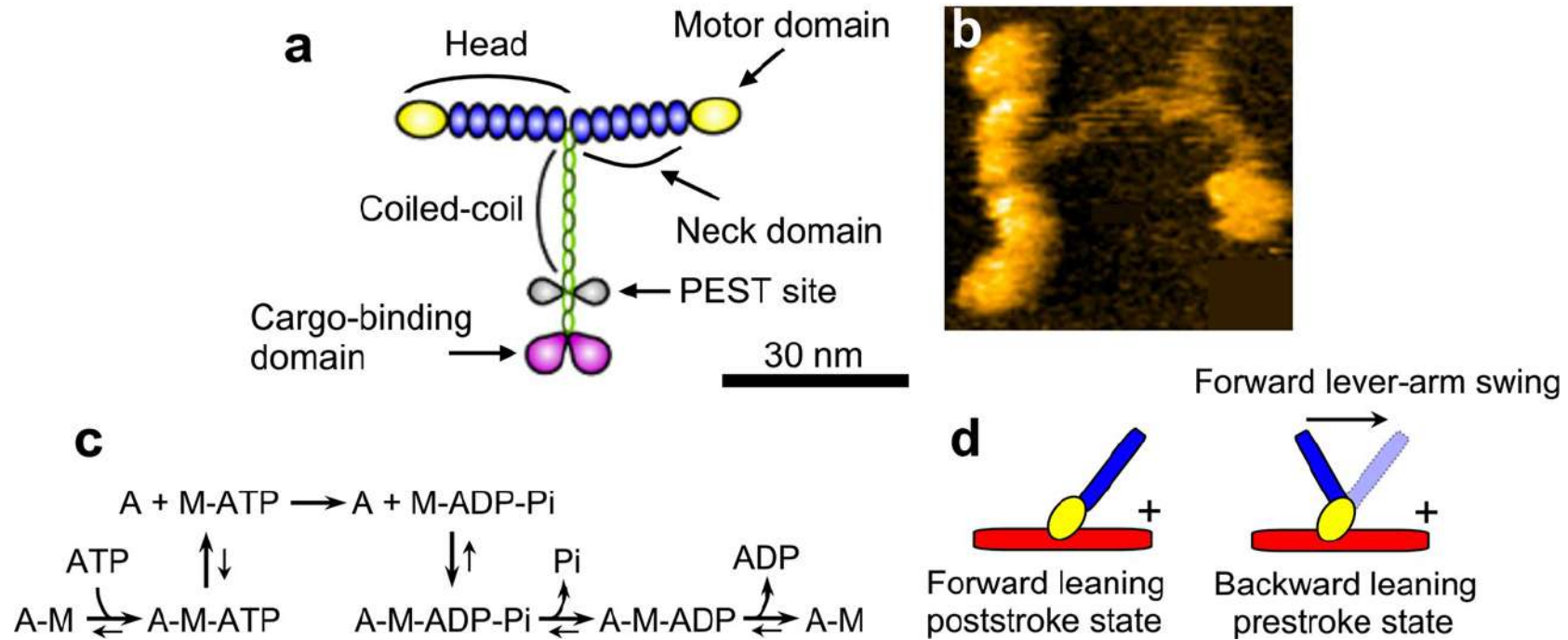
The key idea in the prevailing view on the chemo-mechanical coupling in myosin motility, which has been mainly derived from muscle myosin studies, is that the myosin head is supposed to take two different conformations, prestroke and poststroke conformations corresponding to different angles between the motor domain and the neck domain (often called "lever-arm"), depending on the nucleotide states

(a)

Myosin-coated bead

Actin cables

Chloroplast

+ end
+ end

Cell wall

Coverslip

(b)

Fluorescently labeled actin filament

Myosin

- end

- end

Coverslip

Fig. 4 Schematics showing in vitro motility assay systems for actomyosin. **a** Myosin-coated bead assay. The myosin-coated fluorescent beads are subjected to the polar arrays of actin cables naturally formed on chloroplastd of the alga *Nitella*, and movement of the beads are observed under a florescent microscope. **b** Actin filament gliding assay. Myosin molecules are attached to the surface of a nitrocellulose-coated coverslip and gliding motion of the fluorescently labeled actin filaments are observed under a fluorescence microscope
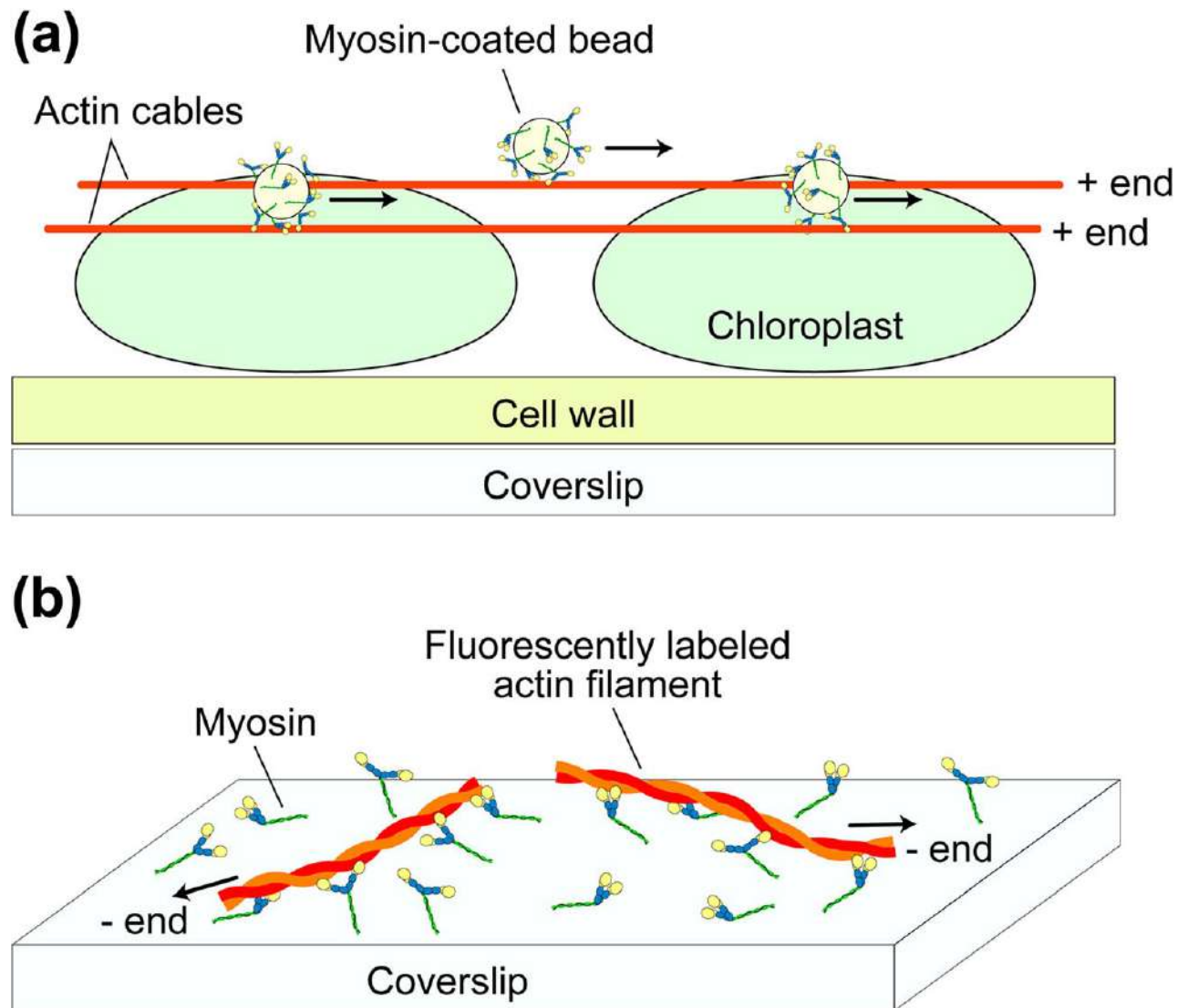
Myosine V walking on actin filaments

a Head / Motor domain / Coiled-coil / Neck domain / PEST site / Cargo-binding domain / 30 nm

b

c

$$A + M\text{-}ATP \longrightarrow A + M\text{-}ADP\text{-}Pi$$

$$A\text{-}M \overset{ATP}{\underset{}{\rightleftharpoons}} A\text{-}M\text{-}ATP \qquad A\text{-}M\text{-}ADP\text{-}Pi \overset{Pi}{\underset{}{\rightleftharpoons}} A\text{-}M\text{-}ADP \overset{ADP}{\underset{}{\rightleftharpoons}} A\text{-}M$$

d Forward lever-arm swing

Forward leaning poststroke state / Backward leaning prestroke state
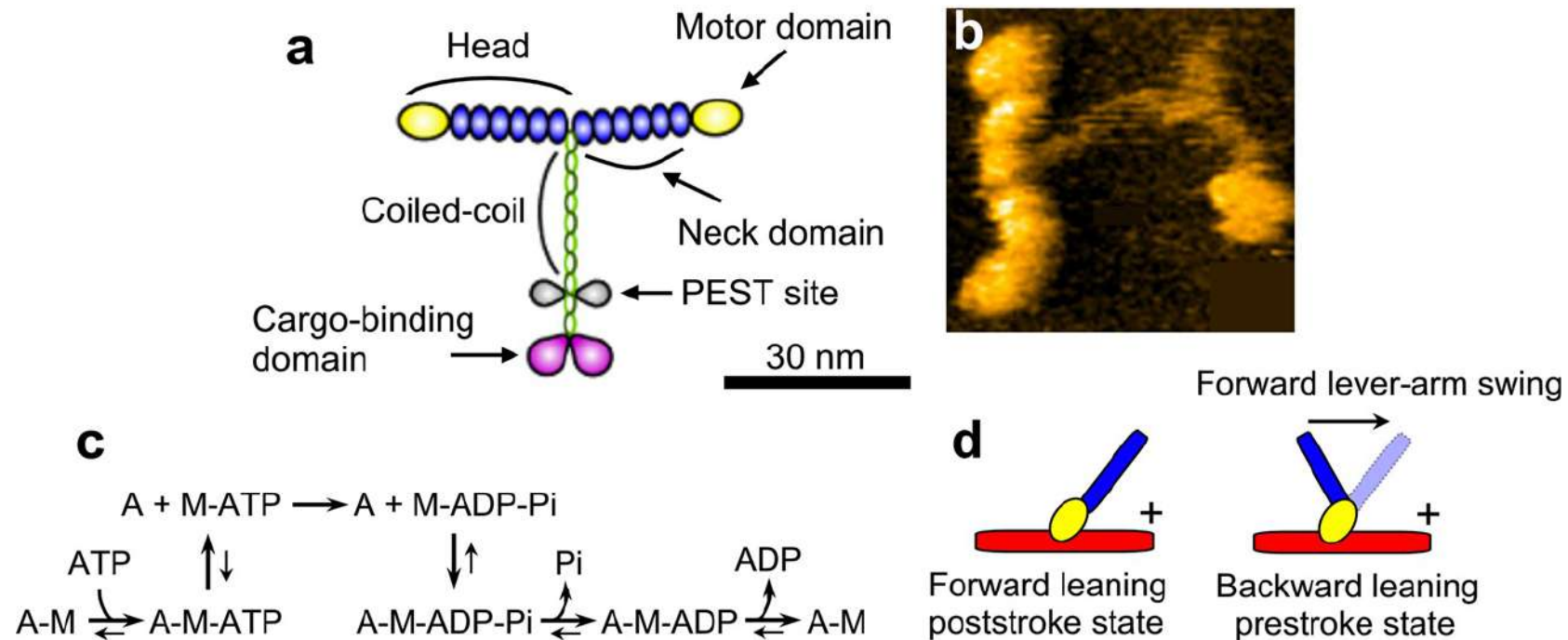
High-speed atomic force microscopy (HS-AFM), allow video-recording the structure and dynamics of functioning biomolecules at single-nanometer resolution, without disturbing their function. It helped to discover that the tension responsible for forward movement can be generated without any chemical transition, meaning that no chemical energy input is required for the tension generation. Moreover, the lever-arm swing (powerstroke) by the leading head spontaneously occurs when the trailing head detaches, thus demonstrating that no chemical energy input is required for the lever-arm swing either.

Myosine V walking on actin filaments

Video imaging by high-speed AFM has been applied to capture the dynamic behaviour of myosin V (two headed motor that functions as cargo transporter in cells) translocating along an acting filament. Moves hand-over-hand, 36 nm per ATP hydrolysis

Supplementary Figure 1 | Schematic of assay system for HS-AFM imaging (not scaled). A mica surface was fully covered with biotin-containing lipid bilayers. Streptavidin molecules (green circles) were partially deposited on the substrate. Biotinylated actin filaments were immobilised on the bilayer surface through streptavidin molecules. M5-HMM was deposited on the lipid bilayers. All imaging experiments were performed in the tapping mode using a laboratory-built high-speed AFM apparatus[5,6].

A positively charged lipid in the mixed lipid bilayer was necessary to assure weak interaction with Myosine and translocation along the actin filament

N. Kodera, D. Yamamoto, R. Ishikawa, T. Ando *Nature* **468**, 72 (2010)
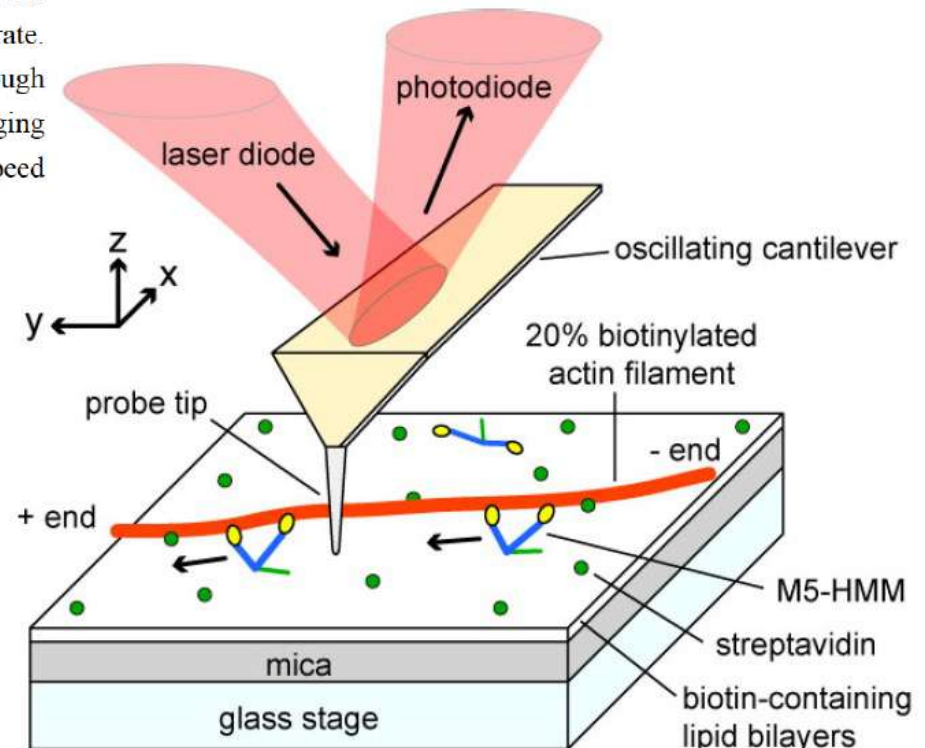
Myosine V walking on actin filaments
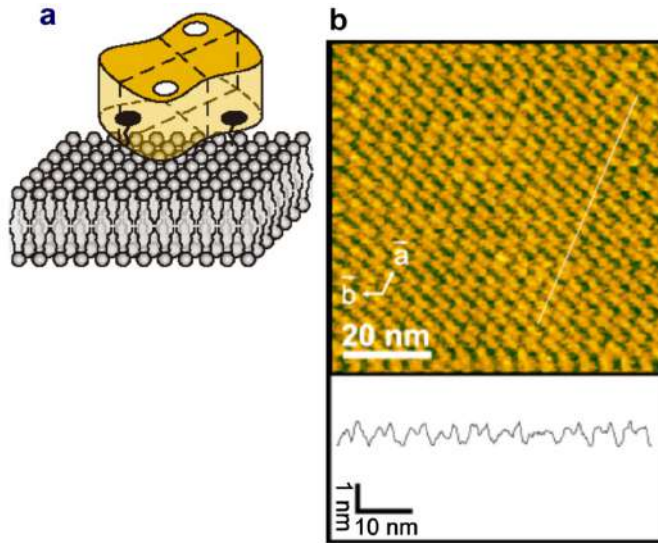
Streptavidin is a homo tetramer with dihedral D2 symmetry. Importantly, it is not favorable to nonspecific binding of many proteins, while each subunit has a high affinity biotin binding site. Streptavidin 2D crystals are easily formed onmthe surface of a fluid SLB containing biotin-lipid.

On the SLBs, two of the four biotin binding sites of streptavidin face the lipid bilayer and are occupied by biotin, whereas the other two are exposed to the aqueous environment and accessible. Therefore, biotinylated samples can be specifically immobilized on the surface of streptavidin 2D crystals
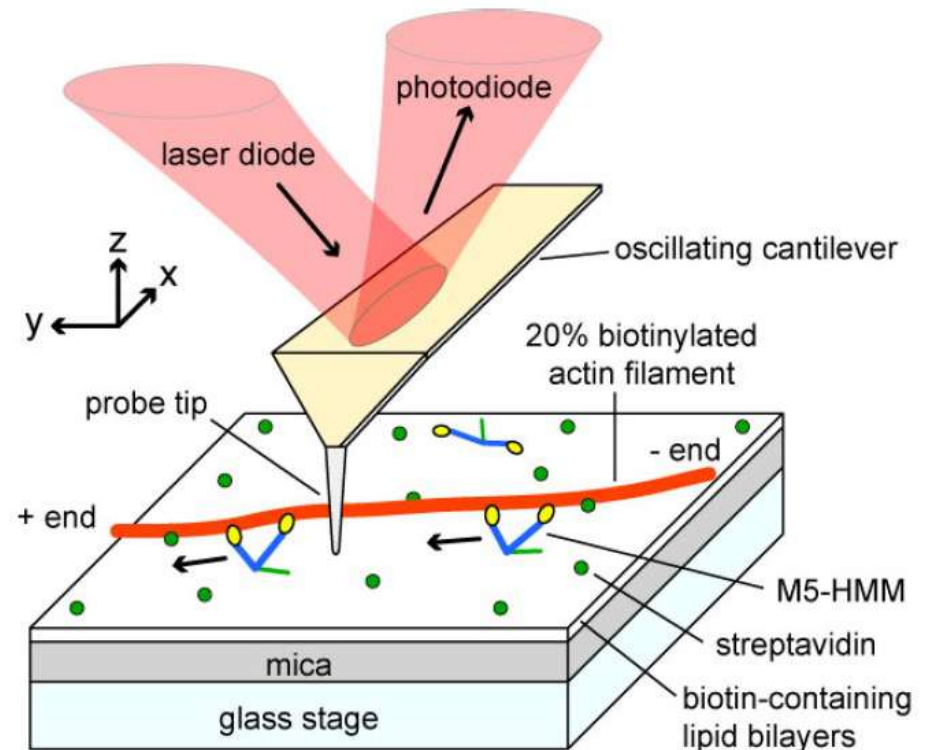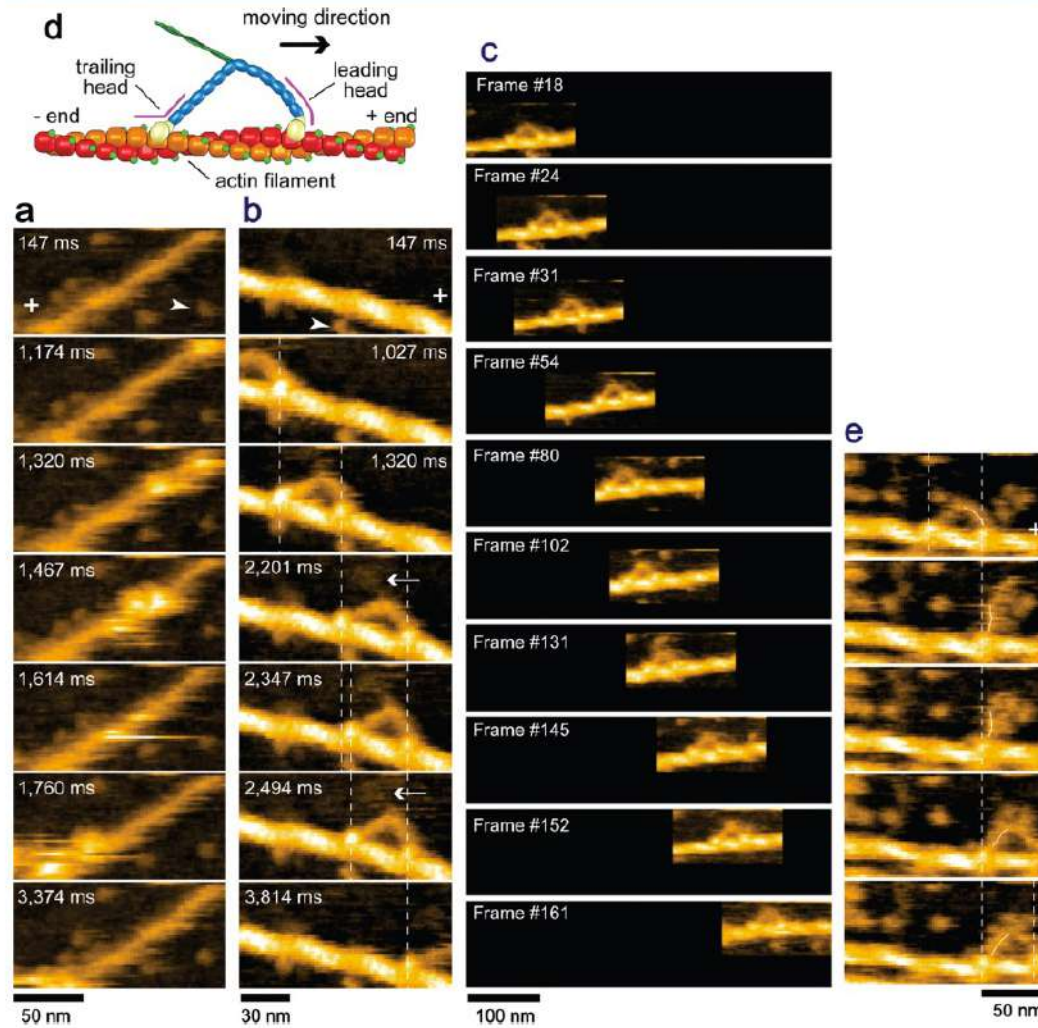
N. Kodera, D. Yamamoto, R. Ishikawa, T. Ando *Nature* **468**, 72 (2010)

Myosine V walking on actin filaments

Myosine V walking on actin filaments

AFM images demonstrate a hand-over-hand movement, with swinging lever-arm motion : the detached T-head rotationally diffused around the advancing neck-neck junction. Extra STV needed as an "obstacle" to slow down the motion to be visualized (100 ms/frame)
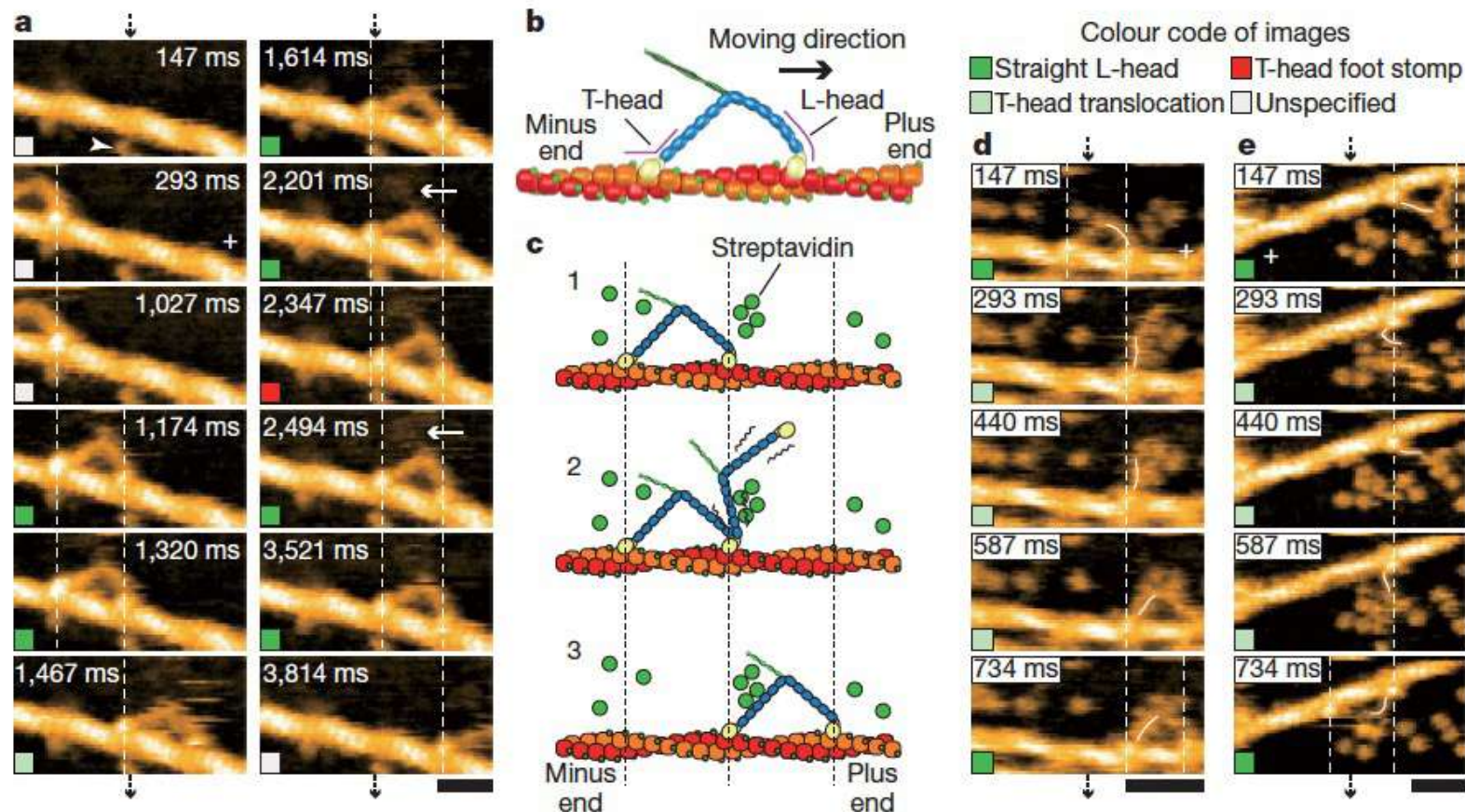
N. Kodera, D. Yamamoto, R. Ishikawa, T. Ando *Nature* **468**, 72 (2010)

http://biophys.w3.kanazawa-u.ac.jp/M5_movies.htm

Myosine V walking on actin filaments

The neck–motor domain junction appears smooth in the leading head (L-head) but is V-shaped in the trailing head (T-head) without exception.
The short coiled coil tail was mostly tilted towards the minus end of actin

N. Kodera, D. Yamamoto, R. Ishikawa, T. Ando *Nature* **468**, 72 (2010)

http://biophys.w3.kanazawa-u.ac.jp/M5_movies.htm

Myosine V walking on actin filaments

The neck–motor domain junction appears smooth in the leading head (L-head) but is V-shaped in the trailing head (T-head) without exception.
The short coiled coil tail was mostly tilted towards the minus end of actin

N. Kodera, D. Yamamoto, R. Ishikawa, T. Ando *Nature* **468**, 72 (2010)

http://biophys.w3.kanazawa-u.ac.jp/M5_movies.htm
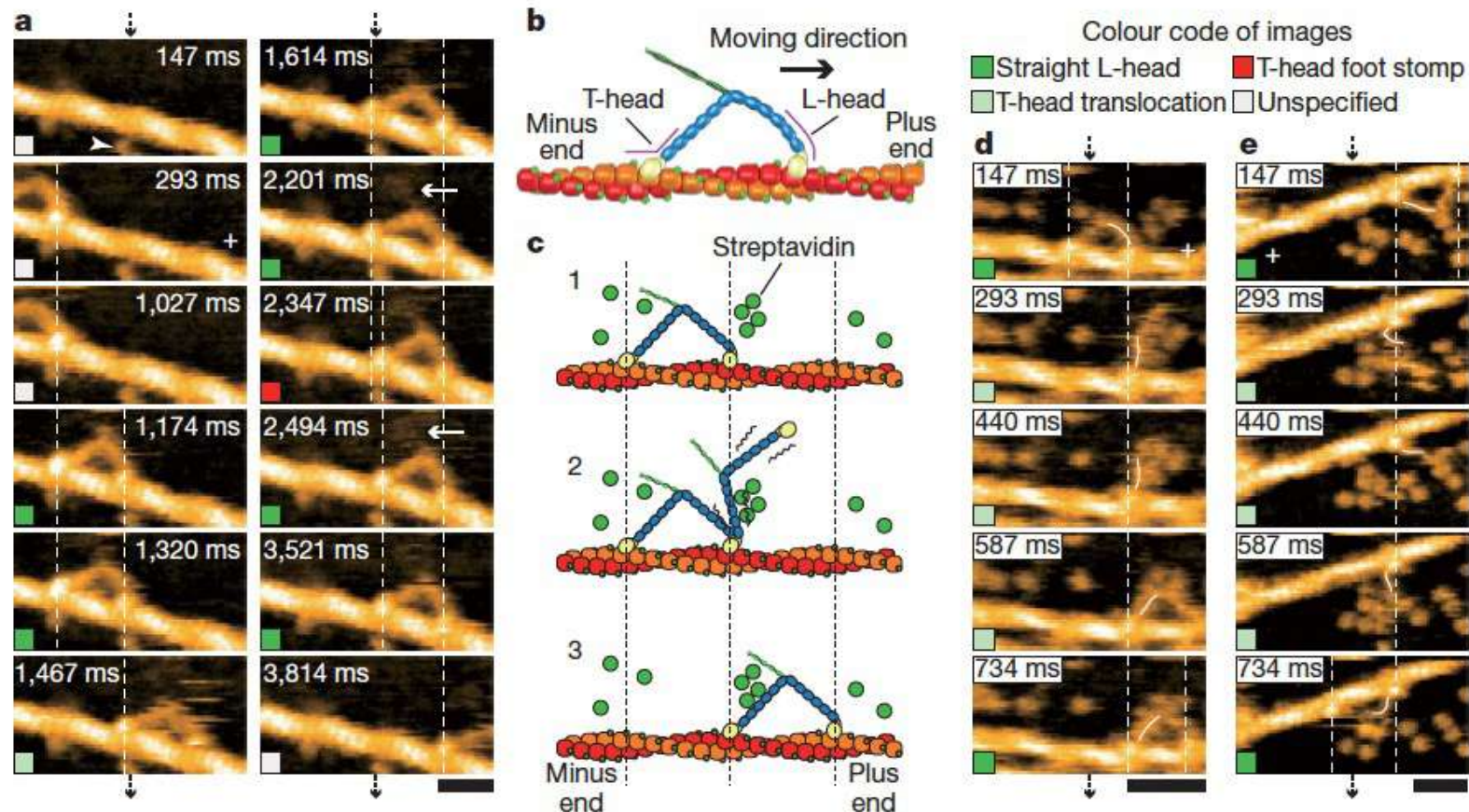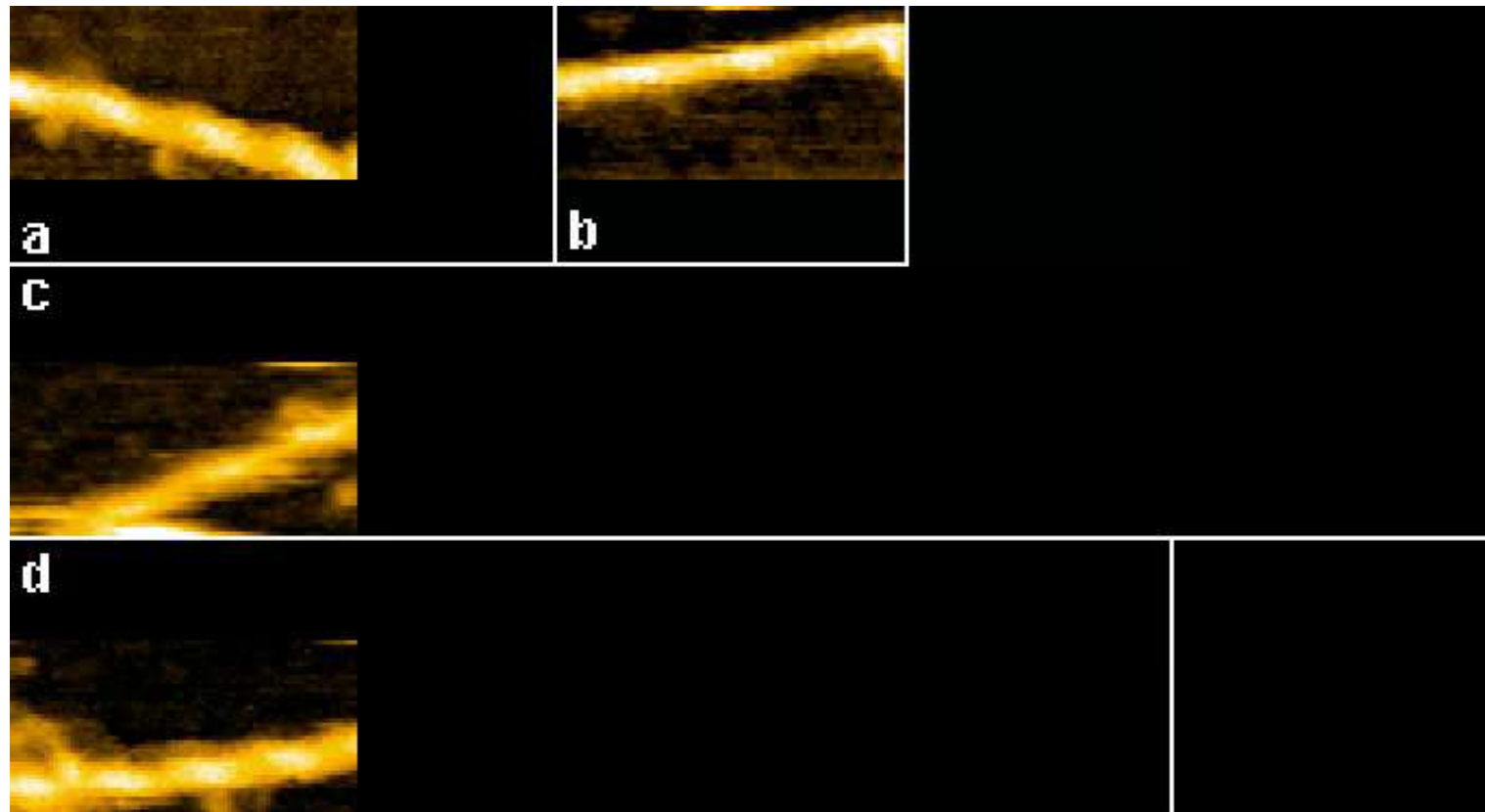
Myosine V walking on actin filaments

After T-head detachment, the nearly straight leading neck swung from the reverse arrowhead (R-ARH) orientation to the arrowhead (ARH) orientation confirming the swinging lever-arm motion initially proposed for muscle myosin. The detached T-head rotationally diffused around the advancing neck–neck junction (no translational diffusion on the actin occurs) and then bound to a forward site on the actin filament, completing one step.
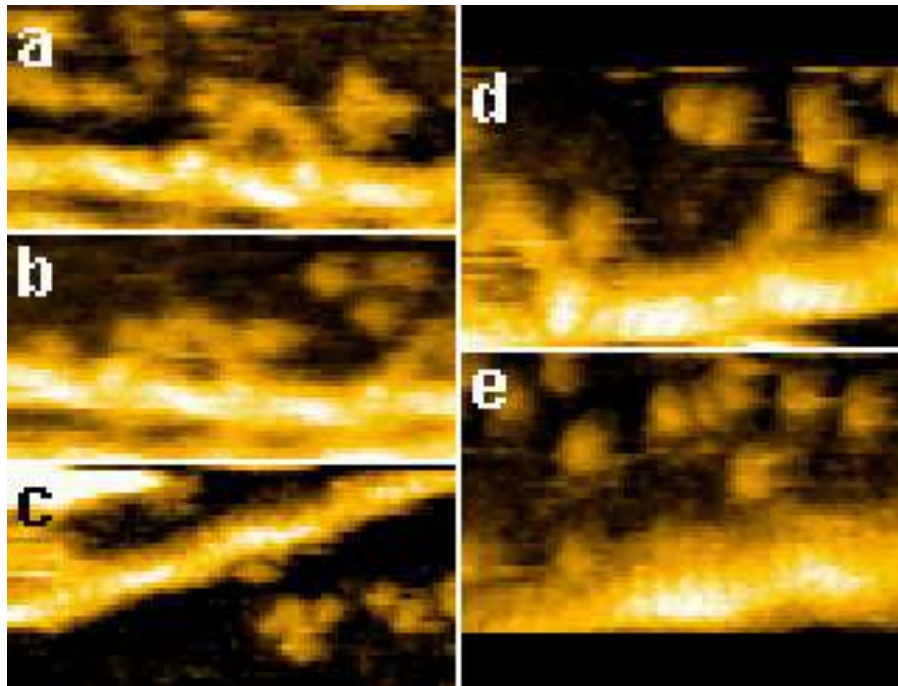
The captured images show that the forward movement is driven not by bending but by rotation of the L-head. The rotation seems to occur spontaneously after T-head detachment, suggesting that intramolecular tension driving the L-head swing exists in the two-headed bound molecules.

N. Kodera, D. Yamamoto, R. Ishikawa, T. Ando *Nature* **468**, 72 (2010)

Myosine V walking on actin filaments

Moreover, it was observed that the leading head of the two-headed bound M5-HMM was often sharply bent in the nucleotide-free condition while it was mostly straight in ADP and ATP. Therefore, just by looking at the shape of the leading head, we can judge whether or not the leading head contains nucleotides. ADP dissociation rate constant at the leading head is 0.1 s-1. This means that ADP is released from the leading head every 10 s, on average. M5-HMM walks many

steps for 10 s. Thus, we can conclude that during walking ADP does not dissociate from the leading head. ADP dissociation, and the subsequent ATP binding,

and the resulting detachment from actin solely occurs at the trailing head.

Just before foot stomping at the leading head, the head never showed the sharply bent conformation which is unique to the nucleotide-free leading head. This fact reinforces our conclusion that the leading head performing foot stomp carries ADP and thus the brief detachment from actin (i.e. the initial stage of foot stomp process) is not caused by binding of new ATP to the leading head.

Polymeric fibers: cytoskeleton

MICROTUBULES   INTERMEDIATE FILAMENTS   MICROFILAMENTS
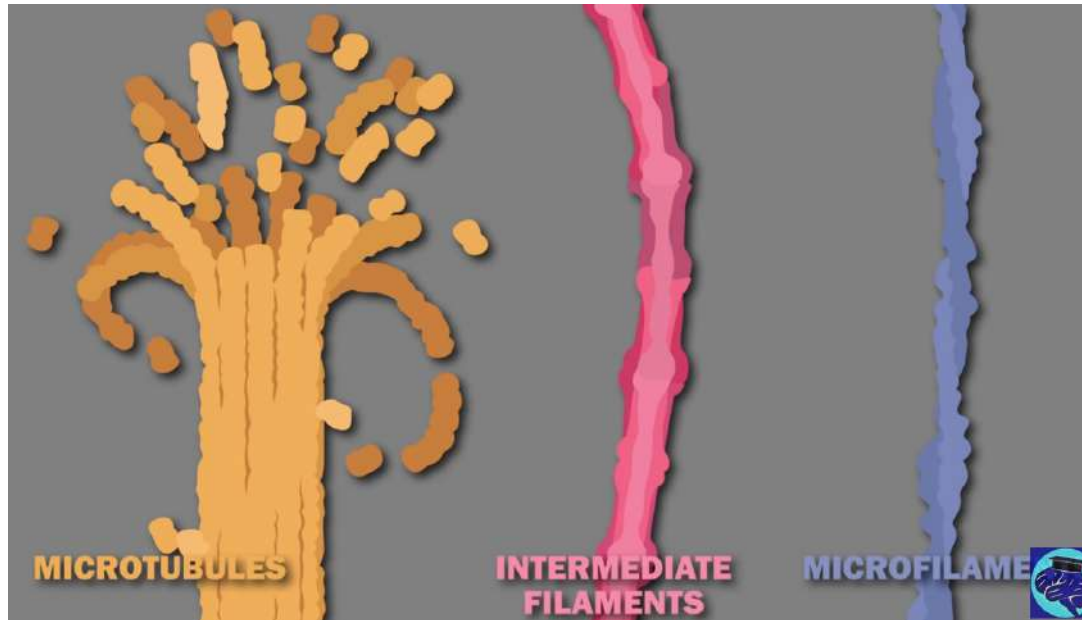
Weak, non covalent interactions
More filaments bind together

POLAR SUBUNITS   WEAK, NONCOVALENT LINKAGES   "POLYMERS"

ASSEMBLY

DISASSEMBLY

NUCLEATION OF A CYTOSKELETAL POLYMER IS THE RATE-LIMITING STEP

Actin filaments

actin molecule

plus end

plus end

37 nm

NH₂

HOOC

ATP
(ADP when
in filament)

minus end

minus end

(B)

(C) 25 nm
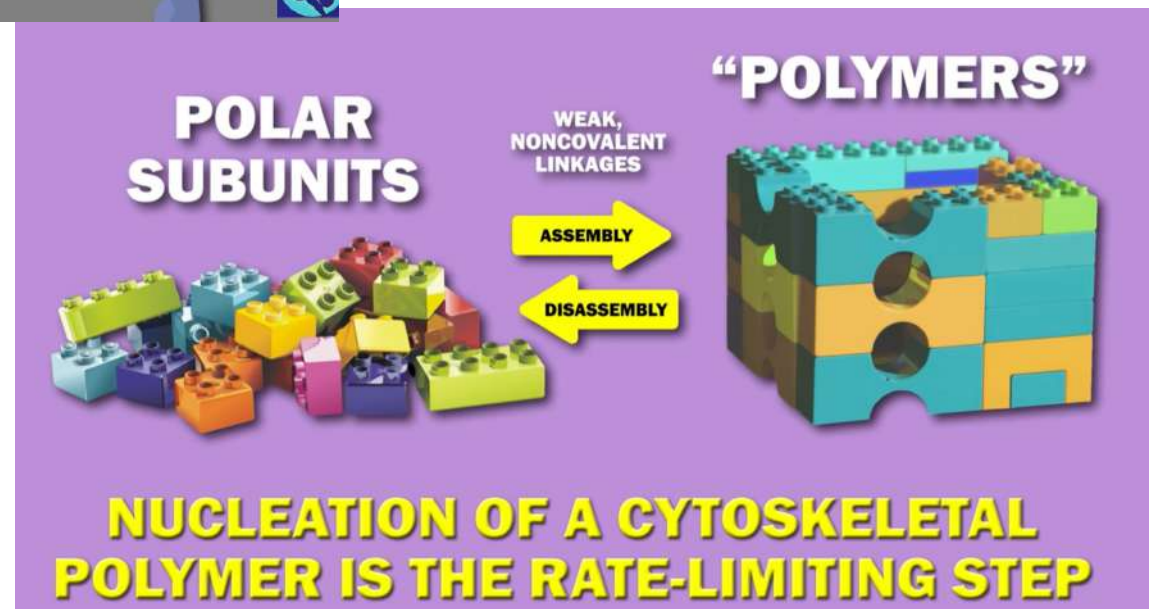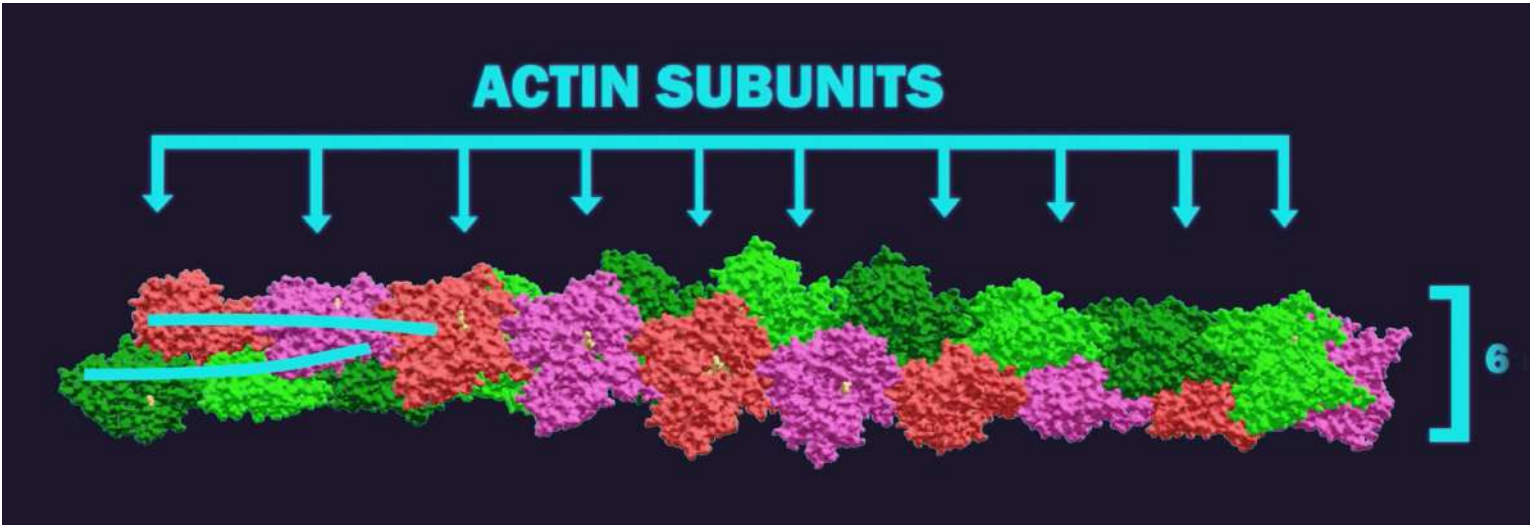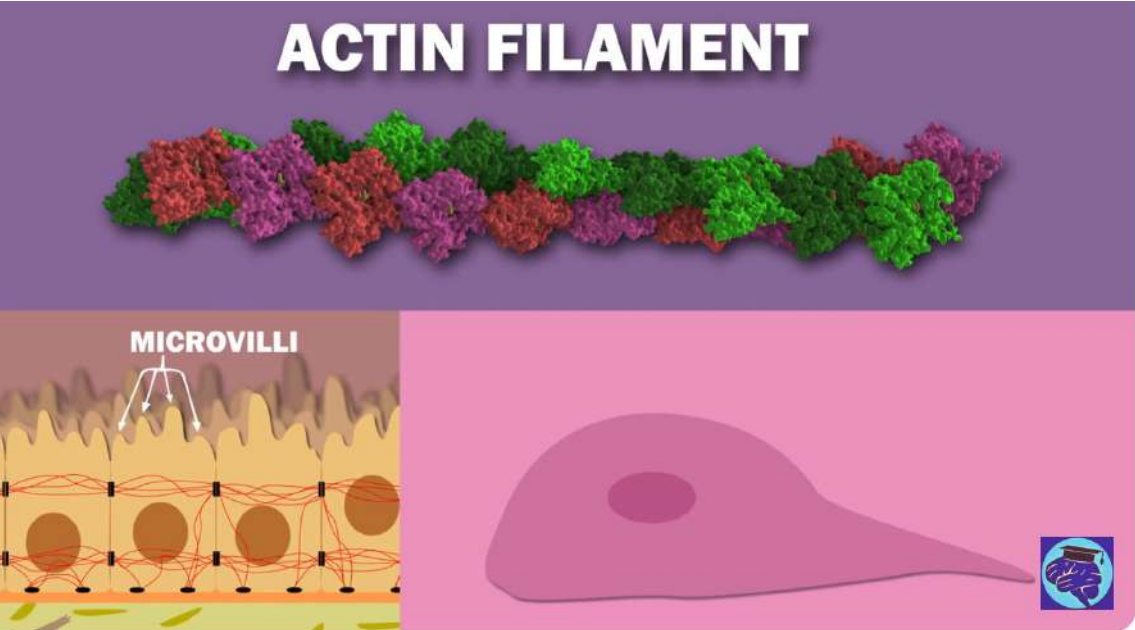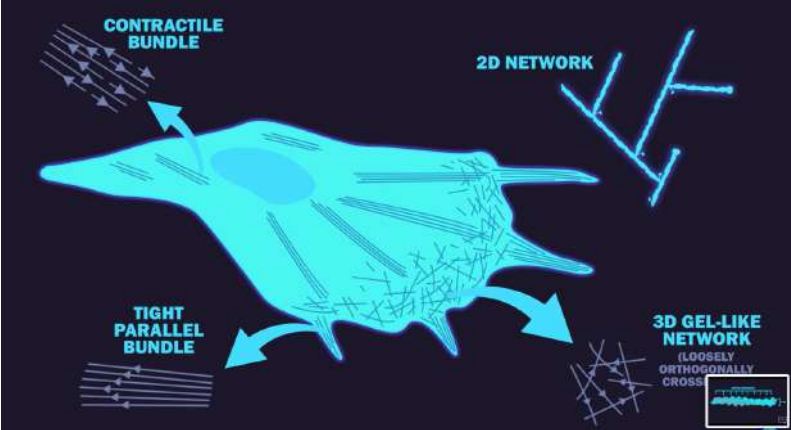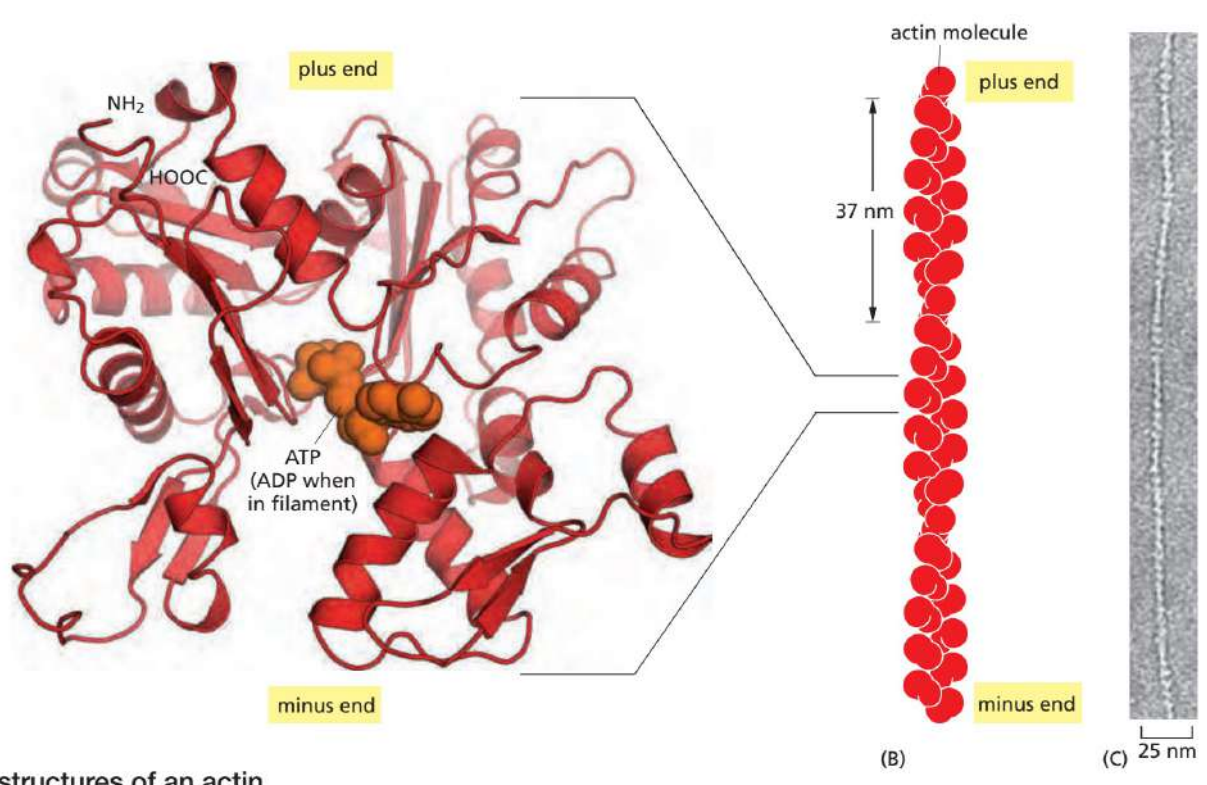
Figure 16–11 The structures of an actin monomer and actin filament. (A) The actin monomer has a nucleotide (either ATP or ADP) bound in a deep cleft in the center of the molecule. (B) Arrangement of monomers in a filament consisting of two protofilaments, held together by lateral contacts, which wind around each other as two parallel strands of a helix, with a twist repeating every 37 nm. All the subunits within the filament have the same orientation. (C) Electron micrograph of negatively stained actin filament. (C, courtesy of Roger Craig.)

Individual actin filaments are quite flexible. The stiffness of a filament can be characterized by its persistence length, the minimum filament length at which random thermal fluctuations are likely to cause it to bend. The persistence length of an actin filament is only a few tens of micrometers. In a living cell, accessory proteins bundle filament together—more rigid

Alberts, Bruce; Johnson, Alexander; Lewis, Julian; Morgan, David; Raff, Martin; Roberts, Keith; Walter, Peter. Molecular Biology of the Cell (p. 898). W. W. Norton & Company. Kindle Edition.

I filamenti di actina hanno una polarità: per convenzione l'estremità "-" cresce lentamente mentre l'estremità "+" è quella che si accresce più velocemente.
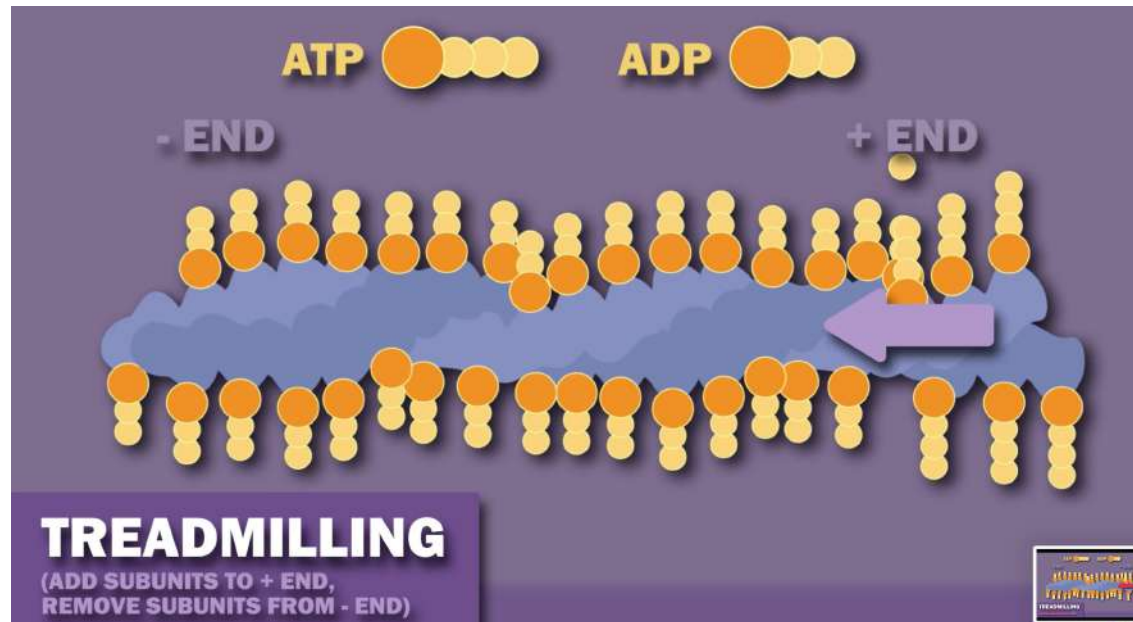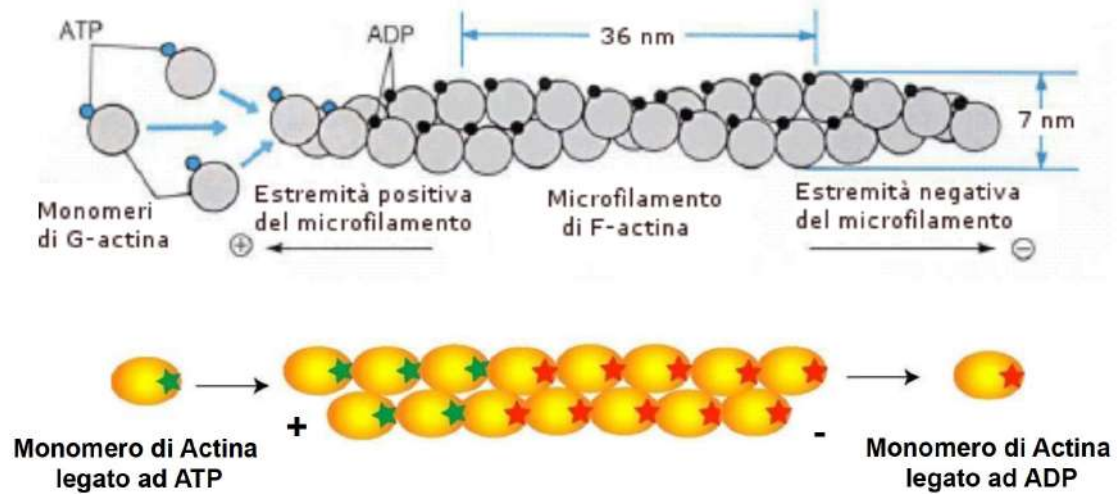
Actin filament dynamics:

actin can catalyze the hydrolysis of the nucleoside triphosphate ATP. For free actin subunits, this hydrolysis proceeds very slowly;

however, it is accelerated when the subunits are incorporated into filaments.

Shortly after ATP hydrolysis occurs, the free phosphate group is released from each subunit, but the ADP remains trapped in the filament structure.

Thus, two different types of filament structures can exist, one with the "T form" of the nucleotide bound (ATP), and one with the "D form" bound (ADP). When the nucleotide is hydrolyzed, much of the free energy released by cleavage of the phosphate–phosphate bond is stored in the polymer. This makes the free-energy change for dissociation of a subunit from the D-form polymer more negative than the free-energy change for dissociation of a subunit from the T-form polymer. Consequently, the ratio of k off/k on for the D-form polymer, which is numerically equal to its critical concentration [Cc(D)], is larger than the corresponding ratio for the T-form polymer. Thus, Cc(D) is greater than Cc(T). At certain concentrations of free subunits, D-form polymers will therefore shrink while T-form polymers grow.

Intermidiate filaments

Cellule epiteliali

Attraversano il citoplasma da una giunzione all'altra, sostenendo la membrana plasmatica

Giunzioni cellula-cellula (desmosomi)

Lamina nucleare

Giunzioni cellula-matrice extracellulare (emidesmosomi)
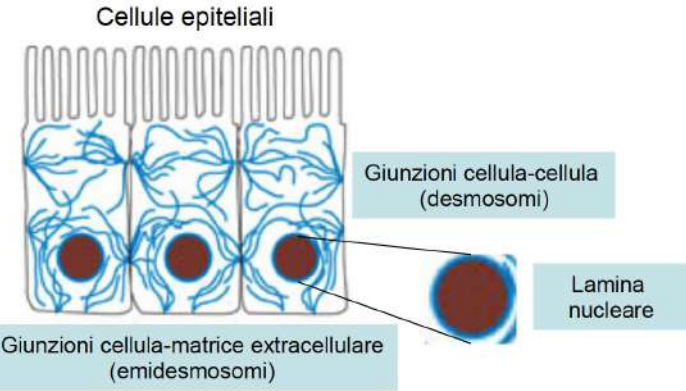
Regolano struttura e funzione dell'involucro nucleare e della cromatina (lamine nucleari)

CITOSOL

involucro nucleare

poro nucleare

làmina nucleare

NUCLEO

cromatina

12
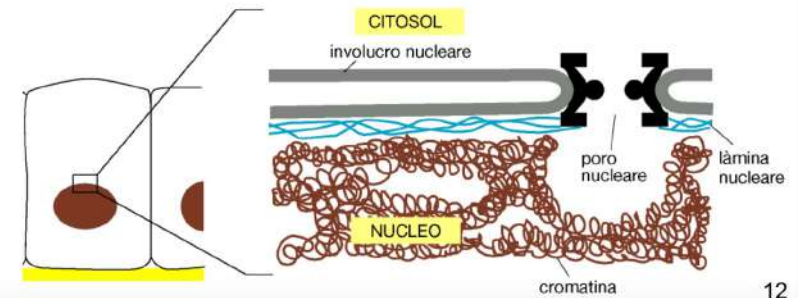
FILAMENTI INTERMEDI - ASSEMBLAGGIO

monomero

(A) regione ad elica α del monomero

NH₂   COOH

dimero parallelo

(B) dimero a spirale ritorta

48 nm

tetramero antiparallelo

(C) tetramero di due dimeri sfalsati e antiparalleli

protofilamento

(D) due tetrameri uniti in filamento con le estremità sfalsate sovrapposte

protofibrilla

(E) otto filamenti pluritetramerici avvolti insieme in un filamento a cordone

10 nm

(F)   0,1 μm

Microtubules

Cellule epiteliali

Disposti come cavi in maniera radiale polaizzata a partire dal Centro Organizzatore dei MicroTubuli (detto anche Centrosoma), cosituito da due **centrioli** perpendicolari

Nucleo

Centrosoma

Centrosoma

Centriolo

9 triplette di microtubuli

Centrioli   **Microtubuli**

Sezione trasversale
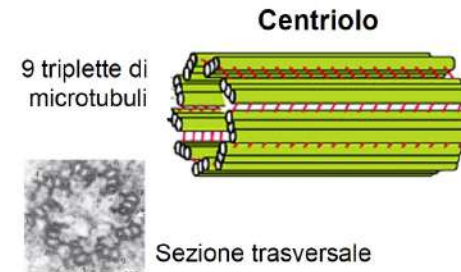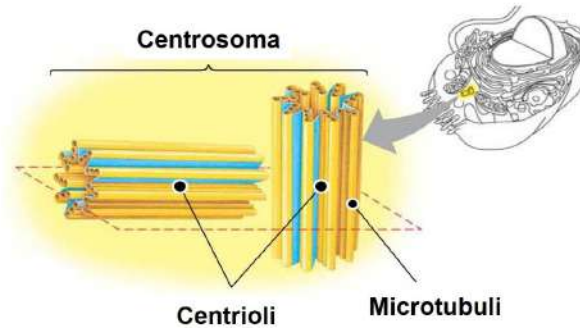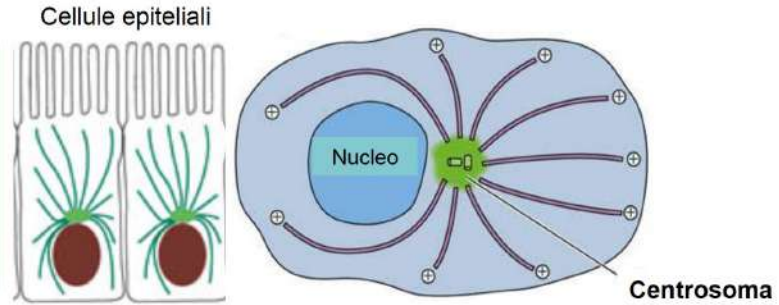
MICROTUBULI - LUNGHEZZA DINAMICA

Estremità +

molecola di tubulina con GTP legato

molecole di tubulina a GTP si aggiungono all'estremità del microtubulo

la polimerizzazione procede più velocemente dell'idrolisi di GTP

cappuccio a GTP

MICROTUBULO IN ALLUNGAMENTO

Estremità -

i protofilamenti di tubulina a GDP sono instabili e si staccano dalla parete del microtubulo

la tubulina a GDP torna libera nel citosol

molecola di tubulina con GDP legato

MICROTUBULO IN ACCORCIAMENTO

STRUTTURA DEI MICROTUBULI

β
α

eterodimero di tubulina (=subunità del microtubulo)

protofilamento

13 protofilamenti disposti a cerchio

lume

+ estremità piú

50 nm

Microtubulo (polarizzato)

- estremità meno

-

Single molecule imaging 1

HR-AFM imaging: DNA

Also, high-resolution AFM imaging has been recently employed to study topological details of DNA/RNA – enzymes interaction. For example, the upstream interaction of Escherichia coli RNA polymerase (RNAP) in an open promoter complex (RPo) formed at the PR and PRM promoters of bacteriophage λ.

I. Mangiarotti, S. Cellai, W. Ross, C. Bustamante, C. Rivetti, *L. Mol. Biol.* **385**, 748 (2009)
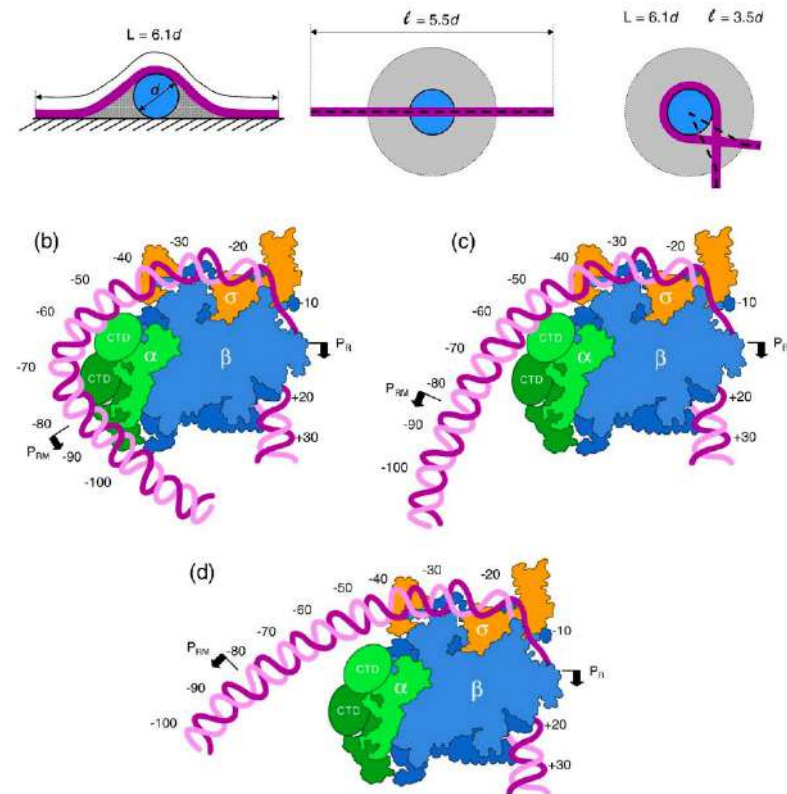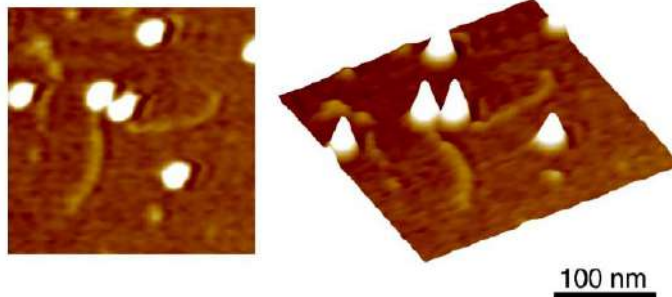
Prokaryotic transcription

Core promoter   Position +1

DNA

RNA polymerase attaches to the core promoter

RNA polymerase

Conversion of closed to open promoter complex

Initiation of RNA synthesis

Promoter clearance

RNA
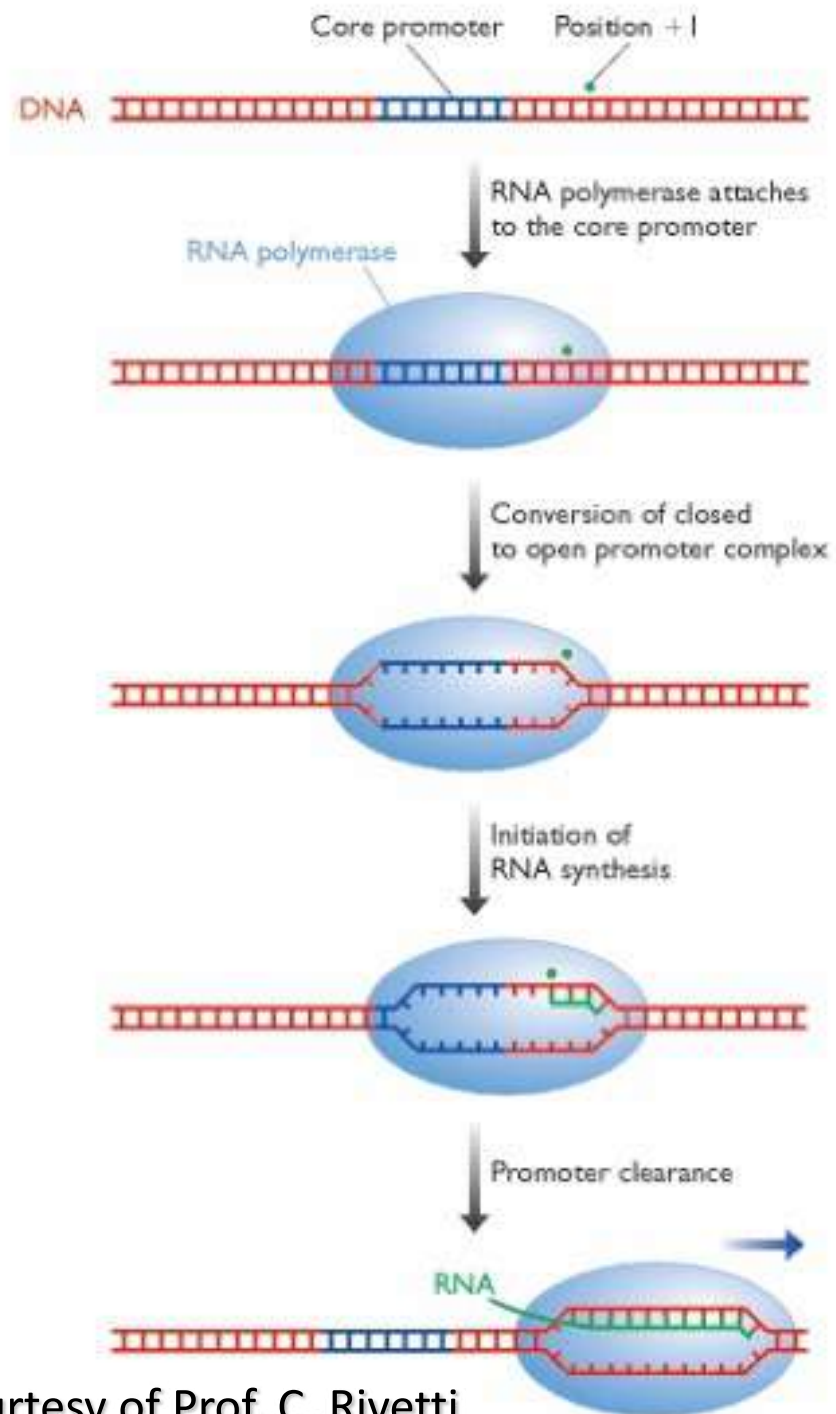
Courtesy of Prof. C. Rivetti

Struttura del DNA

coda 5'

Adenina

Timina

coda 3'

Scheletro fosfato-deossiribosio

coda 3'

Guanina

Citosina

coda 5'

$\varnothing$ = 2 nm

3.4 nm
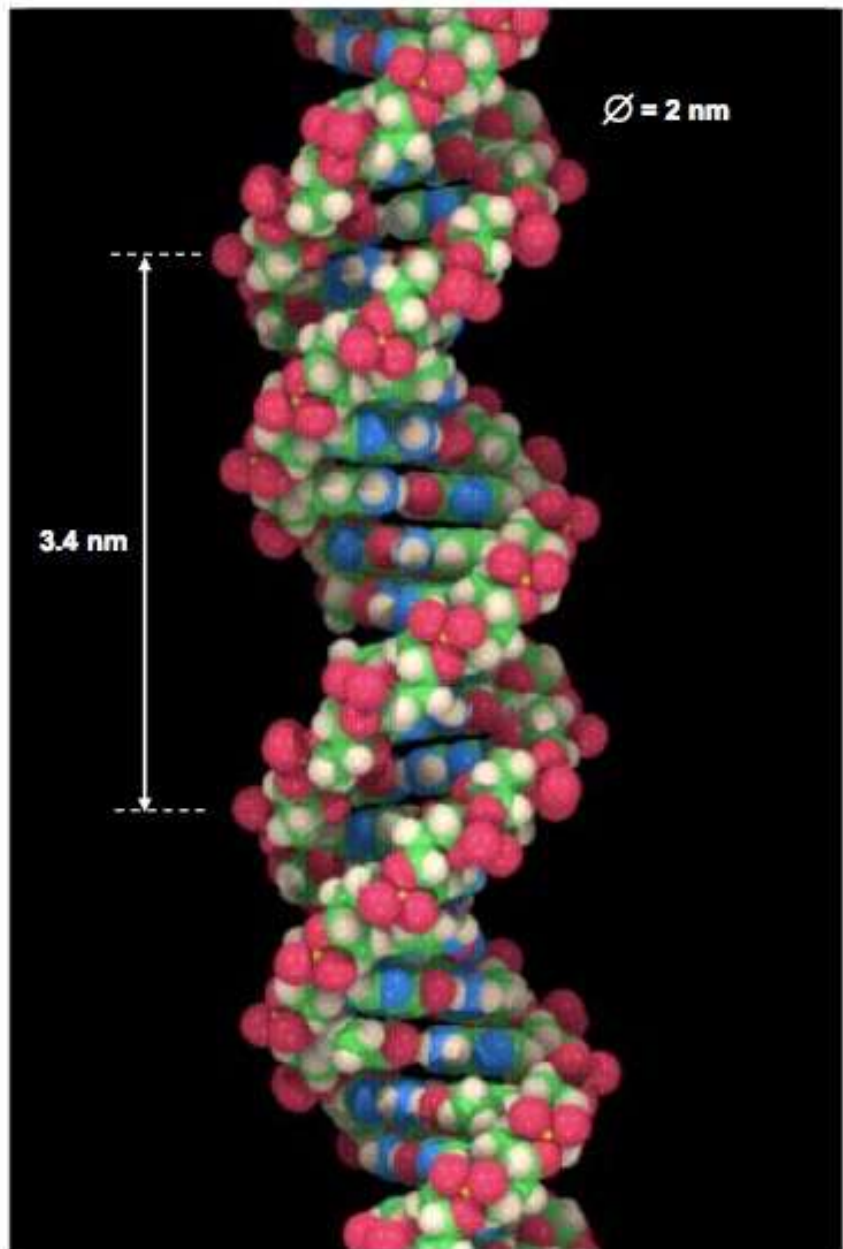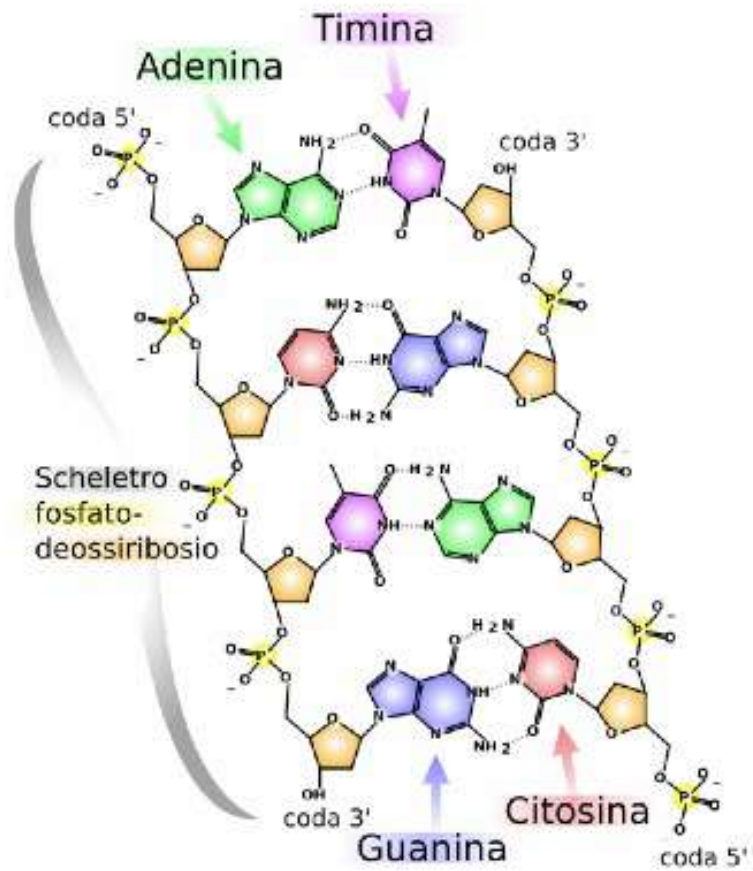
DNA

Watson and Crick, 1953
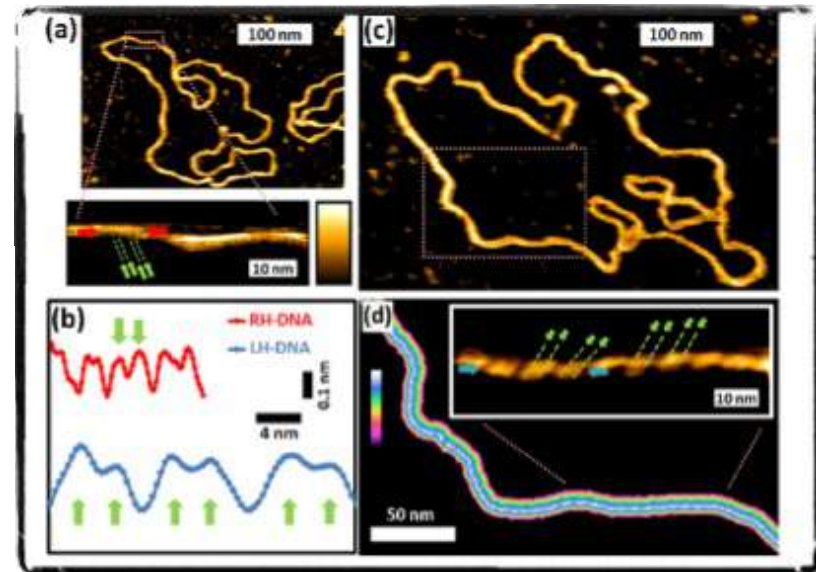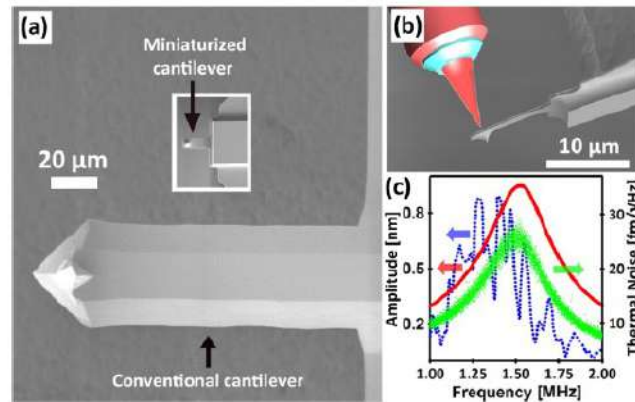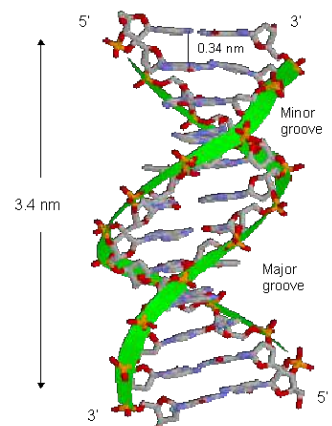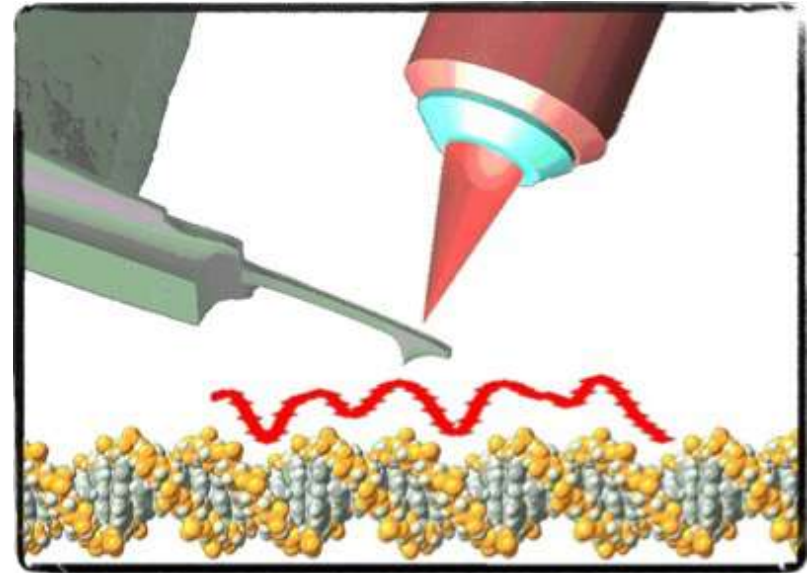
Leung et al., Nanoletters 2012

AFM image simulation of DNA

Rc = 7.0 nm

Rc = 5.0 nm

Rc = 4.0 nm

Rc = 2.0 nm

Rc = 1.0 nm

Rc = 0.5 nm

Rc = 0.1 nm

20 nm

Rc = 0.1 nm

3.0 nm
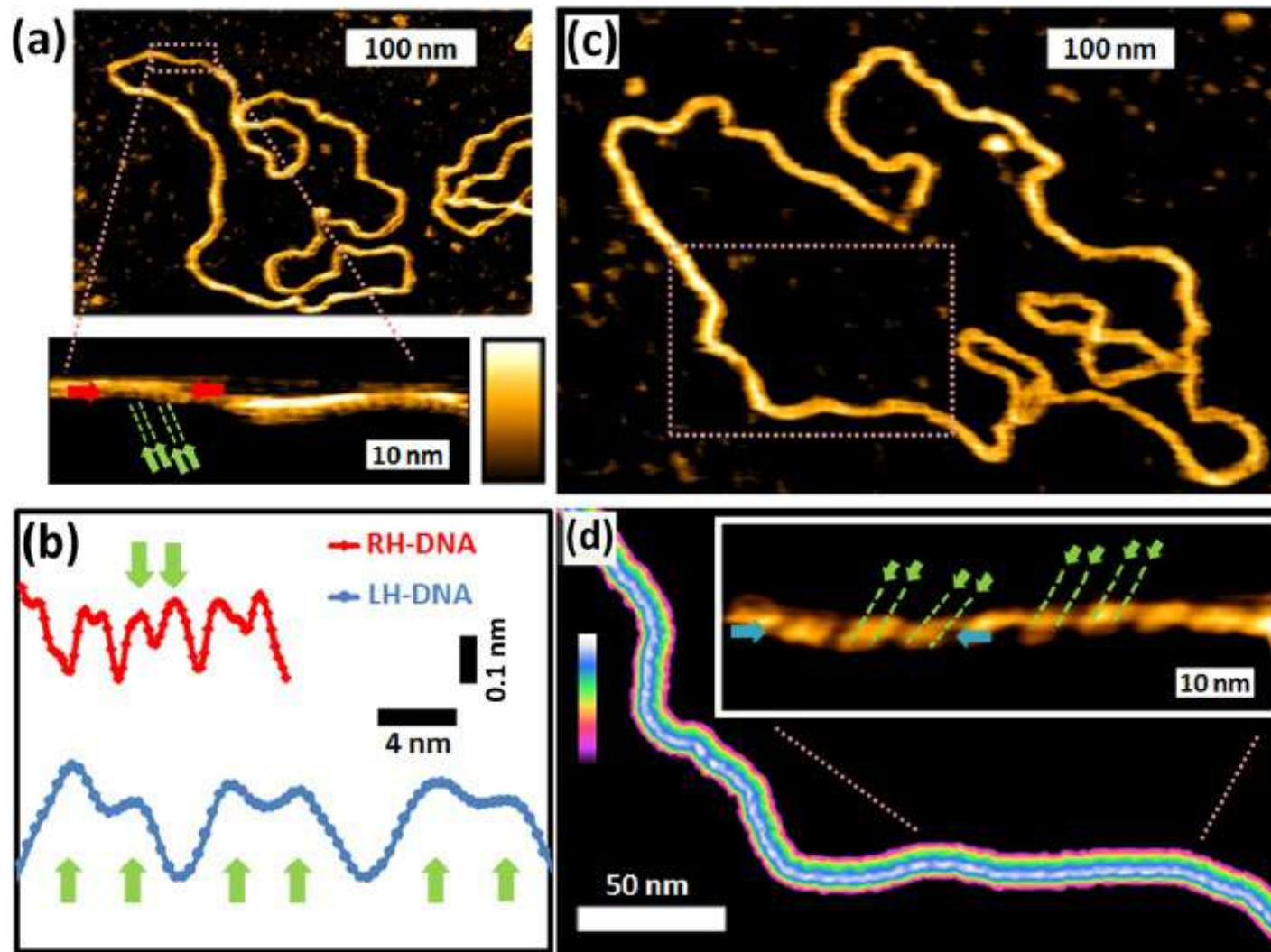
Figure 4. High-resolution AFM on plasmid DNA. (a) 3486 bp plasmid DNA, which on magnification shows a right-handed double helix, superposed to substantial height differences on and along the DNA. (b) Profiles along right-handed (RH) and left-handed (LH) DNA, acquired along the lines marked by the red and blue arrows in the insets of A and D. (c) Elongated configuration of the 3486 bp plasmid DNA displayed at the same scale as part a. (d) On subsequent magnifications of the dashed rectangle in c, an elongated left-handed double helix is resolved. Color scale: 1.5 nm (a); 1.1 nm (a, inset); 1.5 nm (c); 1.1 nm (d); 0.7 nm (d, inset). Green arrows indicate the two strands of the double helix, separated by the minor groove (depth ≲0.1 nm). The major groove (depth ∼0.2 nm) separates the subsequent turns of the double helix.

DNA adhesion on mica

Courtesy of C. Rivetti

MICA

Biotite

tetrahedral layer

octahedral layer

M2   M1

4.64 A

K⁺   (001)

← K

→ O
→ Si

→ O (OH)
→ Al
→ O (OH)
→ Si
→ O

(a)

b

c

Si⁴⁺

Al³⁺

K⁺

O²⁻

OH⁻

(b)

b
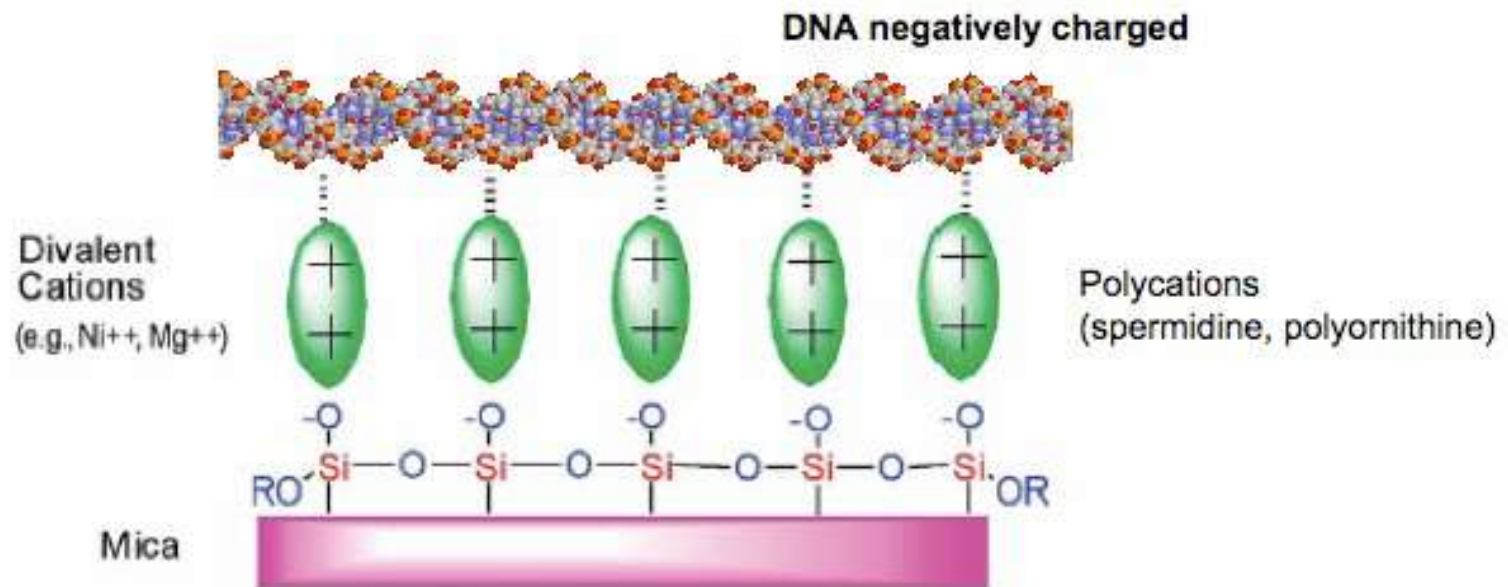
a
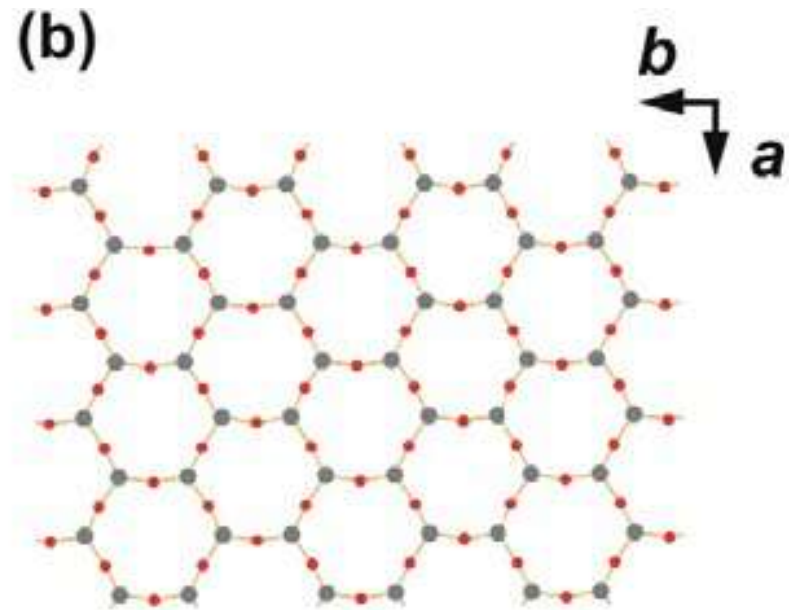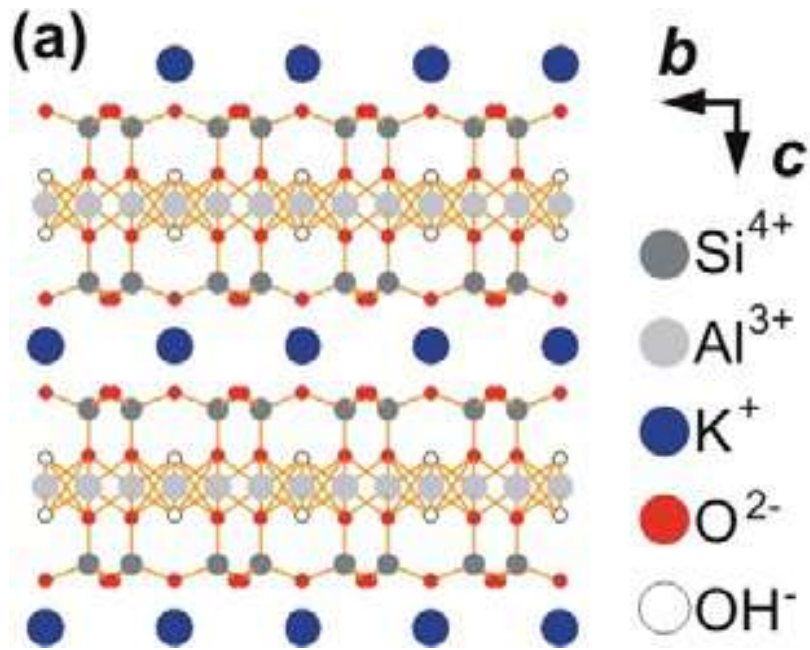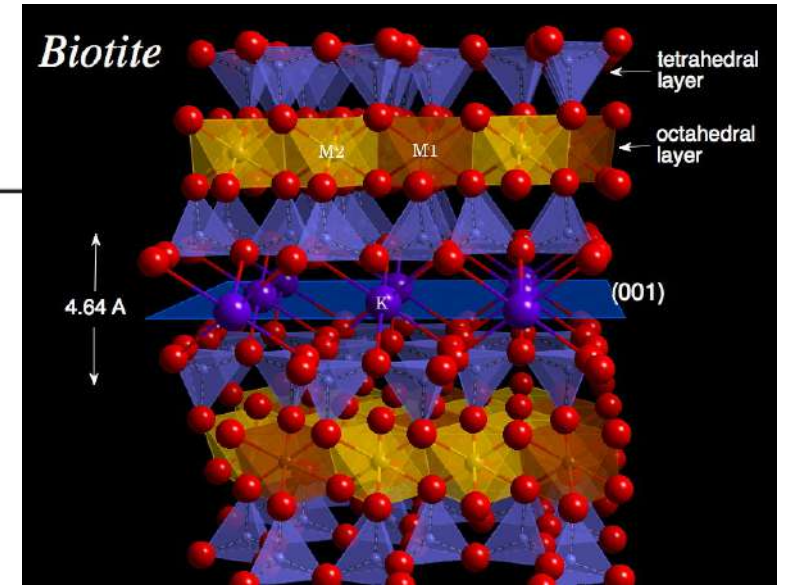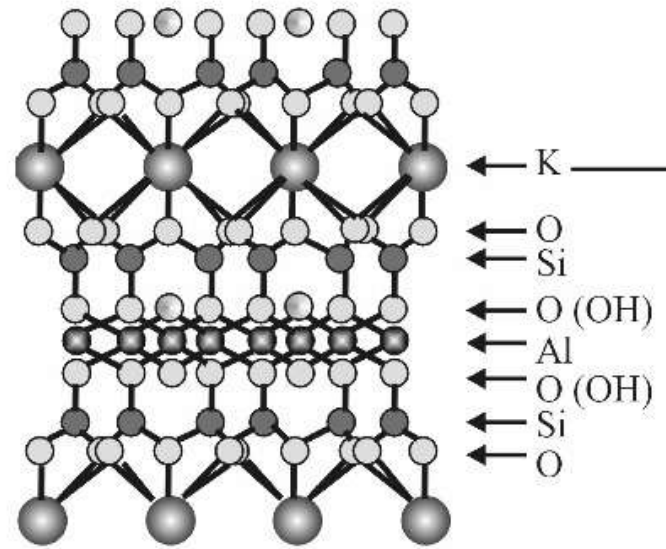
DNA deposition methods
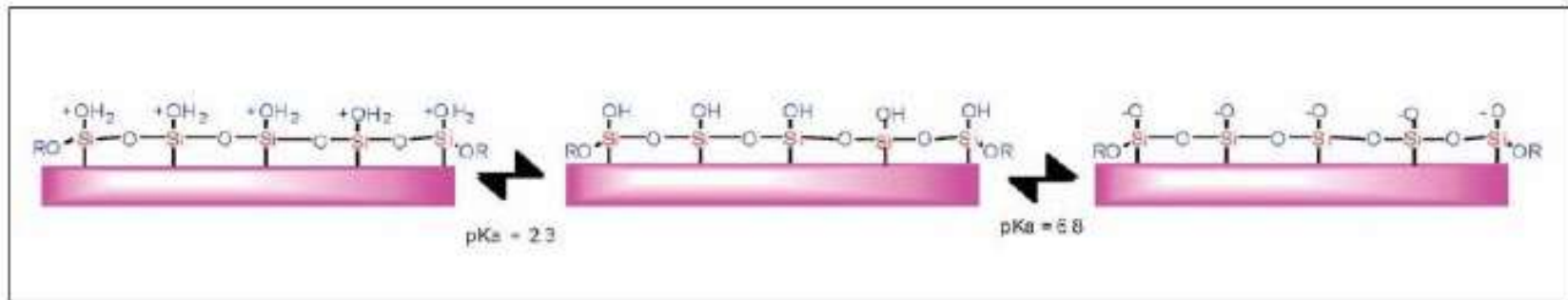
Figure 1. Siloxy groups on the surface of freshly cleaved mica.
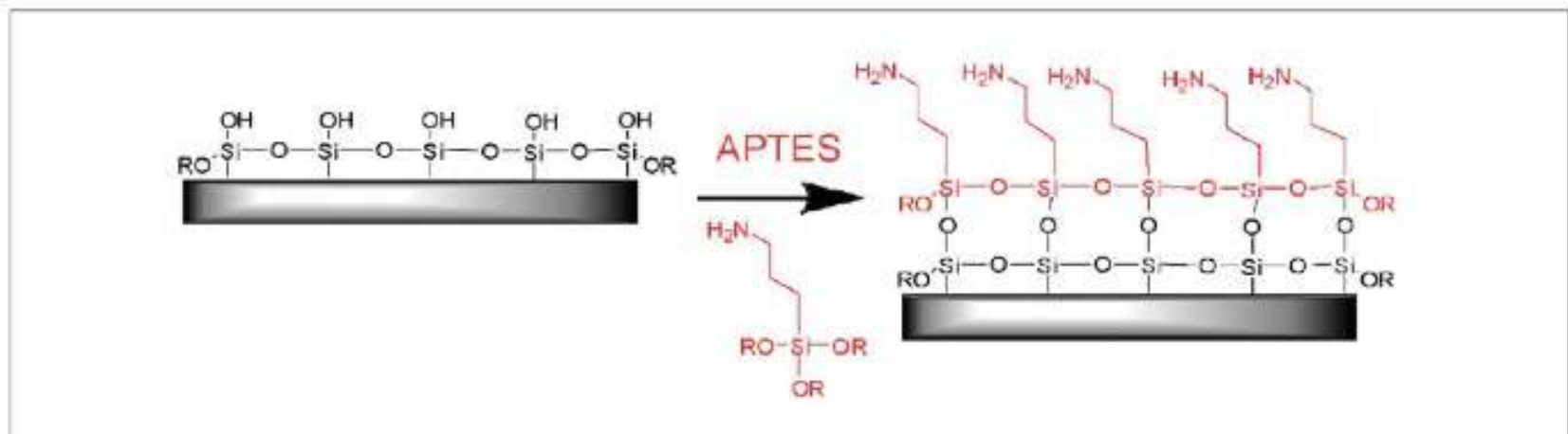
Figure 2. APTES treated mica substrate.

Courtesy of C. Rivetti
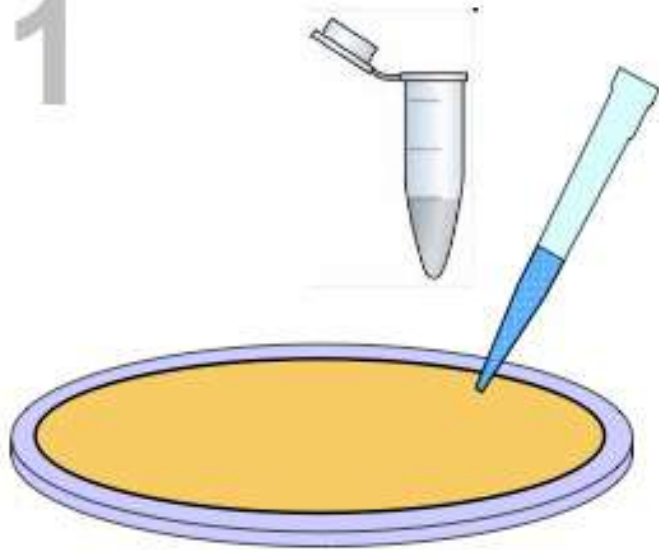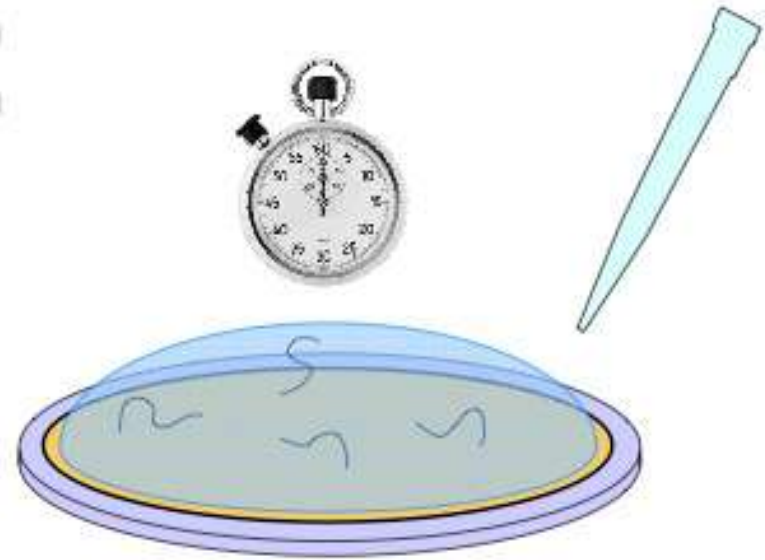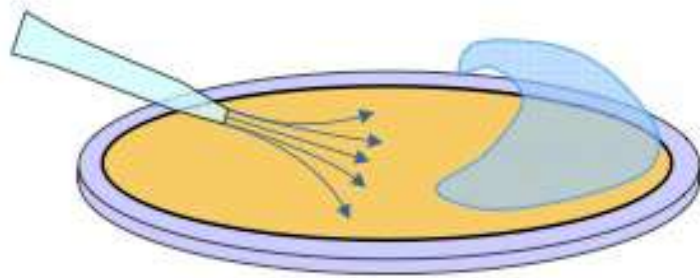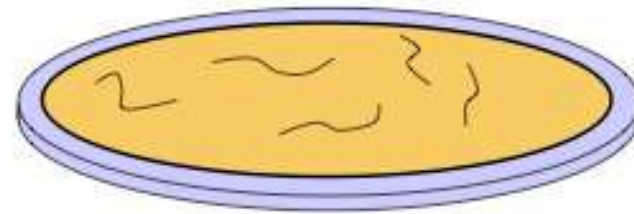
DNA deposition steps
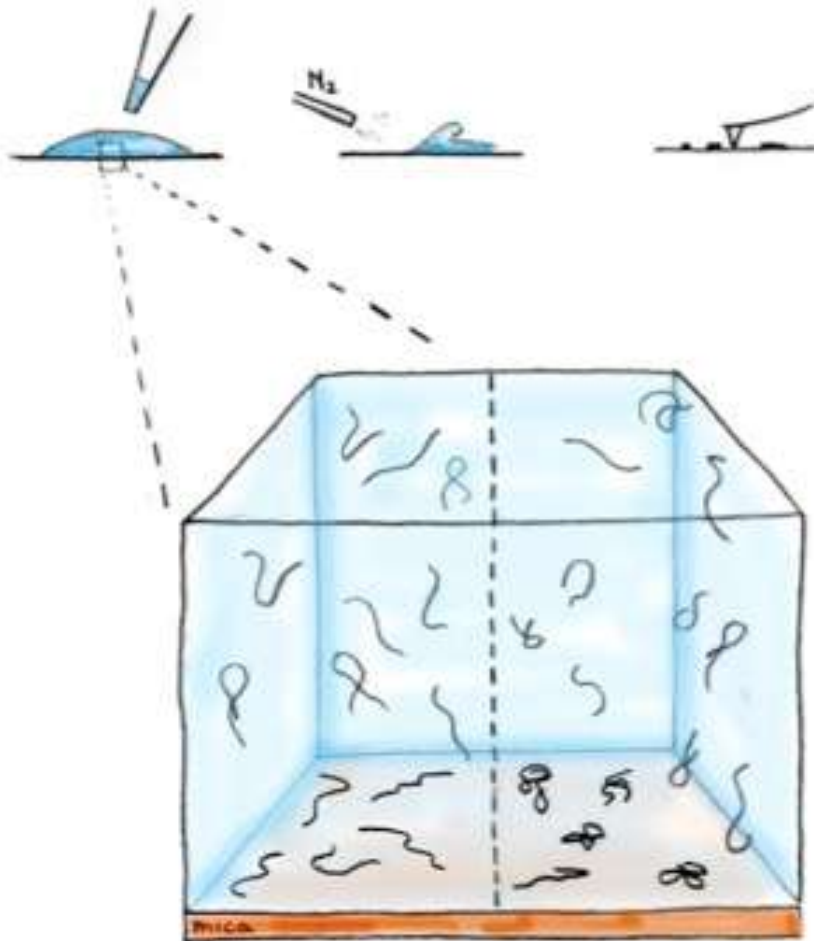
- How do DNA molecules go from solution to the surface?

- Once bound to the surface can they go back into solution?

- What happens to the molecules on the surface before removing the buffer?
  Can they move in 2D or are they trapped in a single conformation?

Can we quantitatively distinguish between the different cases?

Courtesy of Prof. C. Bustamante

DNA Deposition onto Untreated and Treated Mica

Freshly cleaved — Glow discharged — H+-exchanged

2 μm — 2 μm — 2 μm

4 nm — 0 nm

Courtesy of Prof. C. Bustamante
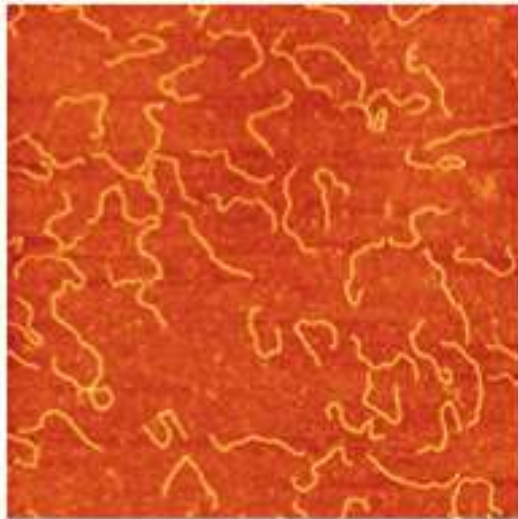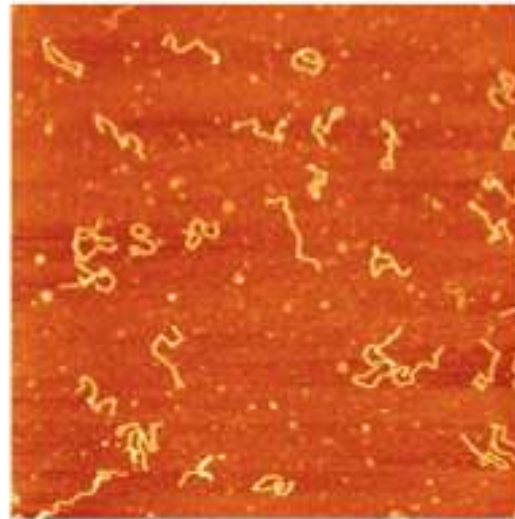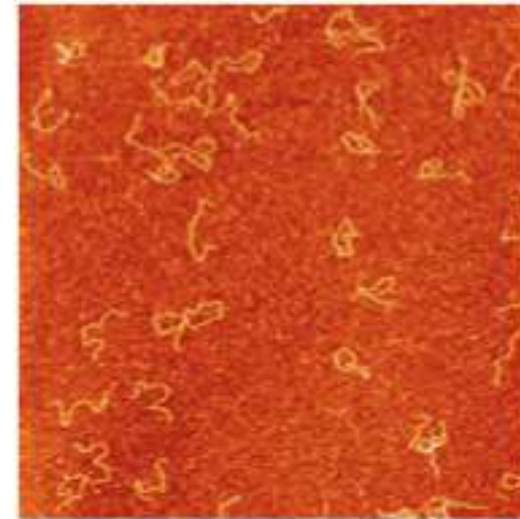
Number of DNA Molecules on the Surface vs. Time

On cleaved mica, transfer of DNA from solution to the surface is solely governed by diffusion:

n_0 initial DNA concentration in molecules/cm^3
D diffusion coefficient
t time of deposition

$$n_F = \frac{\text{N. of Molecules}}{\text{Area}} = \frac{2}{\sqrt{\pi}} \, n_0 \sqrt{Dt}$$

slope = 0.49±0.04
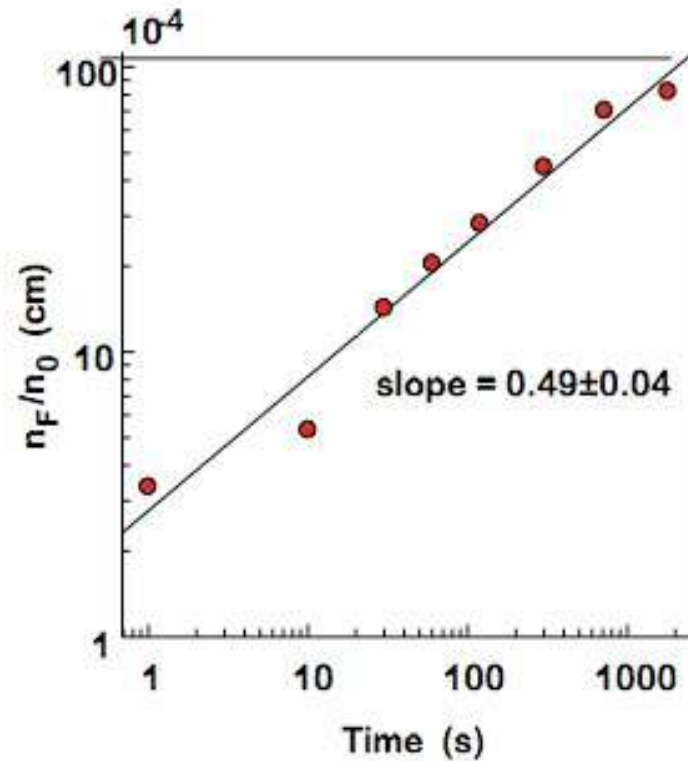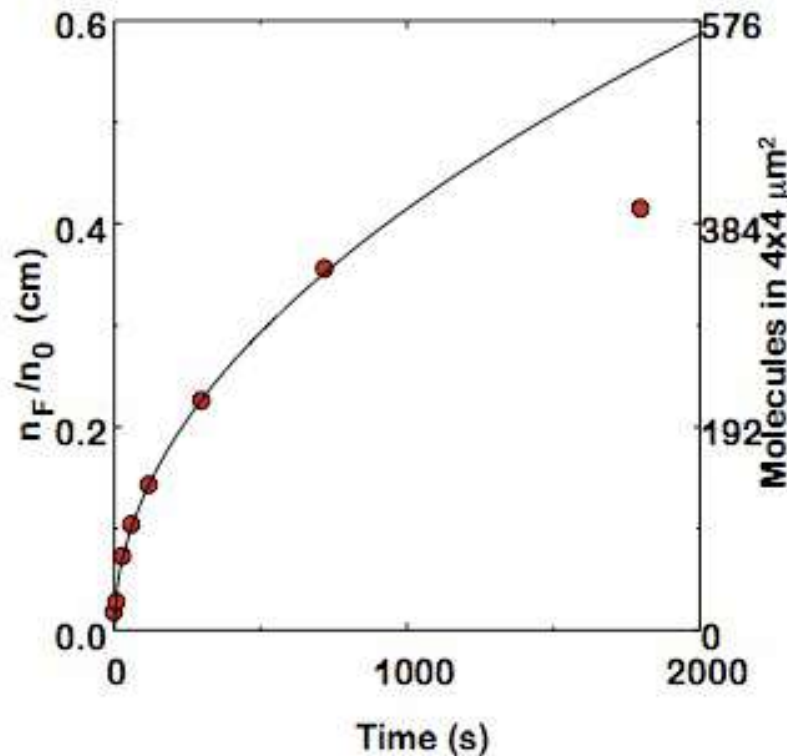
$$D = (5.4\pm0.2)10^{-8} \ cm^2/s$$

Valid if:

- The molecules are irreversibly adsorbed to the surface
- Convection currents do not contribute to the transport of the molecules to the surface
- The solution is not significantly depleted of DNA molecules and the surface is not saturated during the time of deposition

Courtesy of Prof. C. Bustamante

Diffusive dynamics
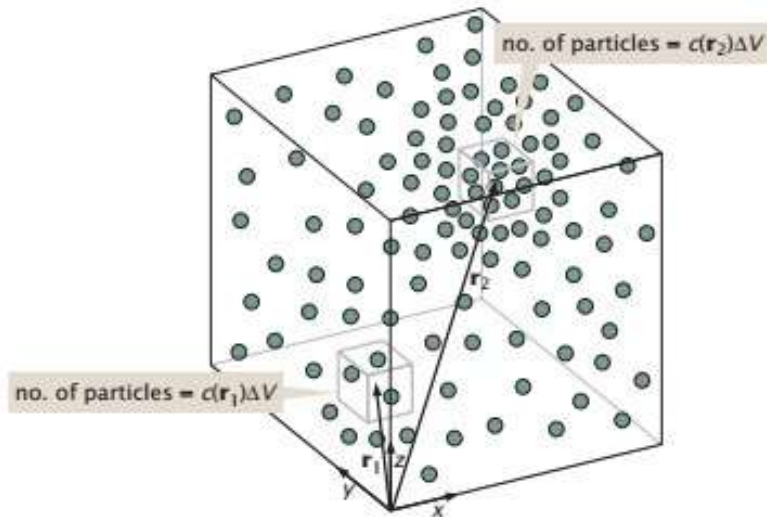
we divide space up into a bunch of small boxes, large enough to include many molecules, but small enough so that the density is nearly uniform over the scale of the box.

We use the notation c($\mathbf{r}$,t) to signify the concentration in a box centered at position $\mathbf{r}$ in three-dimensional space (with units of number of particles per unit volume) and c(x,t) to signify the concentration field in one-dimensional problems (with units of number of particles per unit length).

"Concentration gradient" is a spatial variation in the concentration field.

simple concentration profile where on the left-hand side of the domain of interest, the concentration of the molecule of interest is high, while on the right-hand side of the domain of interest, the concentration is low

Phillips, Rob; Kondev, Jane; Theriot, Julie; Garcia, Hernan. Physical Biology of the Cell (Page 516). CRC Press.

Diffusive dynamics

no. of particles = N(x)

no. of particles = N(x+Δx)
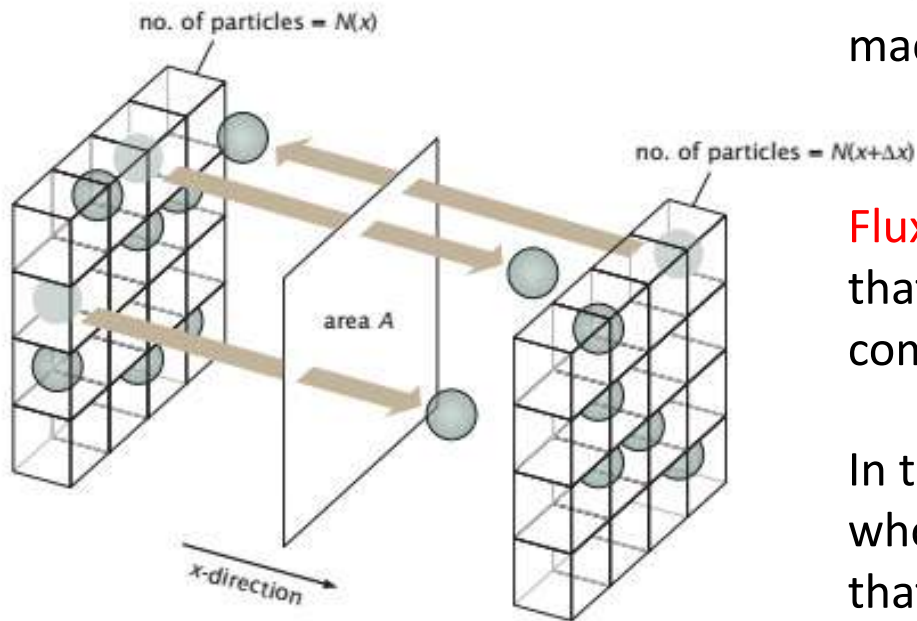
area A

x-direction

The other key quantity of interest for our macroscopic description of diffusion is the flux.

Flux can be seen as the net number of molecules that cross area A per unit time. That is the component of the flux vector in that direction.

In three dimensions, the flux is actually a vector whose components give the flux across planes that are perpendicular to the x-, y-, and z directions.

The goal of our thinking is to determine what amounts to an "equation of motion" that tells how the concentration field changes in both space and time.

Diffusive dynamics

in one dimension, flux is linearly related to concentration gradient:

$$j = -D \frac{\partial c}{\partial x},$$ (13.1)

J = current density, number of particles crossing unit area/ unit time
D = diffusion coefficient

$$[j] = \frac{1}{\text{length}^2 \times \text{time}},$$

$$\left[\frac{\partial c}{\partial x} \right] = \frac{\text{number of particles/length}^3}{\text{length}} = \frac{\text{number of particles}}{\text{length}^4}.$$

[D] = length^2/time, indipendent on dimensionality of space!

Equilibrium Statistic of a Worm-like Chain

Isotropic rod continuously flexible. The worm-like chain model is particularly suited for describing stiffer polymers, with successive segments displaying a sort of cooperativity: all pointing in roughly the same u_1 direction
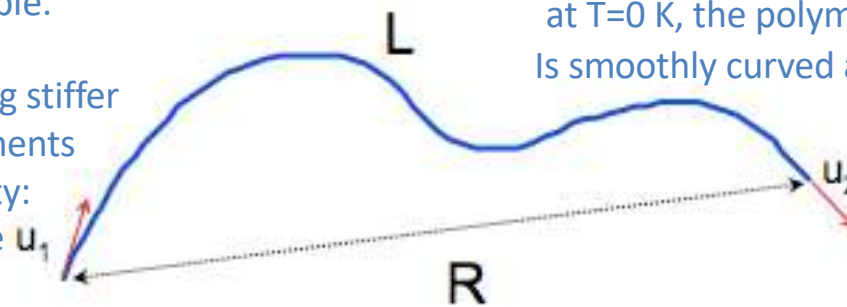
at T=0 K, the polymer adopts a rigid rod conformation
Is smoothly curved at RT

$$\left\langle \vec{u_1} \cdot \vec{u_2} \right\rangle = e^{-\frac{L}{P}}$$

The persistence length of the molecule, P, is the decay length through which the initial orientation of the molecule persist. It is a measure of the stiffness of a polymer chain.

In 2D the mean square end-to-end distance of a worm-like chain of length L, and persistence length P, is:

$$\left\langle R^2 \right\rangle_{2D} = 4PL\left(1 - \frac{2P}{L}\left(1 - e^{-\frac{L}{2P}}\right)\right) \qquad \text{For } L \to \infty \quad \left\langle R^2 \right\rangle_{2D} = 4PL$$

Courtesy of Prof. C. Bustamante

WLC is for semi-flexible polymers.
Assumes polymers are inextensible, has a linear elastic bending energy and is subjected to thermal fluctuations.
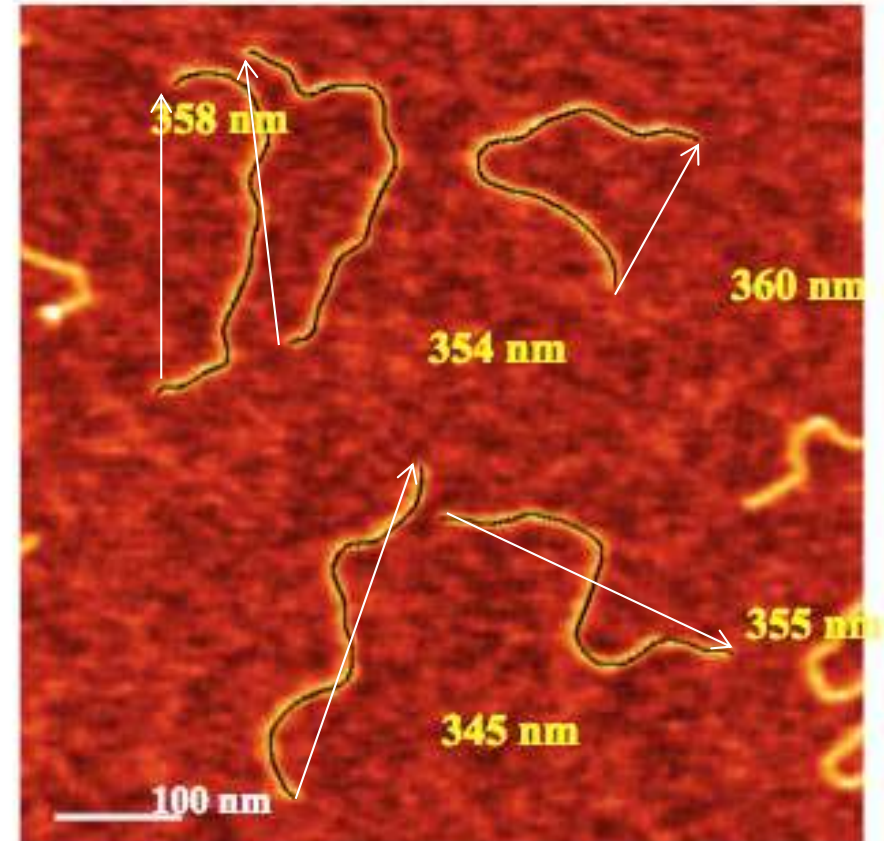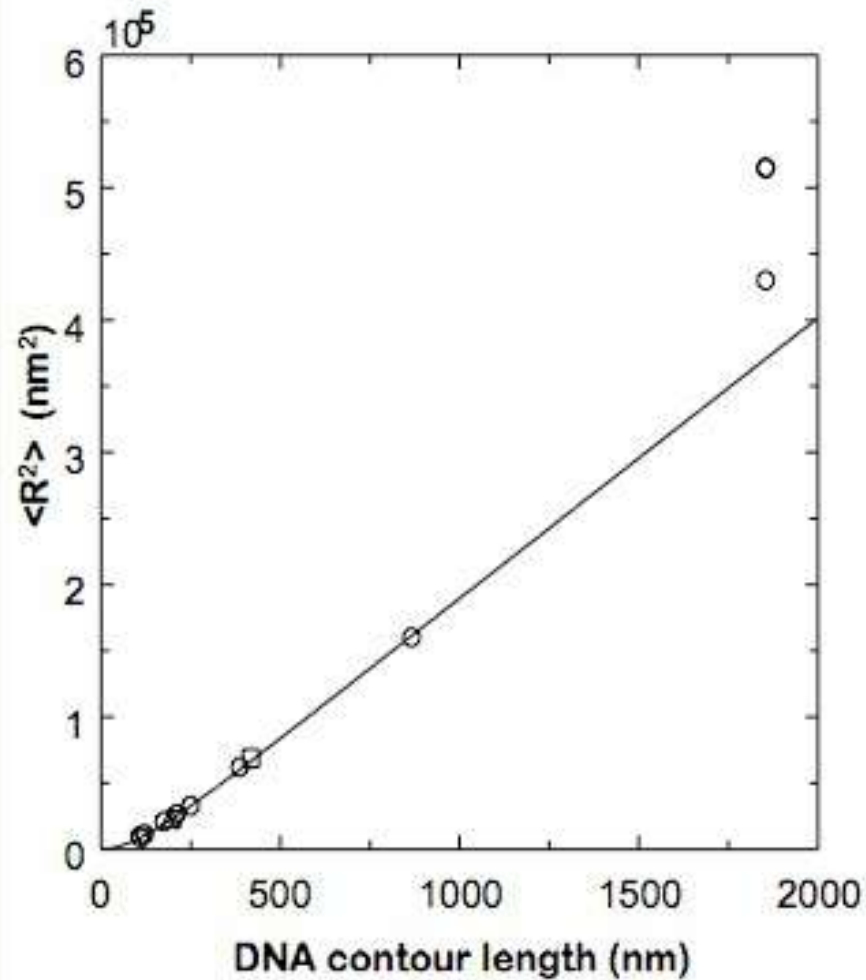
a) L=Nl segments, freely rotating
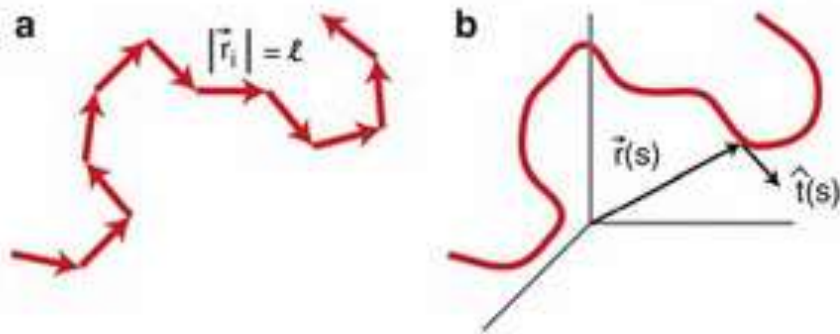
Worm-Like Chain (WLC) Model, Fig. 1 (a) Discrete model of a polymer composed of a chain of segments $\vec{r}_i$ each of length ℓ. (b) Continuous WLC polymer parameterized by the tangent vector $\hat{t}(s) = \frac{\partial \vec{r}(s)}{\partial s}$ along the contour

Adding energy cost associated to the bending:

$$H = -\varepsilon \sum_{i=1}^{N-1} \vec{r}_{i+1} \cdot \vec{r}_i, \qquad (1)$$

which imposes an energy cost of $\varepsilon \ell^2$ times the cosine of the angle between neighboring segments. The right-hand side of (1) can be rewritten using the relation $\vec{r}_{i+1} \cdot \vec{r}_i = \frac{2\ell^2 - (\vec{r}_{i+1} - \vec{r}_i)^2}{2}$. Moving from a discrete model to a continuous model requires taking the limits $N \to \infty$ and $\ell \to 0$. Likewise:

$$\lim_{\ell \to 0} \left(\frac{\vec{r}_{i+1} - \vec{r}_i}{\ell} \right) = \frac{\partial \vec{t}(s)}{\partial s}, \qquad (2)$$

where $\hat{t}(s)$ is a tangent vector at location s along the contour of the polymer (see Fig. 1b). Finally, converting the sum to an integral yields:

$$\frac{H}{k_B T} = \frac{\xi}{2} \int_0^L \left(\frac{\partial t(s)}{\partial s} \right)^2 ds, \qquad (3)$$

WLC is for semi-flexible polymers.
Assumes polymers are inextensible, has a linear elastic bending energy and is subjected to thermal fluctuations.
a) L=Nl segments, freely rotating
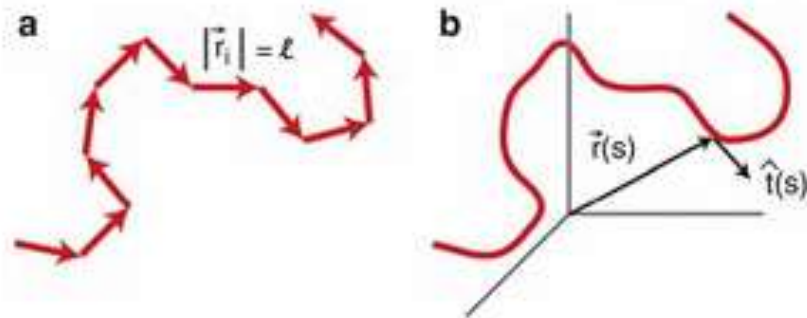
Worm-Like Chain (WLC) Model, Fig. 1 (a) Discrete model of a polymer composed of a chain of segments $\vec{r}_i$ each of length ℓ. (b) Continuous WLC polymer parameterized by the tangent vector $\hat{t}(s) = \frac{\partial \vec{r}(s)}{\partial s}$ along the contour

which is the Hamiltonian for the WLC model assuming that the contour length L is very large (Doi and Edwards 1988). Note the introduction of the persistence length $\xi = \frac{\epsilon \ell}{k_B T}$. The persistence length serves as a characteristic length scale over which two tangent vectors along the polymer remain correlated, i.e.:

$$\langle \hat{t}(s) \cdot \hat{t}(s') \rangle = e^{-\frac{|s-s'|}{\xi}}. \qquad (4)$$

The WLC describes a polymer that is stiff over short distances and flexible at longer ones, with the persistence length setting the length scale of this transition in characteristic behavior. Moreover, while

Mean Square End-to-End Distance of DNA Molecules vs. their Contour Length

Courtesy of Prof. C. Bustamante and C. Rivetti

$$\langle R^2 \rangle_{3D} = 2PL \left(1 - \frac{P}{r} \left(1 - e^{-\frac{L}{P}} \right) \right)$$

$$\langle R^2 \rangle_{2D} = 4PL \left(1 - \frac{2P}{L} \left(1 - e^{-\frac{L}{2P}} \right) \right)$$

$$\langle R^2 \rangle_{proj} = \langle R_x^2 \rangle + \langle R_y^2 \rangle = \frac{2}{3} \langle R^2 \rangle_{3D}$$

Theoretical model for a 1258 bp DNA	$\langle R^2 \rangle$ nm²
Ideal worm-like chain in 3D	35600
Ideal worm-like chain in 2D	60500
Orthogonal 3D → 2D projection	23700

$\langle R^2 \rangle = 61300$ nm² $\langle R^2 \rangle = 26000$ nm² $\langle R^2 \rangle = 25100$ nm²
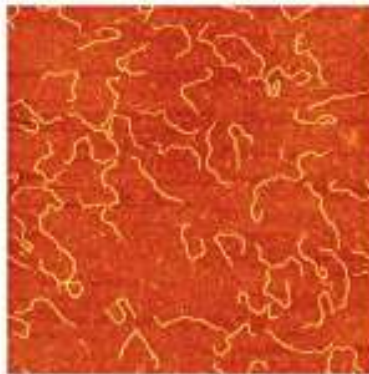
Freshly cleaved   Glow discharged   H⁺-exchanged
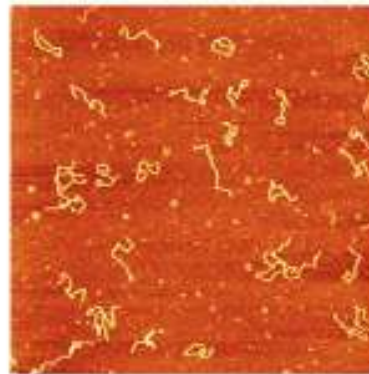
Courtesy of Prof. C. Rivetti

AFM under Liquid
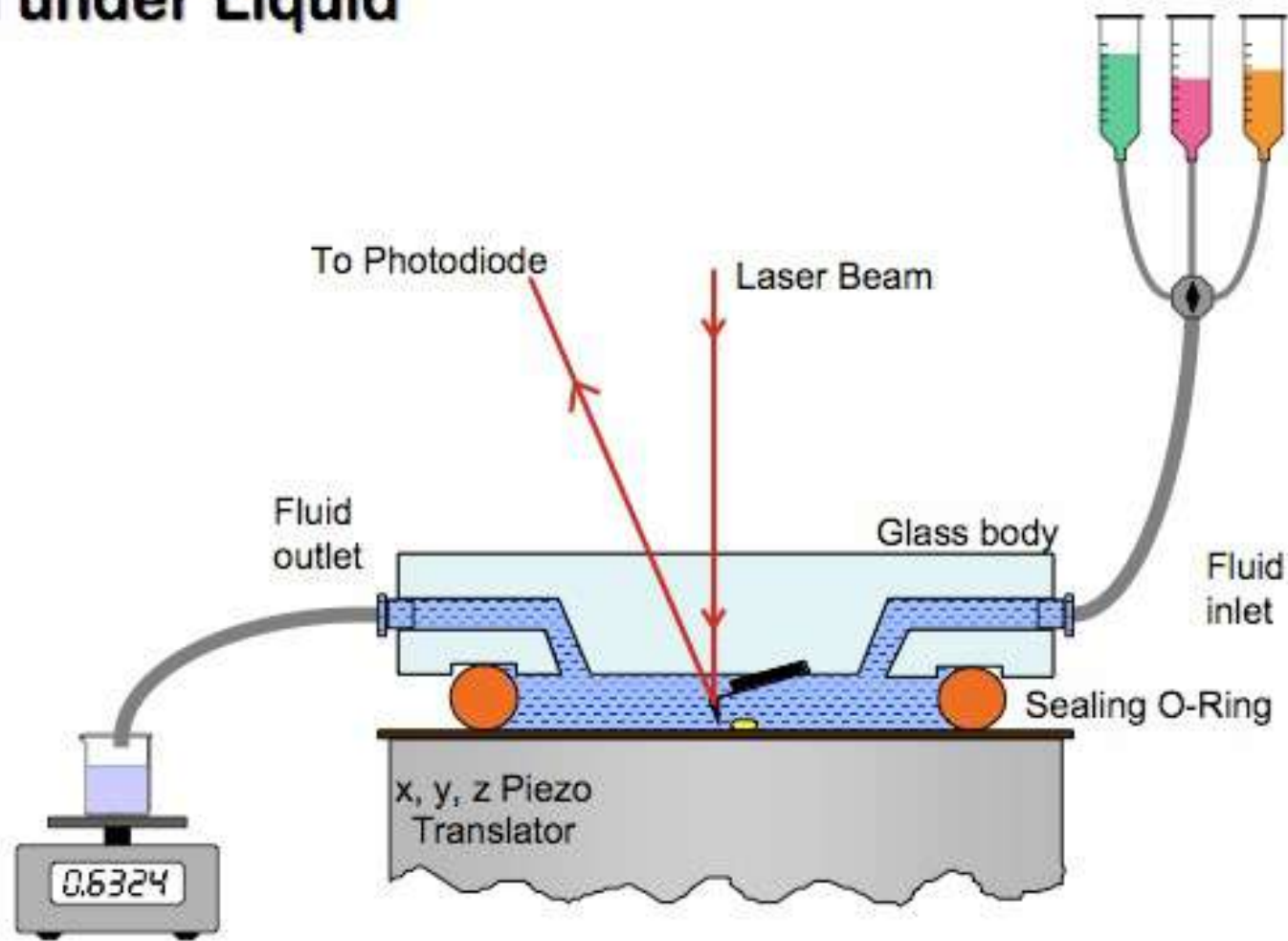
Courtesy of Prof. C. Rivetti

DNA imaged in liquid
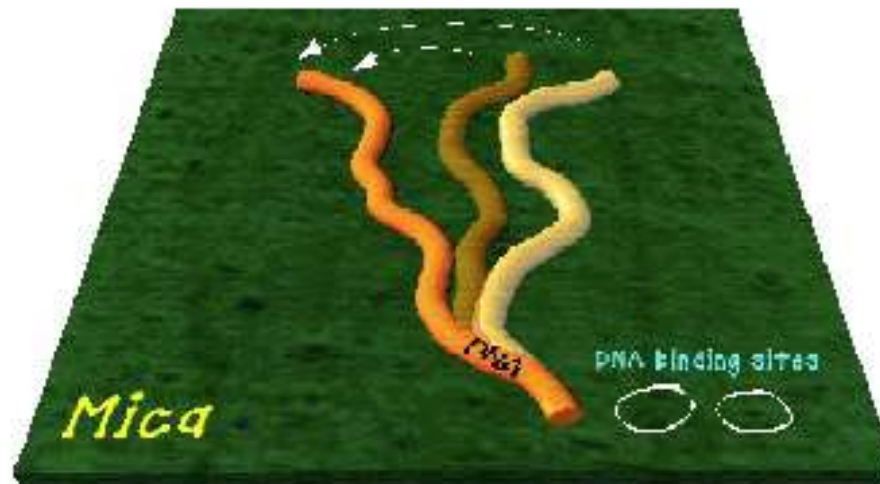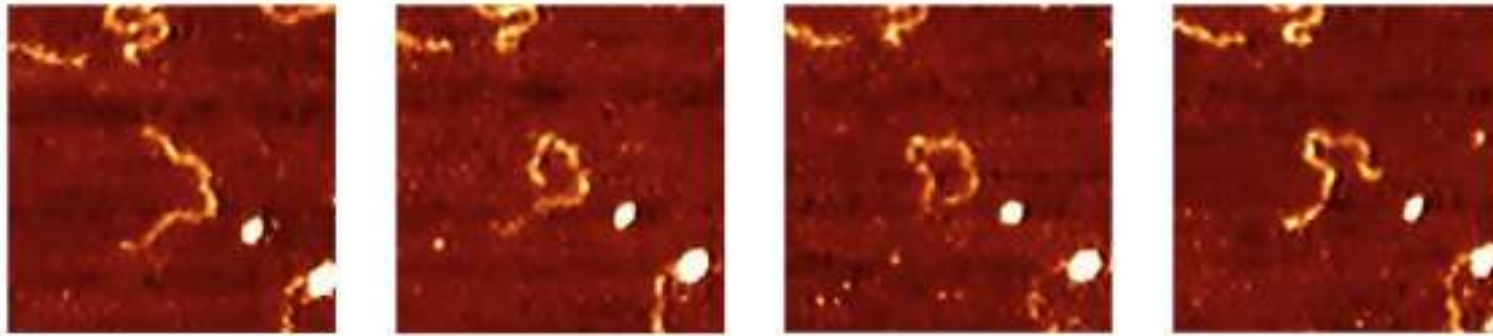
Courtesy of Prof. C. Rivetti

DNA bend angle measurements

A-tract

10 bp

AAAAAACGCG AAAAAACGCG AAAAAACGCG AAAAAACGCG
TTTTTTGCGC TTTTTTGCGC TTTTTTGCGC TTTTTTGCGC
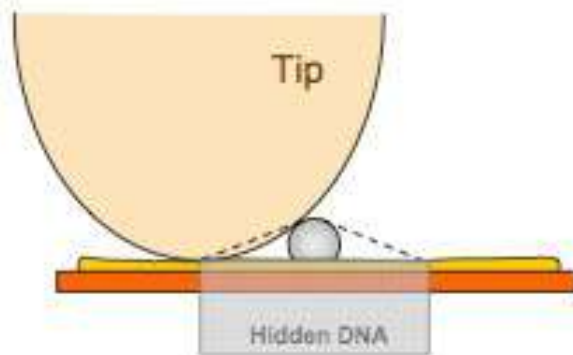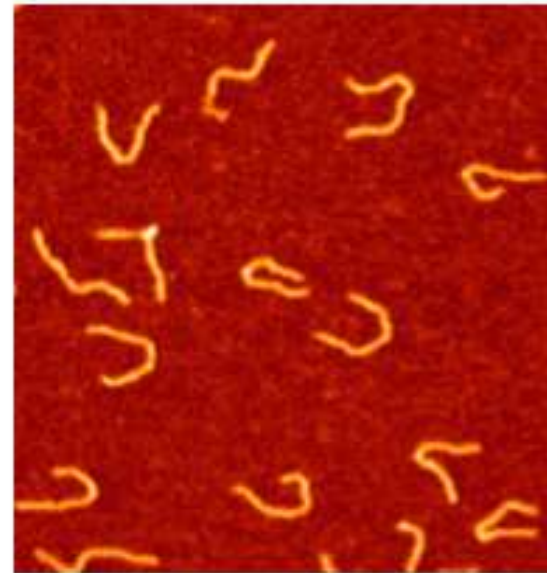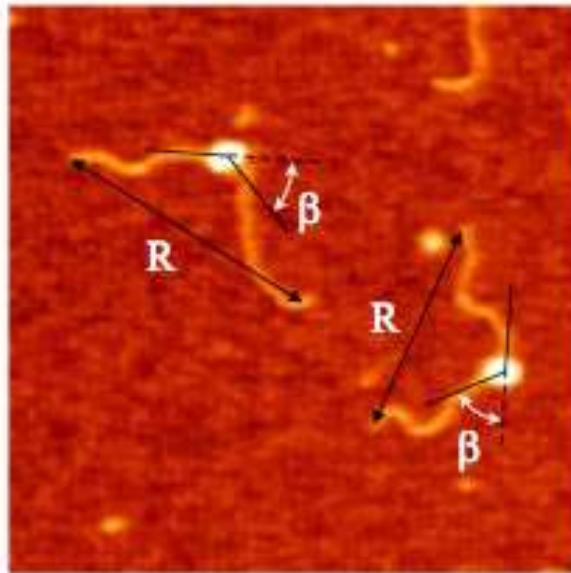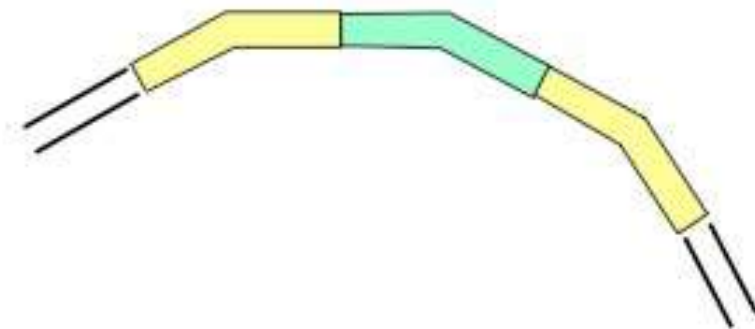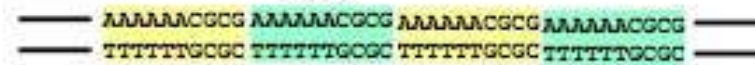
Using the end-to-end Distance to Determine Bend Angles

For a polymer molecule that is bent at any location along the chain, the mean square end-to-end distance is given by:
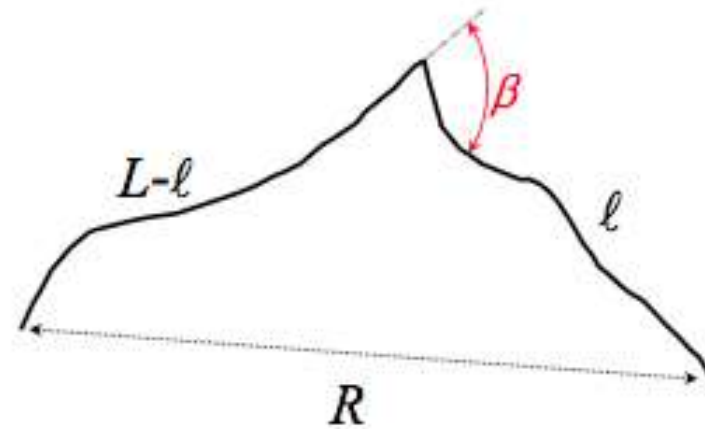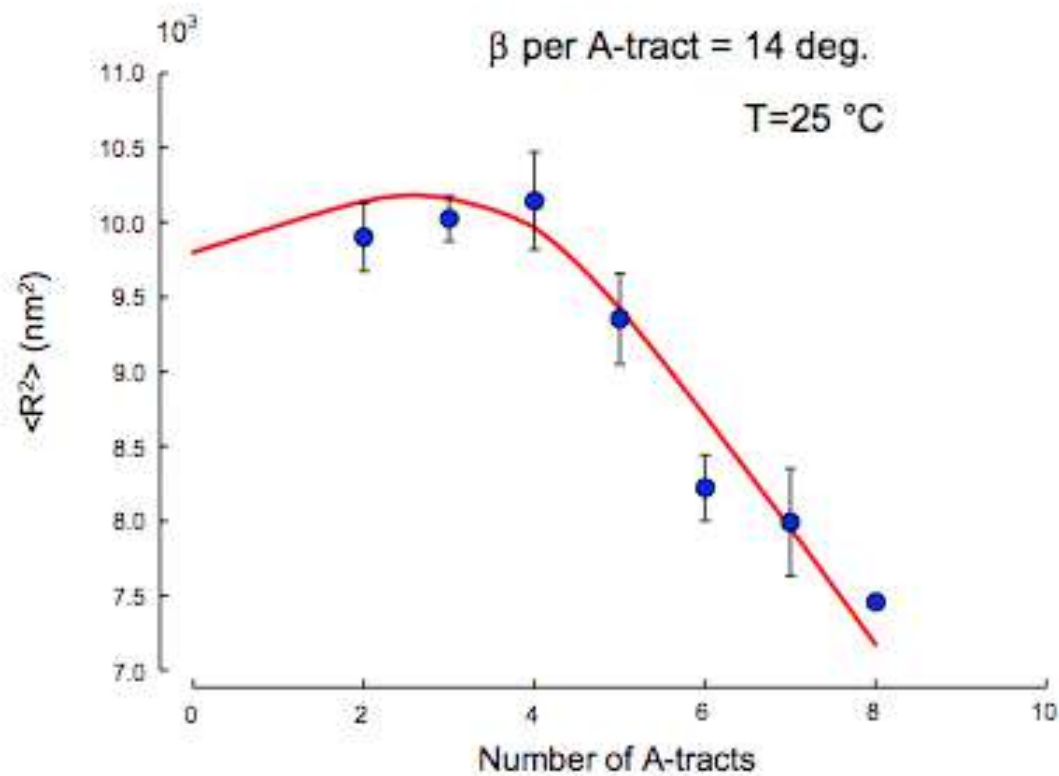

$$\left\langle R_{\beta}^{2} \right\rangle_{2D} = 4PL\left\{1 - \frac{2P}{L}\left[\left(1 - e^{-\ell/2P}\right) + \left(1 - e^{-(L-\ell)/2P}\right) - \cos(\beta)\left(1 - e^{-\ell/2P}\right)\left(1 - e^{-(L-\ell)/2P}\right)\right]\right\}$$

DNA fragments containing A-tracts

2 A-tracts

4 A-tracts

6 A-tracts

8 A-tracts

2 A-tracts

3 A-tracts

4 A-tracts

5 A-tracts

6 A-tracts

7 A-tracts

8 A-tracts

2 μm

50 nm
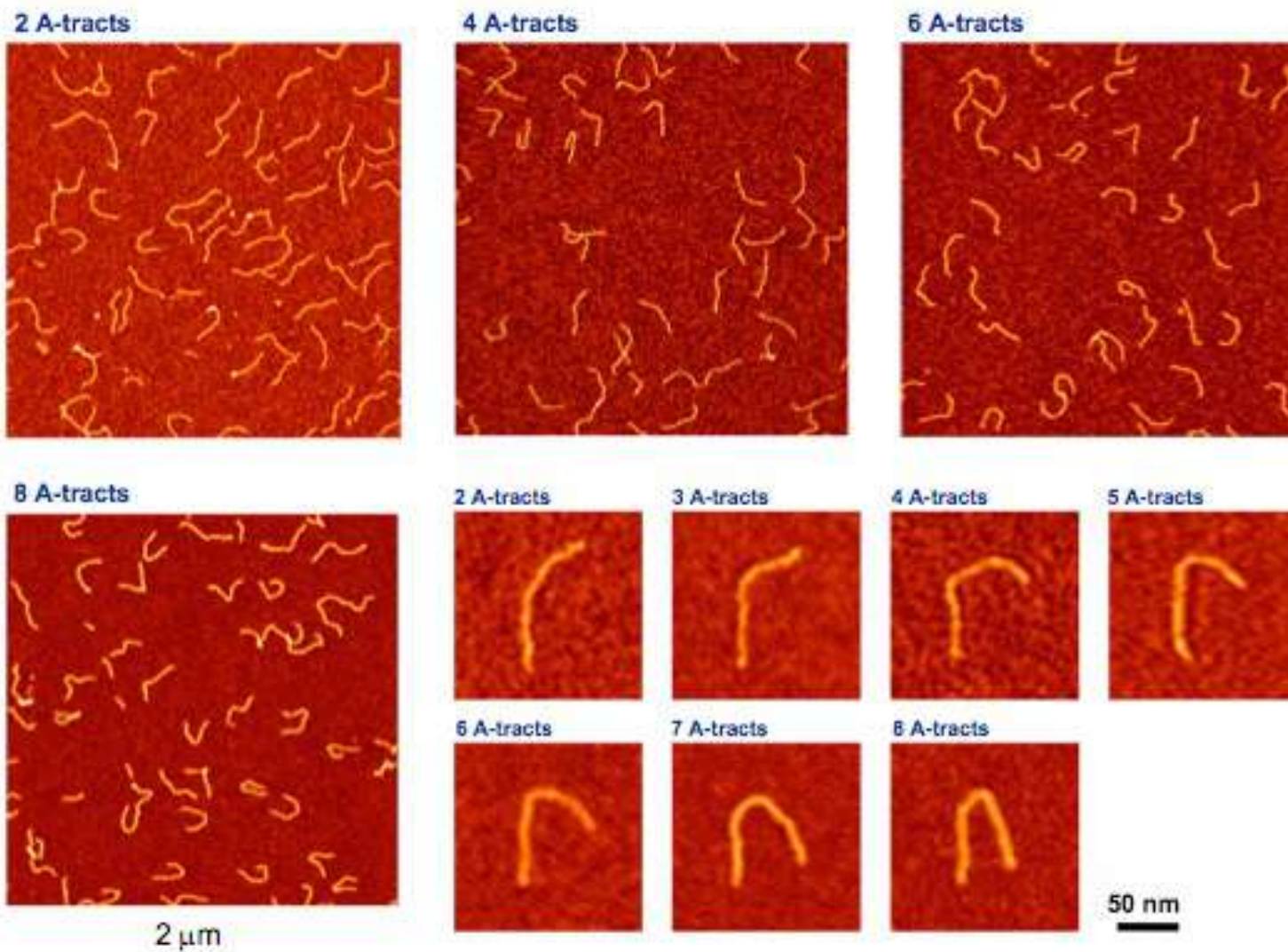
Mean square end-to-end distance as a function of the number of A-tracts

β per A-tract = 14 deg.

T=25 °C

10^3

$\langle R^2 \rangle$ (nm^2)

Number of A-tracts

155 bp

206 bp

[AAAAAACGCG]$_{n=1-8}$

Structure of the E. coli RNA Polymerase
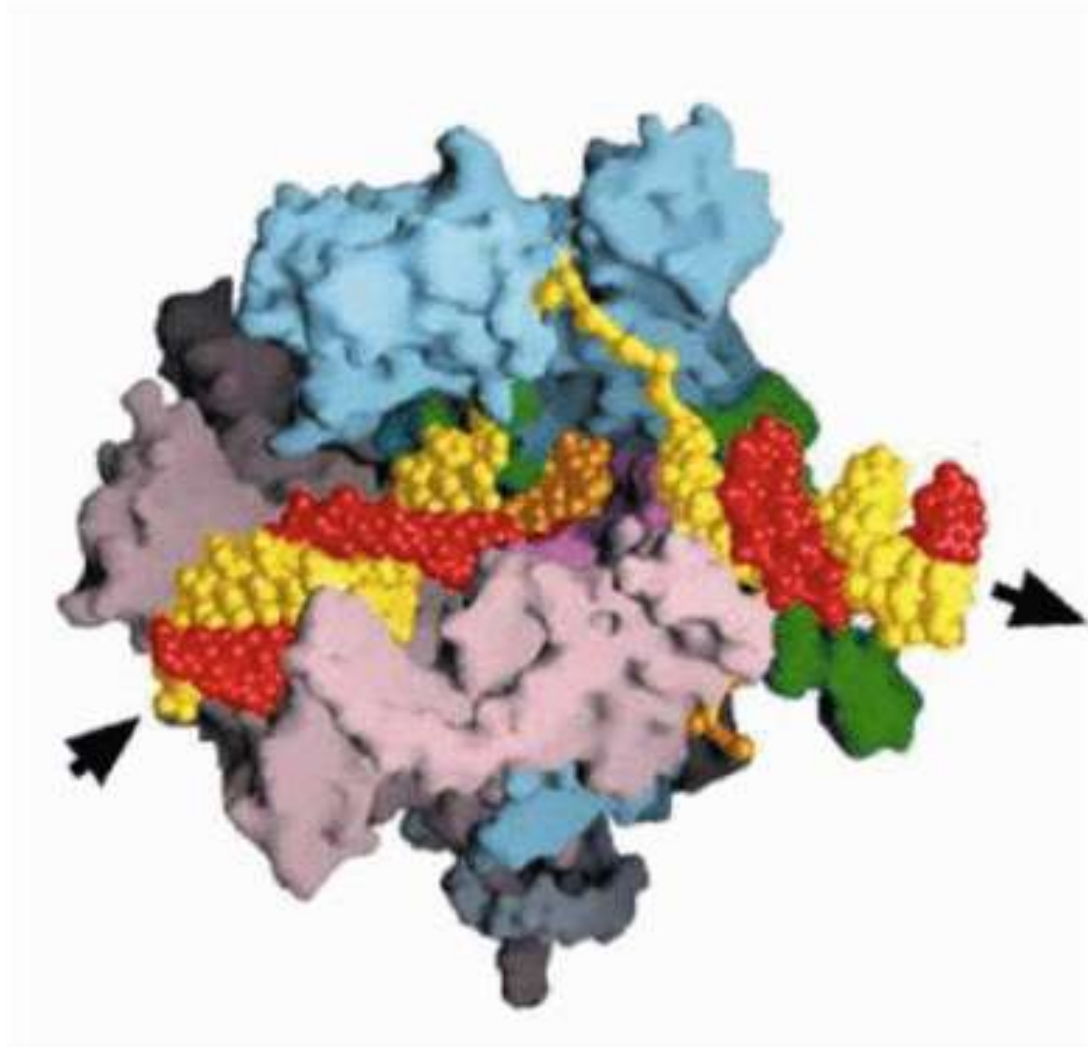
Courtesy of Prof. C. Rivetti
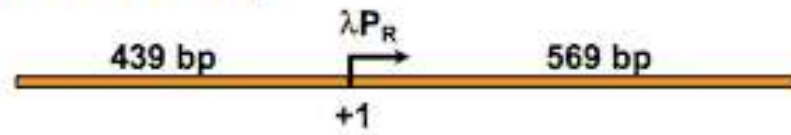
Courtesy of Prof. C. Rivetti
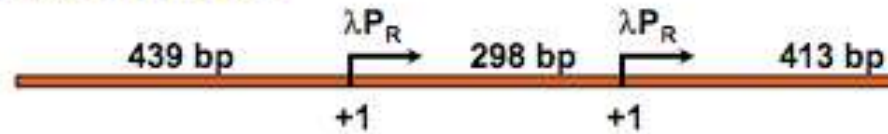
AFM image of Open Promoter Complexes
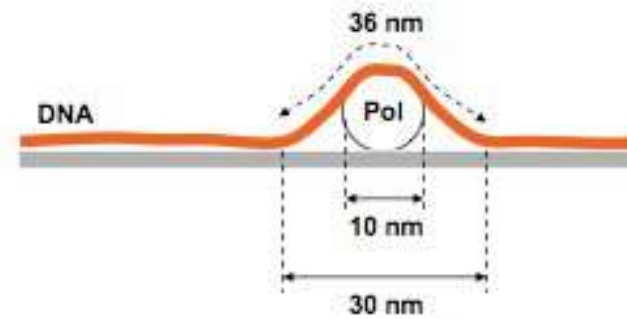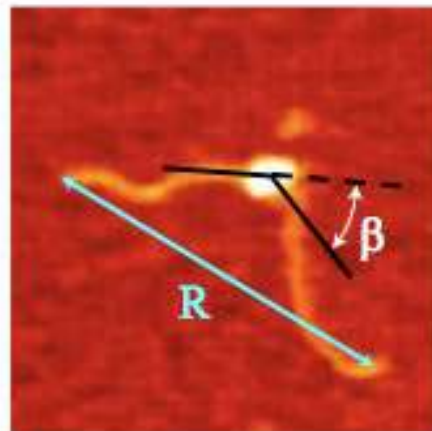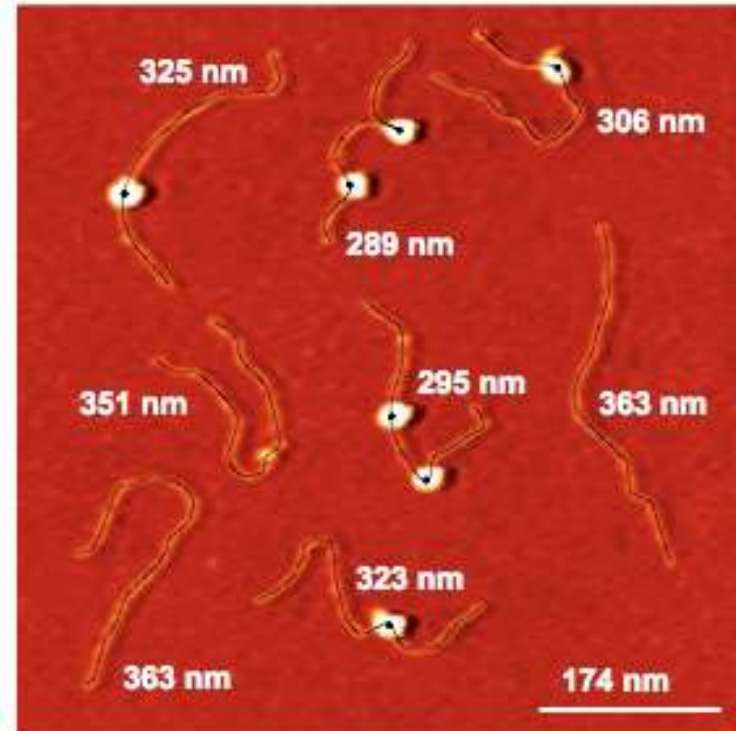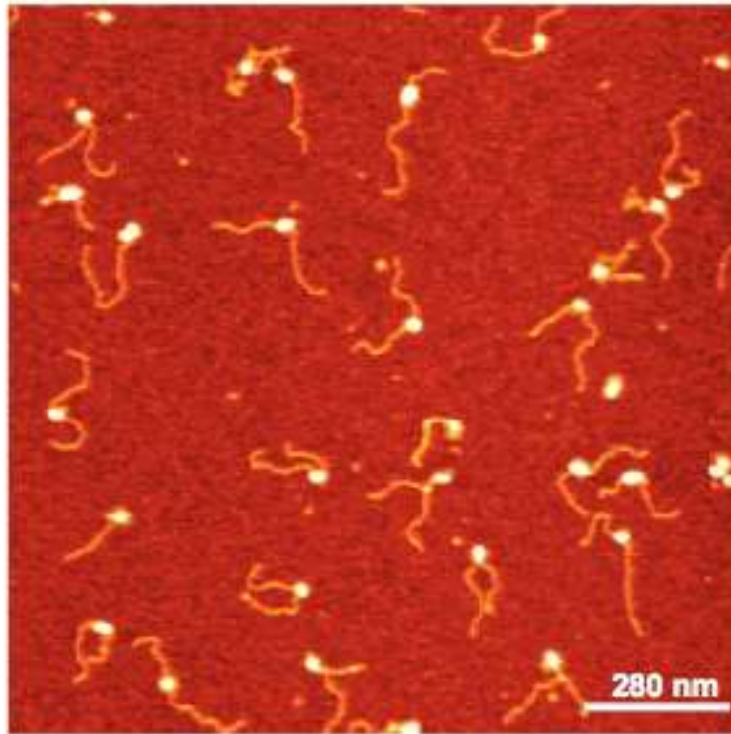
Courtesy of Prof. C. Rivetti

DNA Contour Length Measurements of Open Promoter Complexes
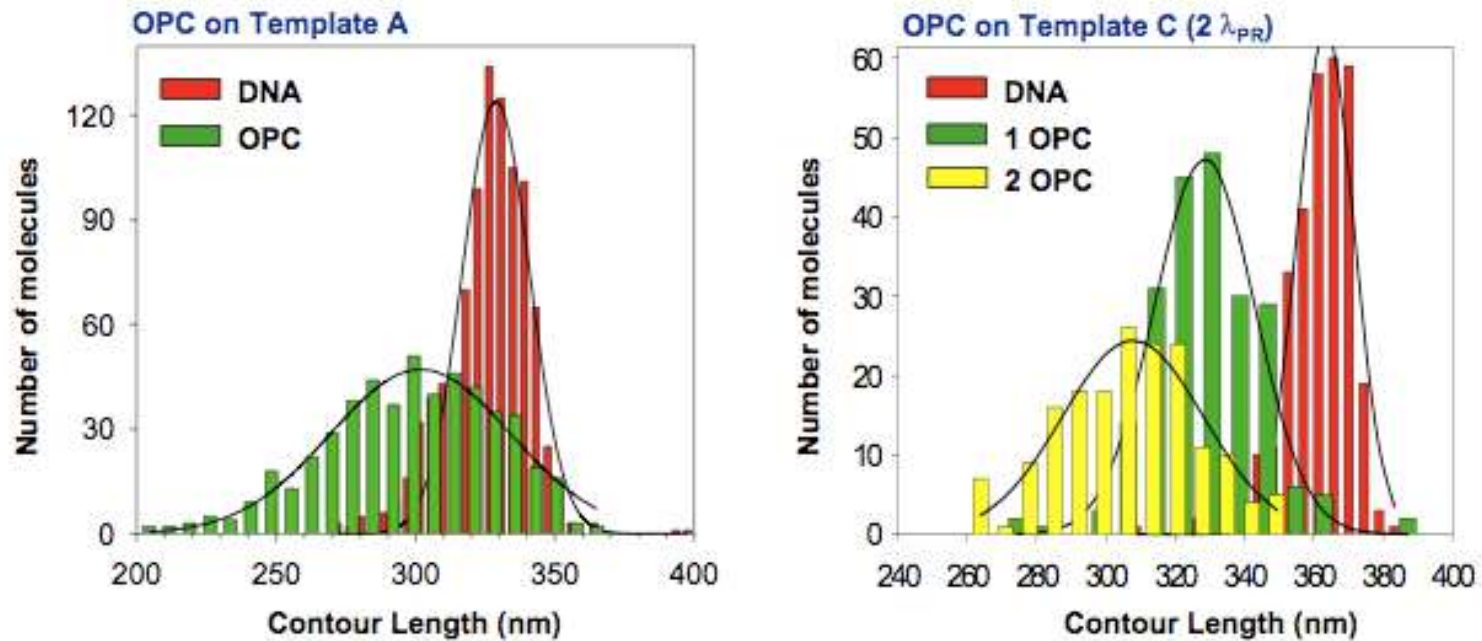
	Contour length (nm)	Compaction (nm)	N. of molecules
DNA (A)	329 ± 12		947
OPC (A)	297 ± 34	32	514
DNA (C)	363 ± 8		317
One OPC (C)	332 ±14	31	157
Two OPC (C)	308 ± 20	55	173

(a)
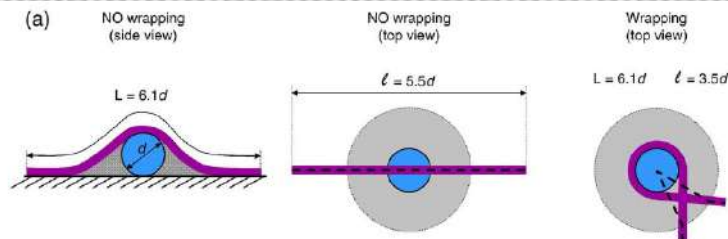
Proposed model for the open promoter complex at λ_{PR}

Courtesy of Prof. C. Rivetti